The effects of Checkpoint Kinase 1 and the Cell Cycle

on Secondary Immunoglobulin Diversification

Dissertation

To Fulfill the

Requirements for the Degree of

„doctor rerum naturalium" (Dr. rer. nat.)

Submitted to the Council of the Faculty

of Biological Sciences

of the Friedrich Schiller University Jena

by M.Sc. Amanda Bello

born on 13th August 1988 in Modugno, Italy

Abstract

In vertebrates, the process of immunoglobulin (Ig) diversification via VDJ recombination leads to the generation of a vast repertoire of B lymphocytes that are reactive to a wide variety of pathogens. Upon recognition of their cognate antigen, the reactive B cells undergo clonal expansion within organs such as the spleen and lymph nodes forming germinal centers (GCs). At the same time, the Ig genes of activated B cells undergo deliberate damage by the enzyme activation-induced deaminase (AID) that converts cytosines to uracils with the purpose to "adapt" the antibody response to the antigen to be defeated. In cells other than the B cells, U:G mismatches are faithfully repaired but in mouse and human B cells the AID-induced lesions are processed by error-prone repair mechanisms. As a consequence, mutations accumulate leading to antibody affinity maturation via somatic hypermutation (SHM) and deletional events of recombination can occur resulting in the Ig isotype switch via class switch recombination (CSR). The mechanisms responsible for the shift from error-free towards error-prone mechanisms of DNA repair at the Ig genes are not yet completely understood.

In GC B cells, the attenuation of the signaling via checkpoint kinase 1 (Chk1) is believed to allow for better DNA damage tolerance, therefore preventing cell cycle arrest and/or apoptosis. Our previous work in *in vitro* models has shown that Chk1 downregulation is beneficial for the process of SHM as such, revealing a possible mechanism for the facilitation of error-prone repair in hypermutating B cells. With the intent to reproduce those findings *in vivo*, we generated a mouse model that allows for a conditional downregulation of Chk1 in B cells and investigated the impact of Chk1 signaling attenuation on the humoral response. We find that adequate levels of Chk1 are indispensable for proper SHM by preventing proliferation and/or survival defects in hypermutating B cells, hence ensuring mutations to be passed on. Nevertheless, we found that decreased levels of Chk1 favour the activity of the non-canonical mismatch repair pathway involved in the introduction of mutations at A:T base pairs during SHM but, at the same time, allow for sustained mutagenesis outside the Ig loci.

AID-induced off-target mutagenesis is associated with the development of various forms of B-cell lymphoma, therefore the mechanisms of Ig diversification must be tightly regulated. The possible temporal limitation of the activity of AID and the error-prone DNA repair mechanisms during the cell cycle has been hypothesized and investigated, leaving, though, some open questions. We ectopically restricted the activity of AID to the G_1 or the S/G_2 phase of the cell cycle in different *in vitro* systems and found that the limitation of AID nuclear accumulation may be the main mechanism that prevents its activity in S/G_2 and that most of the error-prone DNA repair pathways acting during secondary Ig diversification are more active in the G_1 phase.

Zusammenfassung

In Wirbeltieren ermöglicht der Prozess der Diversifizierung von Immunglobulin (Ig) über die VDJ-Rekombination die Generierung eines ausgedehnten Repertoires an B-Lymphozyten, die auf eine Vielzahl von Krankheitserregern reagieren. Nachdem sie ihr jeweiliges Antigen erkannt haben, durchlaufen die reaktiven B-Zellen eine klonale Expansion in als Keimzentren bezeichneten Strukturen, welche sich in Organen wie der Milz und den Lymphknoten befinden. Parallel werden die Ig-Gene aktivierter B-Zellen durch das Enzym Aktivierungs-Induzierte-Desaminase (AID) vorsätzlich geschädigt, welches Cytosin in Uracil umwandelt, um die Antikörperantwort an das zu bekämpfende Antigen „anzupassen". Während die resultierenden U:G-Fehlpaarungen in anderen Zellen fehlerfrei repariert werden, verarbeiten B-Zellen von Mäusen und Menschen die AID-induzierten Läsionen durch fehleranfällige Reparaturmechanismen. Infolgedessen können einerseits Mutationen akkumulieren, welche über somatische Hypermutation (SHM) zur Reifung der Antikörperaffinität führen und andererseits deletierende Rekombinationsereignisse auftreten, die in einem Ig-Isotypwechsel durch Klassenwechsel-Rekombination resultieren. Bisher sind die Mechanismen, welche für den Wechsel von einer fehlerfreien zu einer fehleranfälligen DNA-Reparatur der Ig-Gene verantwortlich sind, noch nicht vollständig geklärt.

Es wird angenommen, dass in Keimzentrums-B-Zellen eine verminderte Signalübertragung der Checkpoint-Kinase 1 (Chk1) für eine höhere DNA-Schädigungstoleranz sorgt und somit ein Anhalten des Zellzyklus und/oder eine Apoptose verhindert. Unsere vorherigen Arbeiten mit in-vitro-Modellen haben gezeigt, dass die Herunterregulation von Chk1 den SHM-Prozess als solchen fördert, was auf einen möglichen Mechanismus zur Begünstigung einer fehleranfälligen Reparatur in hypermutierenden B-Zellen hinweist. Um diese Ergebnisse in vivo zu reproduzieren, haben wir ein Mausmodell erstellt, welches eine konditionale Herunterregulation von Chk1 in B-Zellen ermöglicht und den Einfluß eines verminderten Chk1-Signals auf die humorale Reaktion untersucht. Wir konnten feststellen, dass adäquate Chk1-Mengen für eine funktionierende SHM unerlässlich sind, weil dadurch Proliferations- und/oder Überlebensdefekte in hypermutierenden B-Zellen verhindert werden, wodurch die Weitergabe der Mutationen sichergestellt wird. Dennoch konnten wir zeigen, dass ein verringerter Chk1-Spiegel sowohl die Aktivität des nicht-kanonischen Fehlpaarungs-Reparaturweges begünstigt, welcher an der Mutation von A:T-Basenpaaren beteiligt ist, als auch eine anhaltende Mutagenese außerhalb der Ig-Gene ermöglicht.

Da die AID-induzierte Off-Target-Mutagenese mit der Entwicklung verschiedener Formen von B-Zell-Lymphomen verbunden ist, müssen die Mechanismen der Ig-Diversifikation streng reguliert werden. Obwohl eine zeitliche Begrenzung der Aktivität von AID und den fehleranfälligen DNA-Reparaturmechanismen während des Zellzyklus vermutet und untersucht wurde, bleiben einige Fragen offen. Durch eine ektopische Beschränkung der AID-Aktivität auf die G_1- oder S/G_2-Phase des Zellzyklus haben wir herausgefunden, dass die Aktivität in der S/G_2-Phase durch eine eingeschränkte AID-Akkumulation im Zellkern behindert wird und ein Großteil der fehleranfälligen DNA-Reparaturmechanismen während der sekundären Ig-Diversifikation in der G_1-Phase aktiver sind.

Table of Contents

1 Introduction

All living organisms face the challenge of recognizing and neutralizing insults that may be life-threatening. The nature of the insult may greatly differ, as much as its source. Therefore, evolution has shaped disparate mechanisms of protection that act at different levels to put in place the most adequate response.

The immune system of vertebrates represents a very complex level of protection as it involves a multitude of cell types, tissues, and organs. It defends our body from foreign pathogens that may overcome the natural barriers provided by the epithelia. In such case, the early local protection mediated by the components of the innate immune response guarantees a quick reaction that, on the one hand, prevents or slows down the establishment of the infection and, on the other hand, buys time until the components of the adaptive immune response are ready. As a result, antigen-specific T and B lymphocytes are deployed so that a specific and systemic response takes place, aimed at the eradication of the threat and the generation of immunological memory.

On a much smaller scale, the cells of our body continuously deal with the danger posed by DNA damage and are therefore able to orchestrate a sophisticated network of DNA damage sensors and transductors whose ultimate function is either the repair of the damage or the limitation of its propagation.

B cells in the course of the humoral immune response represent an exceptional paradigm: not only the DNA damage but also the attenuation of the DNA damage response is necessary to achieve effective immune protection.

1.1 The adaptive immune response

The immune system of vertebrates is not only able to protect the body against ideally every kind of pathogen, but also generates long-lasting protection and ensures that the defensive reaction does not harm one's own tissues. These duties are compartmentalized into two distinct but interconnected levels, namely the innate and the adaptive immunity [1]. In the case of infection by pathogens, the innate immunity is the first line of defence and it is required to react quickly. The threat is recognized mainly by phagocytic and granulocytic cells via mechanisms that are highly conserved across animal phyla and encoded in the germline genome, hence *innate*. This protection is immediate but incomplete, as it recognizes limited sets of antigens and is not specific to the kind of threat. Importantly, it only provides a short-term memory of

the encounter [2]. The evolutionary process needed additional hundreds of millions of years to compensate for those deficiencies and eventually shape the adaptive immune response [3].

T and B lymphocytes of the adaptive immunity are able to meticulously discriminate among antigens and to react with great specificity. During the lymphocyte development in the bone marrow and thymus, the genes encoding for the antigen receptors on T and B cells, the T cell receptor (TCR) and the B cell receptor (BCR), respectively, undergo recombination processes, which lead to the generation of a very large number of unique receptors that specifically react to their cognate antigens [4]. Given the extremely high number of receptors and antigens, the likelihood of a spontaneous antigen encounter needs to be maximized. Naive T and B lymphocytes mainly reside in secondary lymphoid tissues, such as the lymph nodes, which continuously receive a representative sample of the antigens that are circulating in the interstitial fluid [1]. T cells recognize antigens presented in association with major histocompatibility complex (MHC) proteins. Extracellular antigens, such as bacterial or fungal proteins, are processed and presented to the T cells by antigen presenting cells (APCs) among which are a specialized type of phagocytes of the innate immune system referred to as dendritic cells (DCs). Antigens delivered intracellularly, such as viral particles, are packaged into MHC proteins and exposed on the surface of the harboring cells [5]. B cells recognize antigens in their native form via their BCRs, which are membrane-bound immunoglobulins (Ig) or antibodies in association with accessory proteins [6]. Upon antigen recognition, T and B lymphocytes massively proliferate in order to increase the number of clones that react against the antigen and differentiate into specialized cell subsets. T helper cells potentiate the immune response by secreting cytokines and chemokines, and are also needed to activate the B cells. Cytotoxic T cells are able to directly eliminate cells that have been infected by viruses or that express aberrant proteins, such as cancer cells [7-9]. Activated B cells may undergo further "adaptation" of their BCR to the cognate antigen and ultimately differentiate into antibody-secreting plasma cells [10, 11]. The long-lasting protection provided by the adaptive immune system is guaranteed by the generation of memory T and B cells, which ensures a quicker activation of the adaptive immune system upon repeated encounters with a known antigen [12].

1.1.1 B cells and antibodies

Mature B cells are the product of a developmental process that is initiated at the embryonic stage in the fetal liver and then relocated to the bone marrow after birth. Fetal liver-derived B cells are referred to as B1 cells and populate predominantly serous cavities such as the

peritoneum and pleura. The most common B cells, referred to as B2 cells, arise from the bone marrow and populate the secondary lymphoid organs such as the spleen and lymph nodes [13]. The humoral response is triggered by the recognition of an antigen by a B cell and its subsequent activation.

The recognition is mediated by the BCR, which is a complex formed by a membrane-anchored IgM coupled with the two accessory protein chains Igα and Igβ [14]. The signaling transduced by the BCR alone is not sufficient to fully activate a B cell, thus additional signals are required. The nature and the source of such co-stimulatory signals are specified by the antigen itself. Protein antigens usually trigger a humoral response defined as thymus-dependent (T-dependent): The co-stimulatory signals are provided to the B cell by a cognate T cell that has been primed with the same antigen [15]. Antigens such as polysaccharides and lipopolysaccharides are T-independent antigens as they have the intrinsic ability to trigger B cell activation in the absence of T cell help. Those antigens may either provide additional mitogenic signals by binding Toll-like receptors (TLRs) on the B cell membrane or by inducing BCR cross-linking as a response to highly repetitive structures [16]. Either way, the activation of a mature naïve B cell culminates in the generation of memory B cells and antibody-secreting plasma cells.

Memory B cells possess high reactivity to the activating antigen in order to mount a quick humoral response upon a subsequent encounter [17]. Plasma cells represent the final stage of B cell differentiation and the effector branch of the humoral immunity [10]. These cells are specialized in the secretion in the fluids of the body of soluble Igs, which exert immune protection in three main ways: i) the binding of soluble antibodies to the antigen may simply neutralize its pathogenic activity by preventing it from entering into the target cells; ii) antibodies may opsonize the surface of antigens and facilitate their uptake by phagocytes, which recognize the invariable portion of the Igs via their Fc (fragment crystallizable) receptors; iii) antibodies can activate the complement cascade, which in turn may recruit phagocytic cells to the site of infection, facilitate the antigen uptake by opsonization, or eventually lyse certain microorganisms by generating pores in their membrane [18].

The basic structure of an antibody (monomer) is that of a "Y"-shaped protein composed of four glycoprotein chains, more specifically two identical Ig heavy (IgH) chains and two identical light (IgL) chains of the κ or λ isotype; each Ig chain comprises a constant and a variable region (Figure 1) [19]. The constant regions are invariant domains; in the case of IgH chains, they specify for the Ig isotypes (IgM, IgD, IgG, IgA, and IgE) and, therefore, for the effector functions of the antibody [20]. The variable regions are the domains that physically interact

with the antigens and their amino acid sequence greatly differs between different Igs, determining different antigen specificities. The variable regions of the heavy and light chains (V_H and V_L, respectively) together constitute the antigen-binding site [21].
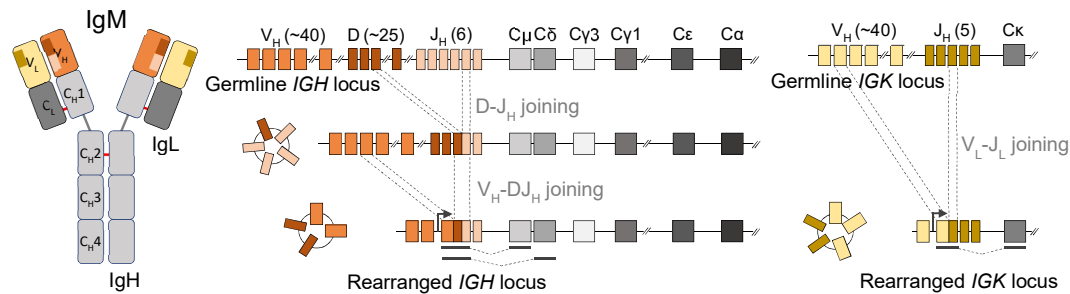
Figure 1: Immunoglobulin structure and primary diversification via V(D)J recombination.
On the left, a representative scheme of an IgM monomer is shown. Each Ig chain comprises a variable region (in orange and yellow) and a constant region (light and dark grey); the constant region of the IgH chain of an IgM comprises four structural domains. The Ig chains are connected via disulphide bonds (in red). On the right, events of V(D)J recombination at the human *IGH* and *IGK* loci (explained in the text) are shown; variable (V), diversity (D), joining (J), and constant (C) gene segments are depicted. Each recombination event leads to the excision of the intervening portion of DNA as extrachromosomal DNA circle. The transcription is initiated from a leader sequence located upstream of the rearranged V(D)J sequence and the splicing of the primary transcript removes the region between the V(D)J segment and the constant region. The figure is adapted from Murphy *et al*. [1].

1.1.2 Primary Ig diversification via V(D)J recombination

The generation of a huge antibody repertoire allows our body to react against, ideally, any kind of antigen. It has been estimated that, in humans, up to 10^{11} different antigens can be recognized by the pool of naïve B cells [22]. The diversification of the variable region starts during the B cell development in the bone marrow through a recombination process known as primary Ig diversification or V(D)J recombination (Figure 1) [23]. The germline organization of the Ig loci comprises clusters of contiguous gene segments classified as following: variable (V), joining (J), diversity (D), and constant (C) [24]. While the constant domain of the Ig is encoded by a single C segment, the gene portion encoding the variable domain is the product of the recombination between more than one gene segment and more specifically it derives from the joining between one V, one J, and, in case of IgH chains, one D segment [23]. The recombination begins at the *IgH* locus with a D to J_H joining. The proteins encoded by the recombination-activating genes 1 and 2 (RAG-1 and RAG-2) bind to conserved recombination signal sequences at randomly chosen D and J_H segments [25]. The synaptic interaction between two RAG complexes activates their endonuclease activity leading to the generation of double-strand breaks (DSBs) in the proximity of the D and J_H segments to be joined [26]. The DNA ends are subsequently ligated together by the non-homologous end-joining (NHEJ) pathway and the intervening region is removed from the genome [27]. The recombination proceeds then

with a second rearrangement between a V_H segment and the newly generated DJ_H segment [28]. Together with the combinatorial diversity provided by the recombination between different gene segments, the extent of the diversification at the *IgH* locus is further increased by junctional diversity as a result of random addition of nucleotides at the junctions by the enzyme terminal deoxynucleotidyl transferase (TdT) [29]. The recombination at the IgL chain begins only if a functional V_HDJ_H rearrangement has been achieved. The pairing between different IgH and IgL chains further amplifies the repertoire of naïve B cells and, as a consequence, the repertoire of unique BCRs [22].

Once a naïve B cell recognizes its cognate antigen and becomes activated, it may undergo further diversification of its Ig genes through processes referred to as secondary Ig diversification.

1.1.3 The germinal center reaction

Upon antigen encounter, a naïve B cell may become activated and generate a multitude of clones expressing BCRs with increased antigen-binding ability [11]. This process is known as antibody affinity maturation and relies on the formation of germinal centers (GC), which are structures that develop within secondary lymphoid organs upon T-dependent B cell activation [30, 31]. In these organs, B and T cells occupy distinct regions referred to as the primary follicle and the T cell area, respectively (Figure 2) [32]. In the primary follicle, resting B cells densely gather around a network of a specialized cell type, namely the follicular dendritic cells (FDCs), due to the expression on the B cell surface of the chemokine receptor CXCR5, which senses the chemoattractant CXCL13 secreted by the FDCs [33].

The GC reaction begins with the recognition by a B cell of its cognate antigen within the follicle and its subsequent migration to the T cell/B cell border in order to interact with a cognate antigen-primed T cell that could provide the signals needed for its full activation (Figure 2) [34, 35]. B cells are professional APCs: Upon antigen recognition, they are able to internalize the antigen, degrade it intracellularly and expose peptides of the antigen on their surface in association with MHC-II proteins for recognition by a cognate T cell [36]. The TCR:MHC-II contact promotes the expression of CD40 and CD40L on the surface of B and T cells, respectively [35, 37]. CD40:CD40L interaction, together with other signals produced by the T cells such as interleukin (IL)-4 or IL-21, provides the co-stimulation needed for a complete B cell activation [38, 39]. The competition among different antigen-specific B cell clones for T cell help poses a first selective pressure aimed at favouring the activation of those clones with
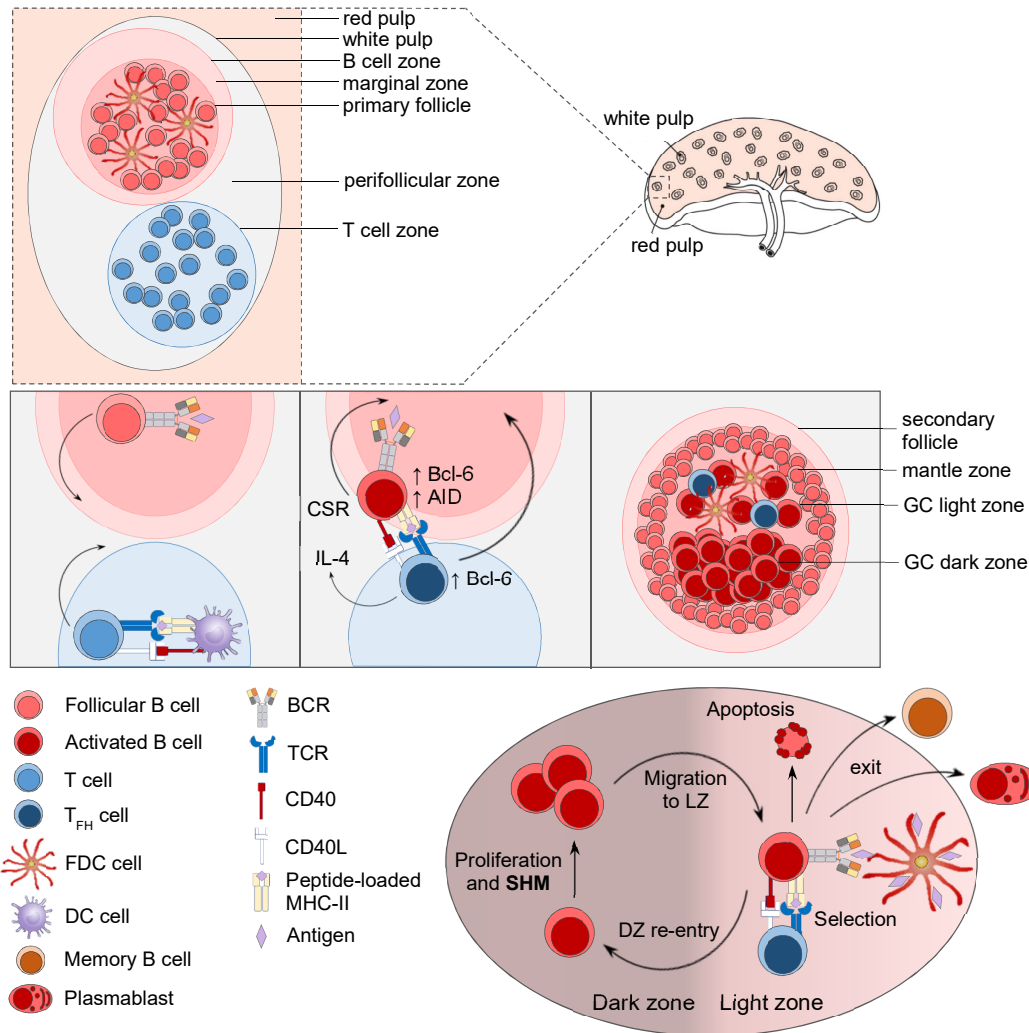
Figure 2: B and T cell dynamics in the generation and progression of the germinal center reaction in the spleen.
B and T cells are found in the white pulp, while the red pulp is populated by different cell types and mostly by macrophages that filter the blood and carry out the clearance of aging red blood cells. Antigen-primed B and T cells interact at the B/T cell border; B cells that do not upregulate Bcl-6 upon interaction can differentiate into early memory cells and short-lived plasma cells, while expression of Bcl-6 commits the B cells to the GC program and the T cells towards the differentiation to T_{FH} cells. B cells start expressing activation-induced deaminase (AID) and may undergo CSR upon stimulation with cytokines such as IL-4. Bcl-6-expressing B and T cells migrate to the center of the follicle generating a secondary follicle characterized by the presence of GCs. Here B cell undergo affinity maturation of their BCR in the dark zone (DZ) followed by selection in the light zone (LZ). From the LZ, B cells may leave the GC or recirculate to the DZ for further rounds of proliferation and Ig diversification. The figure is adapted from De Silva *et al.* [31].

a higher relative affinity for the cognate antigen. Among the responsive B cell clones, the ones with high antigen affinity may directly differentiate into memory B cells and short-lived plasma cells, while the ones with lower affinity may seed GCs in which they undergo affinity maturation of their BCR [40, 41]. Interacting B and T cells start expressing the master regulator of the GC reaction, namely the B cell lymphoma 6 (Bcl-6) protein, which commits T cells

towards the differentiation into T follicular helper (T_{FH}) cells and induces the GC program in activated B cells [42-44]. T_{FH} cells acquire the ability to migrate into the follicle by expressing CXCR5, followed by GC-committed B cells, which move to the center of the follicle and start proliferating, therefore forming early GCs, usually detectable four days after immunization [31, 45]. By day 7 post-immunization, the massive proliferation of the B cell blasts leads to the formation of a mature GC, showing a phenotypical/functional polarization into two microenvironments known as dark and light zone (DZ and LZ) [46]. B cells in the DZ (centroblasts) proliferate at a high rate determining the histological appearance of the DZ as a densely populated region [47]. In the DZ, not only clonal expansion but also Ig diversification via somatic hypermutation (SHM) takes place (Figure 2). During this process, the accumulation of random point mutations in the regions encoding for the Ig variable domains has the purpose of generating clones with higher antigen affinities [48]. Since not every mutation is necessarily advantageous, the newly diversified BCR needs to be "tested". At this point, B cells shuttle from the DZ to the LZ, mainly through the downregulation of the chemokine receptor CXCR4, responsible for retaining B cells in the DZ [49]. The LZ appears sparsely populated by B cells (knows as centrocytes) and hosts other cell types, such as FDCs and T_{FH} cells [47]. FDCs in the LZ function as antigen reservoirs, as these cells are specialized in capturing and retaining antigens in their native form on their surface, which is maximized by dendritic protrusions [50]. Once in the LZ, B cells expressing a BCR with relative higher affinity may have an increased ability to internalize the antigen and to present it to the T_{FH} helper cells. In doing so, these B cells receive survival signals and are positively selected [51]. The intraclonal competition for T cell help leads, once again, to selective pressure, therefore clones that have not received adequate survival signals (either because of low antigen affinity or stochastic reasons) activate the apoptotic program [52]. Positively selected B cell clones may now either leave the GC as memory B cells or long-lived plasma cells or recirculate to the DZ for further clonal expansion and diversification of their Ig genes [53, 54]. GCs are transient structures that disappear within three weeks from the first immunization, leaving memory B cells and plasma cells, which may persist in the body for decades [55-57].

Another process of Ig diversification is class switch recombination (CSR), which leads to the switch of the constant region of the IgH chain and, therefore, the antibody isotype. Through CSR, the antibodies acquire different and more specialized effector functions, more adequate to the pathogen to defeat [20]. CSR was believed for a long time to occur in the LZ of the GC, but more recently it has been identified as a process that precedes the GC formation and that does not frequently occur in mature and established GCs [58].

1.2 Molecular mechanisms of secondary Ig diversification

The processes of SHM and CSR taking place in human and mouse B cells rely on the deliberate introduction of point mutations in the variable region of the Ig genes (both IgH and IgL) and on the region-specific deletional recombination of the IgH chain, respectively [59]. These processes are triggered by the targeted introduction of lesions in the DNA by the enzyme activation-induced deaminase (AID) and by the subsequent unfaithful resolution of those lesions by error-prone mechanisms of DNA repair that allow for the purposeful mutagenesis and recombination.

The secondary Ig diversification in animals like chickens and rabbits occurs via a process of templated mutagenesis referred to as Ig gene conversion (IgGC) that relies on the repair of AID-induced lesions via homologous recombination (HR) (Figure 3), which acts in an error-free fashion [60, 61].
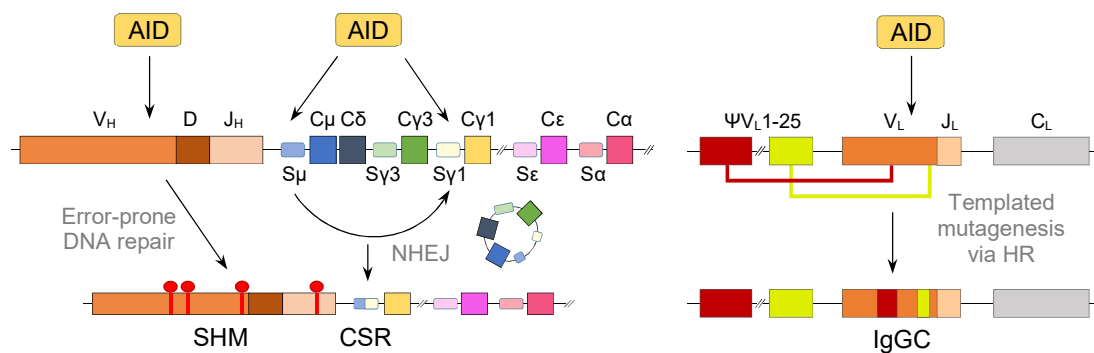
Figure 3: Secondary Ig diversification via SHM, CSR and IgGC.
On the left, a representation of secondary Ig diversification at the *IgH* locus in mouse B cells via SHM and CSR is shown. Point mutations (nucleotide substitutions, insertions/deletions) occur in the VDJ region upon error-prone repair of AID-induced lesions during SHM and are shown as red circles and lines. An event of CSR to IgG1 is depicted. CSR is initiated by AID targeting at the switch (S) regions; in the depicted event the Cγ1 gene segment is brought into proximity of the VDJ region by NHEJ and the DNA portion between the targeted Sμ and Sγ1 is excised from the genome. On the right, the diversification via IgGC at the *IgL* locus in chicken B cells is shown. AID targets the variable region; each of the 25 upstream pseudo (ψ) genes can contribute to the diversification via HR-mediated repair of AID-induced lesions. Figure adapted from Wang [62] and Tang *et al.* [63].

1.2.1 Somatic hypermutation (SHM)

SHM is the process by which B cells diversify the variable regions of their Ig genes in order to develop antibodies characterized by higher affinity for their cognate antigen, allowing them to be more effective in the fight against the foreign substance. Nucleotide substitutions, and more rarely insertions and deletions, are generated in the Ig genes with a frequency of 10^{-3} mutations/base pair (mut/bp), many orders of magnitude higher than the frequency of mutations

arising spontaneously in the genome of somatic human cells of around 10^{-9} mut/bp [64]. Mutations start appearing 100–200 bp downstream of the transcription start site (TSS) and are found in a region spanning ca. 2 kb, with the constant regions spared from mutagenesis [65, 66]. The peak of mutation frequency is observed within three hypervariable regions designated as complementary-determining regions (CDR), as they determine the complementarity to the cognate antigen [67].

AID preferentially deaminates cytosines in the context of WRCY motifs (W=A/T, R=A/G, Y=T/C) that are referred to as SHM hotspots [68, 69]. Cytosine deamination results in the conversion of cytosine into uracil, an event that leads to the generation of the full spectrum of mutations: Transitions, i.e. purine to purine or pyrimidine to pyrimidine base substitutions, and transversions, i.e. purine to pyrimidine or pyrimidine to purine base substitutions, are introduced at C:G and also at A:T base pairs. The collective underlying mechanisms are often described through a scheme referred to as "deamination model" or "Neuberger model", named after the immunologist who has provided a great contribution to the understanding of uracil processing in the course of SHM, Michael Neuberger (Figure 4, explained in chapter 1.2.5) [70, 71].

1.2.2 Class switch recombination (CSR)

Mature naïve B cells co-express IgM and IgD as a result of alternative mRNA splicing of the primary mRNA transcript [72]. CSR is initiated upon AID activity in regions called switch (S) regions, which are located upstream of each of the C_H genes, with the exception of Cδ (Figure 3) [24]. The efficient AID targeting in these regions is driven by the presence of overlapping, highly repetitive and palindromic 5'-AGCT-3' motifs and by the induction of transcription from promoters located upstream of the switch regions (for the link between AID activity and transcription, see chapter 1.2.4), generating sterile germline transcripts, so-called because they are transcribed from unrearranged genes that do not encode for proteins [73, 74]. AID-mediated deamination of cytosines on opposite DNA strands in the S regions results in the generation of DSBs (see chapter 1.2.5) whose error-prone repair leads to the deletional DNA recombination occurring between the donor Sμ region and an acceptor Sx region via NHEJ, so that a new C_HX gene is placed directly downstream of the rearranged variable region [75]. The specificity of the Ig isotype is determined by locally secreted cytokines, which activate the transcription from promoters located upstream of the acceptor Sx regions to be recombined. IL-4, for example, stimulates the transcription of the Sγ1 and Sε regions, therefore directing AID activity to those regions and leading to CSR to IgG1 and IgE; IL-10 leads to the switch to IgG1 and IgG3 [76, 77].

1.2.3 Ig gene conversion (IgGC)

Birds and some farm animals, such as horses and rabbits, have evolved another mechanism of altering antibody specificity and affinity, namely IgGC (Figure 3). The gut-associated lymphoid tissue of birds, named the *bursa of Fabricius,* is the main tissue where IgGC has been investigated [78].

In these animals, the primary antibody diversification via V(D)J recombination yields a very limited antibody repertoire caused by the reduced availability of functional V, D, and J gene segments [79]. Diversity is introduced into the rearranged V(D)J portion by a mechanism of templated mutagenesis: AID activity at the V(D)J regions may result in the formation of single-stranded breaks (SSBs) or DSBs (see chapter 1.2.5), which are repaired by HR using pseudo V genes (ψV) located upstream of the V segments as donor template [80, 81].

In chicken B cells, the heavy and light chains contain 80 and 25 pseudogenes, respectively, which are not used for V(D)J recombination as they do not generate productive rearrangements [80]. Their 5' regions show high sequence homology with the functional V segment, thus recognized in the course of the homology search, while their 3' ends represent the main source of antibody variability via templated mutagenesis [82].

1.2.4 AID activity and regulation

AID is a cytidine deaminase that catalyzes the conversion from deoxycytidine (dC) to deoxyuridine (dU). AID was discovered in 1999 by Tasuku Honjo's group; due to sequence homology with the apolipoprotein B (apoB) editing complex 1 (APOBEC1), which deaminates the mRNA for apoB, AID was initially identified as an mRNA-editing cytidine deaminase [83]. While the role of AID as a mRNA-editing enzyme is still controversial, its activity as a DNA deaminase was supported by increasing amounts of experimental evidence, among which was the detection of uracils at the Ig loci [84, 85]. AID activity was found to be indispensable for SHM and CSR to occur, in both mice and humans, and later on also for antibody diversification by IgGC in the chicken lymphoma cell line DT40 [86-88]. Humans carrying mutations in the gene that encodes for AID (*AICDA*) develop an immunodeficiency known as hyper-IgM syndrome (HIGM2) characterized by normal or high amounts of circulating IgM with a complete absence of the other antibody isotypes (IgG, IgE, and IgA) and a drastic reduction of SHM, inducing a marked susceptibility to infections [86].

Together with its protective role in eliciting immunity, AID activity functions as a double-edged sword: Aberrant expression of AID has been associated with the production of high-affinity

autoantibodies in autoimmune disorders, and its activity on off-target genes may lead to cancer development [89, 90]. The processing of AID-induced U:G mismatches determines the generation of point mutations, SSBs, and DSBs, which are necessary intermediates for Ig diversification to occur (the molecular mechanisms are explained in detail in chapter 1.2.5). When those same events occur upon AID activity in genes other than the Ig genes, they may lead to various forms of B-cell lymphoma. DSBs generated upon AID activity in non-Ig genes may lead to the generation of chromosomal translocations such as the one observed between the *MYC* proto-oncogene on chromosome 8 and the *IgH* locus on chromosome 14 observed in Burkitt's lymphoma [91, 92]. Off-target mutagenesis is a collateral event upon AID activity, and for this reason, AID is regulated by multiple mechanisms [93].

AID is regulated at the transcriptional level and is expressed in high amounts exclusively in activated B cells: T cell-dependent activation promotes *AICDA* expression via CD40 stimulation, and through cytokines such as IL4, the tumor necrosis factor-alpha (TNF-α), and the tumor growth factor-beta (TGF-β) [94-96]. Among the T cell-independent stimuli that culminate in B cell activation, it is worth mentioning the B cell-activating factor (BAFF), a proliferation-inducing ligand (APRIL), TLR signaling stimulation, and estrogen release [97-100]. The activated pathways converge into the activation of many general and B cell-specific transcription factors, such as NF-κB (nuclear factor 'kappa-light-chain-enhancer' of activated B cells), E2A (a lineage-specific protein belonging to the E-family of transcription factors), STAT6 (signal transducer and activator of transcription 6) and PAX5 (Paired box 5) [101-103]. In the GCs, not only active induction of *AICDA* expression but also the inhibition of transcriptional and post-transcriptional repressor mechanisms contributes to maintaining high AID expression. The GC factor Bcl-6 works as a transcriptional repressor for the microRNA miR-155, which targets the human AID mRNA for degradation, and for the gene *PRDM1,* which encodes the PR domain zinc finger protein 1, also known as BLIMP-1, that represses *AICDA* transcription and activates the plasma cell differentiation program [104, 105].

AID acts in the nucleus, but 90% of the protein is found in the cytoplasm [106]. AID is stabilized in the cytoplasm by the chaperone complex formed by heat shock protein 90 kDa (HSP90) and DnaJ homolog subfamily A member 1 (DNAJA1) [107, 108]. In addition to HSP90, AID is found in a complex containing translation elongation factor 1A (eEF1A), which is responsible to retain AID in the cytoplasm [109]. The pronounced cytoplasmic retention has the function to keep AID out of the nucleus, therefore minimizing its mutagenic effects, and presumably to protect it from the high rate of proteasome-mediated nuclear degradation: In the

nucleus AID has a half-life of 2.5 hours, in comparison to 18- to 20-hour half-life in the cytoplasm [110].

AID is a relatively small protein with a molecular weight of 24 kDa that could passively diffuse through the nuclear membrane pores, therefore the association to the cytoplasmic retention complex may have the additional function to prevent this possibility [111]. AID shuttles between cytoplasm and nucleus and its movements towards or outside the nucleus are regulated by active transport: A conformational N-terminal nuclear localization signal (NLS) is recognized by karyopherins, whereas nuclear exit is mediated by the exportin CRM1 (chromosome region maintenance 1), which recognizes the nuclear export signal (NES) localized at the C-terminal end of AID [112, 113].

AID's catalytic pocket accommodates only single-stranded DNA (ssDNA), which is only rarely accessible [114]. A way for AID to find its target is the interaction with replication protein A (RPA), which stabilizes ssDNA during DNA replication, but also in the context of replication stress and stalling, DNA repair and transcription [115, 116]. The observation that the mutation frequency at the variable regions decreases as the distance from the promoter increases, led to the first link between AID activity and transcription initiation [65, 117]. AID is indeed found at transcriptionally active sites where it associates with RNA polymerase II (RNAPII) through the transcription elongation factor SPT5 [118, 119]. SPT5 stabilizes stalling RNAPII, linking AID to sites of transcription stalling where not only it may have more time to work, since AID is a catalytically slow enzyme, but also it could have easier access to ssDNA exposed as a consequence of premature transcription termination upon stalling [120, 121]. Within the *IgH* locus, transcription stalling at the switch regions may be due to the formation of DNA-RNA R-loops or G quadruplex structures facilitated by high G content, and by the repetitiveness of those sequences. The reasons that would lead to transcription stalling within the variable regions are still unclear, though [122].

AID targets not only the transcribed strand exposed in the transcription bubble but also the non-transcribed one. This seems to be possible through association with the components of the RNA exosome complex that degrades prematurely terminated transcripts near enhancers and promoters [123].

Even though many factors regulate AID occupancy, those same factors recruit AID outside of the Ig loci. AID occupancy, though, does not necessarily result in mutagenesis. Among thousands of genes AID associates with, ~300 have been found mutated in normal B cells. Known oncogenes often mutated in B-cell lymphomas such as *MYC*, *PAX5*, *BCL-6,* and *BCL-2* display intragenic super-enhancers responsible for the occurrence of convergent transcription

(simultaneous on both positive and negative strands of DNA). In these loci, anti-sense and sense transcription clash inducing transcription stalling, premature transcription termination, and RNA exosome activity, factors that make them eligible targets for AID-induced mutagenesis [124, 125].

The reasons why AID targeting is more efficient at the Ig loci than at off-target genes are still under investigation. AID phosphorylation by protein kinase A (PKA) at Ser38 increases AID enzymatic activity and allows AID to interact with RPA [126]. It appears that PKA can be recruited specifically to the Ig loci, therefore enhancing AID predilection for the Ig genes [127, 128]. A mechanism that could limit productive targeting of AID has been recently proposed: AID associates with RNAPII at many TSSs but a "licensing step" is necessary to couple AID to transcription elongation, so to allow AID to act within the gene body [129].

A further level of regulation appears to be mediated by the cell cycle. Even though AID is constitutively expressed throughout the cell cycle, the early G_1 phase seems to provide the window for AID activity, as revealed by uracil detection at the Ig loci in different phases of the cell cycle, whereas in S/G_2 AID seems to undergo a faster nuclear degradation [85, 110, 130]. The factors responsible for this type of regulation are still under investigation: There are indications that the cell cycle orchestrates the AID nuclear/cytoplasm shuttling and that a higher toxicity of AID in S/G_2 may lead to faster degradation but these observations certainly require further research [85, 130-132].

1.2.5 DNA repair during secondary Ig diversification

The presence of uracils in the DNA represents a lesion that is usually repaired faithfully by error-free mechanisms so as to prevent mutagenesis and/or chromosomal aberrations. In cells other than the B cells, the hydrolytic damage and the misincorporation of dUMPs are the main sources of uracils in the genome, which would be repaired by the base excision repair (BER) or the mismatch repair (MMR) pathways or eventually by HR (see chapter 1.3) [133, 134]. Interestingly, many AID off-target genes are mostly spared from mutagenesis but at the Ig loci the deliberate generation of uracils promotes either mutagenesis via SHM, aimed at the maturation of the antibody affinity, or leads to the generation of SSBs and/or DSBs that trigger recombination events during IgGC and CSR (Figure 4).

The simplest type of mutations during SHM occurs when uracils escape the detection and are copied by the replication machinery: Uracil is "seen" as thymine by the replicative polymerase, therefore leading to the incorporation of adenine on the opposite strand, generating transition (TS) mutations at G:C base pairs [135-137]. Alternatively, the U:G mismatch can be detected
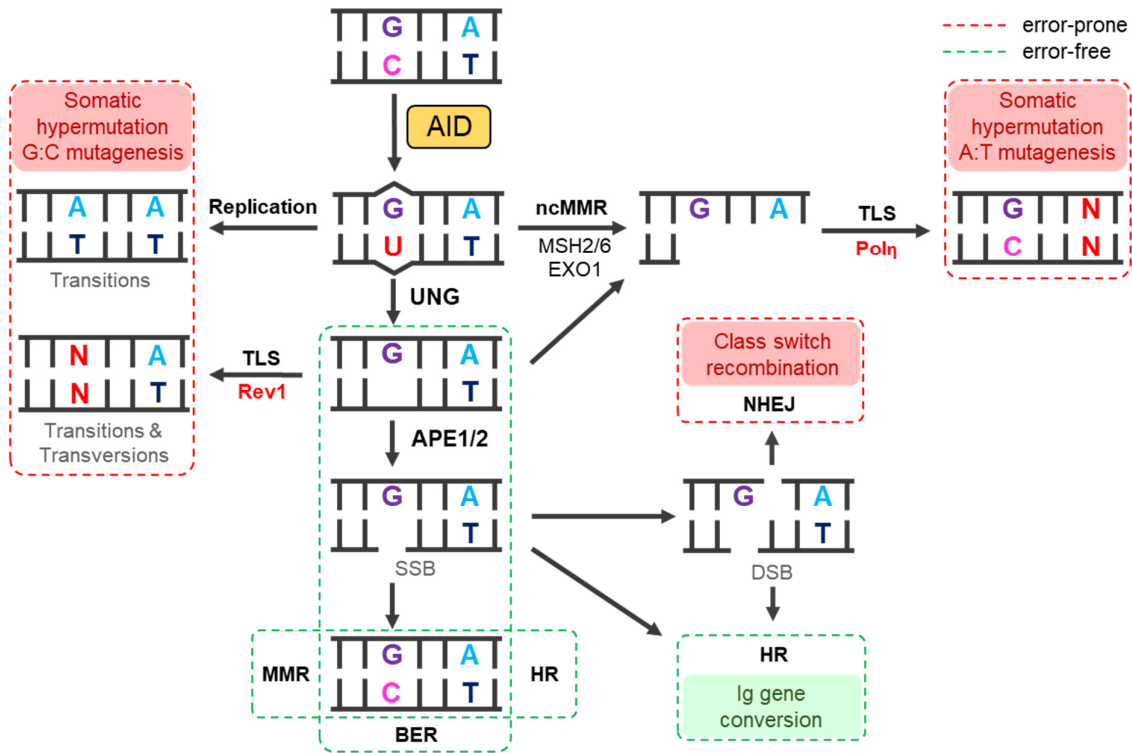
Figure 4: The deamination model: DNA repair during secondary Ig diversification.
The model explains the multiple ways of uracil processing leading to the generation of the full spectrum of mutations during SHM and the generation of SSBs and/or DSBs for IgGC and CSR to occur (see text for details, figure adapted from Di Noia and Neuberger [70]). Error-free repair of AID-induced lesions via BER, MMR and HR could restore the original sequence, but in human and mouse B cells these mechanisms are subverted towards error-prone repair that promotes the Ig diversification (N represents any base). Diversification via IgGC relies on error-free repair via HR.

and processed by the BER pathway: The uracil is excised by the nuclear uracil-DNA glycosylase (UNG), and, at the resulting abasic site, the apurinic/apyrimidinic endonuclease 1 or 2 (APE1/2) mediates an incision in the DNA that would normally provide an entry point for the DNA polymerase β, which would faithfully restore the original DNA sequence, with the DNA ligase 1 or 3 ultimately sealing the nick [138-141]. In B cells, the processing of the uracil by BER is circumvented at later steps: The replication across the non-instructive abasic site generated upon UNG activity is carried out by translesion synthesis (TLS) DNA polymerases (Figure 4). These polymerases are able to bypass replication-blocking lesions, such as abasic sites, at the expense of fidelity. The flexible nature of their active sites allows them to accommodate different DNA lesions and, in the case of a non-instructive abasic site, it may result in the incorporation of a random nucleotide on the opposite DNA strand. Therefore, the activity of TLS polymerases results in the generation of both TS and transversion (TV) mutations at C:G base pairs. Different TLS polymerases are characterized by different nucleotide affinities. Among these polymerases, Rev1 has been identified as the major

contributor to C>G and G>C TVs during SHM, since it bypasses abasic sites preferably by incorporating dCMP [142, 143].

The U:G mismatches may also be processed by the MMR pathway [144]. The recognition of the mismatch by the heterodimeric complex MutSα formed by MSH2-MSH6 is followed by the recruitment of the MutLα complex formed by MLH1-PSM2, which creates an incision in one strand of the DNA. The single-stranded nicks provide an entry point for exonuclease 1 (EXO1), which removes nucleotides with the purpose to excise the error-containing portion of DNA; the process generates a single-stranded gap that would then be re-filled correctly (see chapter 1.3.2). In contrast to the canonical MMR pathway operating in an error-free fashion, the repair taking place in the B cells is error-prone, therefore referred to as "non-canonical" (ncMMR): Mutagenesis at A:T base pairs is the result of gap filling mainly by TLS polymerase η (Polη) recruited upon the monoubiquitination of proliferating cell nuclear antigen (PCNA), an event that promotes replication across replication-blocking DNA lesions by TLS (see chapter 1.3.2) [145-148]. Polη is referred to as the sole contributor to A:T mutagenesis during SHM in the mouse, and, like Rev1, shows a typical mutational "footprint" since it has the tendency to incorporate guanine opposite of thymine in TW motifs generating A>G and T>C TSs (Figure 4) [149].

It has been recently proposed that the UNG- and ncMMR-dependent TLS synthesis may also act in concert in the process of SHM: The nick used as entry point for EXO1 during ncMMR may as well be provided by UNG/APE and UNG activity may be facilitated by ncMMR by exposing uracils on patches of ssDNA, for which UNG is around 1.7-fold more effective than on double-stranded DNA (dsDNA) [150-155].

DSBs are necessary intermediates for CSR to occur: Uracils at the switch regions are converted into DSBs, followed by recombination via the NHEJ pathway, which re-ligates the DNA ends at the 5' portion of the donor Sμ region and at the 3' portion of the acceptor Sx region thereby excising the intervening genomic DNA, which is looped out to form an extrachromosomal DNA circle [156]. The processing of the AID-induced U:G mismatches via UNG and APE1/2 leads to the generation of ssDNA nicks [141, 157-159]. Given the highly repetitive occurrence of the palindromic motifs 5'-AGCT-3' targeted by AID at the switch regions, it is very likely that SSBs would be generated on both DNA strands and, if in close proximity, processed as a DSB (Figure 4). It is also possible that DSB generation is facilitated by MMR activity: In this model MMR excises nucleotides on one strand of the DNA and, as soon as it reaches a nick on the opposite strand, its activity would terminate creating a DSB [160].

For CSR to occur, the activity of UNG and MMR is critical not only for the generation of DSBs but also for their resolution, perhaps by processing DNA ends for successive recombination by NHEJ. The domain between aa 182 and 198 at the C-terminus of AID was found to be required for CSR, but not for SHM as it mediates the recruitment of UNG and the MSH2-MSH6 complex and the accomplishment of CSR [161-164].

In contrast to the diversification by SHM and CSR, the mechanism of antibody diversification via IgGC relies on templated mutagenesis by HR, which operates in an error-free fashion (Figure 3). In human and mouse B cells, the activity of HR would prevent diversification, therefore the repair pathway is interestingly not very active at the Ig loci, even though it contributes to the repair at many AID off-target genes [134]. Its main role in the course of Ig diversification in mouse B cells is to promote survival of the hypermutating B cells as they accumulate DNA damage, and in the faithful resolution of DSBs that may have been left unrepaired by NHEJ [165-168].

GC B cells have the ability to attenuate the ATR/Chk1 (Ataxia telangiectasia mutated and Rad3-related/checkpoint kinase 1) signaling pathway (see chapter 1.3.3.2) and thereby the DNA damage response in order to better tolerate the ongoing DNA damage and to prevent excessive apoptosis while hypermutating. The master regulator of the GC program Bcl-6 has been shown to decrease the expression of ATR, Chk1, p53, and p21 by transcriptional repression [169-172]. Given the threat that such attenuation represents in case of the accumulation of catastrophic genomic aberration, the activity of Bcl-6 may need to be circumvented. Genotoxic stress can activate the response via ATM (Ataxia telangiectasia mutated), which can lead to the ubiquitin-mediated degradation of Bcl-6, therefore restoring a functional ATR/Chk1 signaling and, eventually, apoptosis of the cells that may have accumulated extensive DNA damage [173].

1.3 DNA repair and DNA damage response during the cell cycle

The DNA integrity in every cell of our body is constantly threatened by exogenous and environmental agents, as well as endogenous processes. It has been estimated that every day each cell deals with approximately 70,000 DNA lesion [174]. Exposure to exogenous substances such as alkylating agents, aromatic amines, polycyclic aromatic hydrocarbon and other reactive electrophiles leads to the generation of mutagenic and carcinogenic lesions through the modification of one or more DNA bases, the generation of intra- and interstrand crosslinks, as well as DNA-protein crosslinks that interfere with DNA metabolism [175-179].

Ultraviolet light (UV), though, represents the most prevalent environmental DNA-damaging agent, followed by the abundant forms of ionizing radiation (IR) [180, 181].

Endogenous processes may also cause DNA damage: hydrolytic reactions lead to spontaneous DNA deamination, oxidative reactions generate reactive oxygen species (ROS) that can cause up to 100 different base lesions, and/or methylation of guanines may generate O^6-methylguanine and other related residues, which are highly mutagenic [182-184].

The process of DNA replication per se represents a great source of endogenous threats: every time a human cell replicates, approximately 1 nucleotide misincorporation occurs in every 10^8 insertion events; torsional stress may induce SSBs; replication fork stalling and, eventually, collapse can result in reversed or resected forks and DSB generation [185-188].

The choice of the repair mechanism to use depends on the type of lesion and on the cell cycle phase in which the lesion has occurred [189]. To protect genome integrity, activation of repair mechanisms may not be enough, therefore cells are able to arrest the cell cycle to buy time for efficient repair, or potentially activate programmed cell death whenever the damage has not been successfully repaired. Cells coordinate the cell cycle arrest/progression via cyclin-dependent kinases (CDKs) in a network orchestrated by checkpoint signaling pathways, which is known as DNA damage response (DDR) (see chapter 1.3.3) [190-192].

1.3.1 DNA repair in the G_1 phase of the cell cycle

Accidental damage occurring in G_1 needs to be repaired before the cells start replicating their DNA because primary DNA lesions can induce mutagenesis, replication fork stalling, and/or be converted into hazardous DSBs.

Abnormal DNA bases generated upon oxidative reactions, alkylation, methylation, or deamination are mainly repaired by BER. Various DNA glycosylases detect altered bases and specifically excise them from the DNA by N-glycosidic bond hydrolysis: Different glycosylases have evolved to respond to distinct base alterations, such as UNG that specifically detects and removes misincorporated uracils in the DNA mainly during replication (see chapter 1.3.2) [193, 194]. The resulting abasic site is recognized by an AP endonuclease, mainly APE1, that hydrolyzes the phosphodiester bond 5′ to the lesion, generating a nick in the DNA [195]. Processing of lesions by BER generates SSBs as intermediates, so BER is also the main pathway involved in the resolution of accidentally generated single-stranded nicks. BER can operate by replacing single or multiple nucleotides via short- or long-patch BER, respectively [196]. The cell cycle stage contributes to the repair pathway choice in a way that short-patch BER is predominant in G_1 due to restriction of the long-patch BER genes to the S phase [197].

Via short-patch BER, a single nucleotide-gap is filled mainly by DNA polymerase β, even though also polymerase λ can perform this activity [198, 199]. The complex formed by DNA ligase I or III and cofactor X-ray cross complementation 1 (XRCC1) ultimately seals the nick [200, 201]. Poly ADP-ribose polymerase 1 (PARP1) is required for the repair of SSBs and damaged purine bases by a sub-pathway of BER [202].

An important role in the resolution of damage in G_1 is played by the nucleotide excision repair (NER) pathway, whose activity is however not restricted in this phase of the cell cycle [189]. NER is the main pathway involved in the resolution of UV-induced DNA lesions, such as thymine dimers: The recognition of the damage is followed by the removal of a short ssDNA patch containing the lesion and by subsequent gap-filling [203, 204].

DSBs represent perhaps the most harmful damage to the DNA since they cause chromosomal aberrations, such as translocations, frequently associated to carcinogenic transformation. IR, ROS, and DNA damaging agents (clastogens) may induce DSBs by different mechanisms [205]. The NHEJ and HR pathways are the main mechanisms of repair involved in the resolution of DSBs. The NHEJ pathway may act throughout the cell cycle but is the predominant mechanism of DSB repair in G_1 due to many factors: the sister chromatids required for the templated repair via HR (see chapter 1.3.2) are absent; CDK activity, which influences HR initiation, is low until S phase; HR is suppressed outside S/G_2 [206-209]. For NHEJ to occur, the heterodimeric Ku complex formed by Ku70 and Ku80 recognizes and binds the DSBs, determining the repair pathway choice by preventing DNA end resection [210]. Resection of broken DNA ends is a process indispensable for the initiation of templated repair by HR in S/G_2 (see chapter 1.3.2), while end resection in G_1 may lead to the repair of DSBs by an alternative mechanism of end-joining (alt-EJ) or by single strand annealing (SSA), which is a mechanisms of repair mediated by small or relatively longer homologies [211-213]. Upon Ku binding to the DSBs, the catalytic subunit of DNA-dependent protein kinase (DNA-PK$_{CS}$) is recruited, resulting in the activation of critical downstream factors [214]. Since NHEJ joins DNA blunt ends, single-stranded overhangs are either trimmed off via the protein ARTEMIS, which has endonuclease activity on 5' and 3' overhangs, or they are extended into blunt ends by gap-filling via Polμ and/or λ [215]. After DSB end-processing, the DNA termini are ligated by Ligase IV, which functions as a NHEJ-specific ligase, in a complex with XRCC4 and XRCC4-like factor (XLF) [216]. Since NHEJ-mediated repair occurs in the absence of a complementary template, it may be error-prone: The processing of DNA ends from the same chromosome may result in the deletion or insertion of base pairs, and the ligation between ends from different chromosomes may lead to loss of genetic information and/or translocations [217, 218].

1.3.2 DNA repair during and post replication

Nucleotide misincorporation and small insertion/deletion (indel) loops generated during DNA replication are repaired by the MMR pathway, which is closely coupled to DNA replication [219, 220]. In human cells, the most abundant mismatch-binding factor is MutSα, a heterodimeric complex formed by MSH2-MSH6. MutSα is involved in the repair of base-base mismatches and small indels (one or two extrahelical nucleotides), while the repair of larger indels is carried out by the MutSβ complex composed of MSH2-MSH3 [221]. Upon mismatch recognition, MutSα recruits the MutLα complex formed by MLH1-PSM2; as a sliding clamp, the MutSα-MutLα complex translocates along the DNA, positioning itself at the site where, presumably, the repair will be initiated [219]. Here MutLα generates a single-stranded nick that provides the entry point for EXO1, which is loaded onto the DNA and starts ssDNA degradation in a 5′→3′ direction to remove the misincorporated nucleotide [222, 223]. The ssDNA gap formed upon EXO1 activity is stabilized by RPA till subsequent gap-filling mediated by Pol δ, which is recruited to the 3' terminus of the ssDNA gap by interaction with PCNA [224-226]. DNA ligase I ultimately seals the nick and completes the repair process [227].

Chemically altered nucleotide bases can be repaired by BER also in the S phase of the cell cycle. Even though both short- and long-patch repair may act during replication, the long-patch seems to be favoured, as it uses replication proteins such as DNA polymerase δ/ε, PCNA, and LIG1 for the repair of tracts as long as at least two nucleotides [196]. Misincorporated uracils during replication are mainly removed via BER by UNG; the expression of UNG in S phase reaches its peak, therefore this phase is considered the predominant window for UNG activity [197, 228].

The presence of sister chromatids in S phase allows high-fidelity template-mediated repair by HR, which has always been considered to be primarily involved in the resolution of DSBs but is now also recognized for its activity in the resolution of other replication-blocking lesions. Single-stranded nicks and gaps may also be repaired via HR, as well as interstrand crosslinks, for the repair of which HR acts together with the Fanconi anemia pathway [229-233]. DSBs are recognized by the MRN (Mre11–Rad50–Nbs1) complex, which works together with the endonuclease CtIP (C-terminal-binding protein-interacting protein) to initiate DSB end resection, a process that generates 3'-ended ssDNA required to mediate strand invasion into the sister chromatid for the search of the homologous template [234-236]. At first, the MRN/CtIP complex generates a short 3' overhang of ssDNA, which is subsequently extended by EXO1 or DNA2 [237]. The ssDNA stretches are coated with RPA till subsequent replacement with the effector recombinase Rad51 by BRCA2 (breast cancer-associated gene 2), which is facilitated

upon checkpoint signaling activation (see chapter 1.3.3) [238]. The Rad51/ssDNA filaments perform strand invasion into the homologous sister chromatid and, once Rad51 has been dissociated from the DNA by Rad54, the replication machinery can extend the 3' end of the invading strand using the homologous template [239]. During the S phase of the cell cycle, NHEJ can compete with HR in the resolution of the breaks [240]. Many factors are involved in the repair pathway choice at DSBs: DSB end and chromatin structure; activation of RAD18 and PARP, which seem to favour repair via HR by decreasing the affinity of the Ku complex for the DSB; the opposing activity of BRCA1 and the p53 binding protein 1 (53BP1) in promoting and inhibiting end resection, respectively [241-245].

Stalling of replication forks is a frequent event upon DNA damage due to the inability of high-fidelity replicative polymerases to replicate damaged templates. Specialized DNA polymerases have evolved to accommodate a variety of lesions and to restore replication in such circumstances [246]. This mechanism of DNA damage tolerance or bypass is known as translesion synthesis (TLS) and involves error-prone TLS polymerases, such as Pol η, Pol ι, Pol κ, Pol ξ and Rev1 [247]. Stalled replication forks expose ssDNA that is promptly coated by RPA, which can activate the checkpoint cascade (see chapter 1.3.3.2) and recruit the E3 ubiquitin ligase Rad18 that in turn binds to the ssDNA [248]. Rad18 interacts with Rad6, which is a E2 ubiquitin-conjugating enzyme, and together they monoubiquitinate PCNA on Lys-164 [249, 250]. This is a crucial event that leads to the recruitment of TLS polymerases that temporarily replace the replicative polymerases via exchange mechanisms that are still not completely clear [251-253]. As a consequence, DNA replication is restored, but the process, intrinsically error-prone due to the low-fidelity of the TLS polymerases, may induce mutagenesis [254, 255].

As previously mentioned, the activity of TLS polymerases accounts for the accumulation of mutations in the variable regions of the Ig loci during SHM. Even though the monoubiquitination of PCNA is determinant for the recruitment of TLS polymerases, the activity of Rev1 at the Ig genes in the course of SHM seems not to be strictly dependent on this interaction [147].

Interestingly, PCNA may also be polyubiquitinated in the same position (Lys-164) by the complex formed by UBC13 (ubiquitin-conjugating enzyme 13), MMS2 (methyl methanesulfonate-sensitive 2), and Rad5; in this case another damage tolerance mechanism is initiated, known as template switch, which mediates an error-free DNA damage bypass by using the newly synthetized sister chromatid as template [256].

NER also recognizes a broad spectrum of lesions that distort or disrupt the DNA double-helix and seems to share components with HR during the resolution of crosslink-dependent DSBs, or the error-prone TLS for crosslink repair [257, 258].

1.3.3 Checkpoint signaling activation and functions

The occurrence of DNA damage is one of the most dangerous threats that the cells have to face. The DDR is a multifaceted response that protects genome integrity by activating DNA repair mechanisms, the checkpoint signaling pathways, and, eventually, apoptosis via post-translational modifications of crucial damage sensors, transducers, and effectors, but also by inducing a transcriptional response. The checkpoint-specific DNA damage sensors are two phosphoinositide 3-kinase (PI3K)-related kinases (PIKK), namely ATM (Ataxia telangiectasia mutated) and ATR (ATM and Rad3-related). These two proteins are the initiators of the checkpoint signaling cascades often referred to as the ATM/Chk2 (checkpoint kinase 2) and the ATR/Chk1 axes, which are activated in response to intrinsically different types of damage but their activities converge at multiple levels (Figure 5) [257, 259, 260].

1.3.3.1 The ATM/Chk2 signaling pathway

The ATM/Chk2 axis is activated in response to DSBs; specifically, ATM is recruited to DSBs that have been recognized by the MRN complex by interacting with the C terminus of NBS1 (Figure 5). The MRN and the Ku complexes compete for the recognition of DSBs; another PIKK is involved in the response to Ku-bound DSBs, namely DNA-PK, which promotes the DSB repair via NHEJ [261].

Activated ATM leads to the recruitment of CtIP and BRCA2, but also of 53BP1 through a signaling cascade initiated by the phosphorylation of the histone variant H2AX and mediated by MDC1 (mediator of DNA damage checkpoint protein 1) [262-264]. 53BP1 stimulates DSB repair via NHEJ by inhibiting the initiation of end resection, while CtIP and BRCA2, together with the MRN complex, stimulate the resection process by displacing 53BP1 from the DNA, highlighting a controversial role for ATM in the DSB repair pathway choice (Figure 5) [245].

Chk2 is the downstream transducer of the ATM-initiated response but it can also be activated by DNA-PK [265, 266]. ATM phosphorylates Chk2 on Tyr-68 leading to a conformational change that induces Chk2 dimerization and autophosphorylation [267]. Activated Chk2 plays a role in DNA repair processes, cell cycle arrest/progression and induction of apoptosis (Figure 5) [267]. In the course of DSB repair, Chk2 favours HR over NHEJ by phosphorylating BRCA1
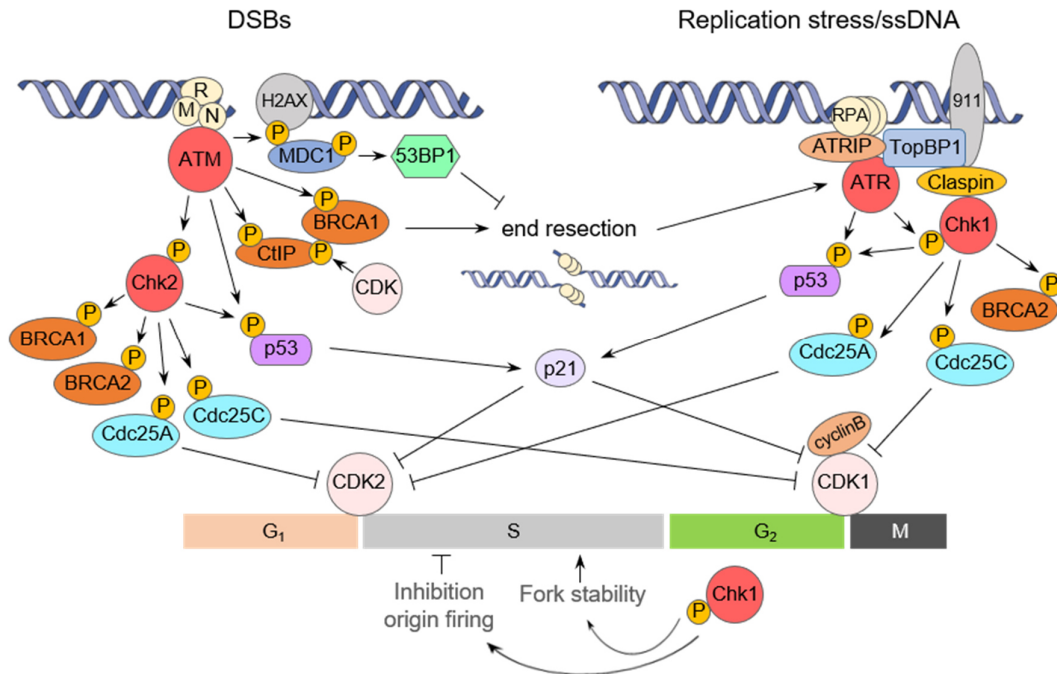
Figure 5: Signaling cascade upon checkpoint activation via ATM/Chk2 and ATR/Chk1.
On the left, activation of the ATM/Chk2 axis by DSBs is shown; on the right, activation of the ATR/Chk1 axis by replication stress/ssDNA is depicted (described in detail in the text). The activation of ATM by DSBs may result in the stimulation of end resection via BRCA1 and CtIP and in an ATM-dependent activation of the ATR/Chk1 signaling pathway via RPA coated resected ends. The ATM-mediated recruitment of 53BP1, on the other hand, inhibits end resection. The activation of the ATR/Chk1 axis stimulates repair via HR by Chk1-mediated phosphorylation of BRCA2. Both checkpoint pathways have redundant roles in the control of cell cycle arrest/progression and in the activation of apoptosis via p53. Chk1 has multiple roles during replication: upon replication stress it may either favour the S-phase progression by stabilizing the replication forks, or induce intra-S-arrest by inhibiting replication from new origins.

and BRCA2, and it participates in the repair of modified bases via BER by stimulating the transcription of XRCC1 [268-270]. Chk2 transiently arrests the cell cycle or delays its progression upon DNA damage providing time for the repair. The progression from G_1 to S phase depends on the activation by dephosphorylation of cyclin-dependent kinase 2 (CDK2) operated by the phosphatase Cdc25A (cell division control protein 25 homolog A); Chk2 induces G_1/S arrest by phosphorylating Cdc25A, therefore targeting it for proteasome-mediated degradation. In a similar way Chk2 induces intra-S and G_2/M arrest by inactivating Cdc25C that can no longer activate by dephosphorylation the complex formed by cyclinB1 and CDK1 responsible for the G_2/M transition [271, 272]. ATM and Chk2 can both directly phosphorylate p53, therefore preventing its degradation via the proteasome. p53 can, on the one hand upregulate the expression of p21, an inhibitor of cyclin-dependent kinases, therefore contributing to cell cycle arrest, and on the other hand activate the apoptotic program in cells unable to repair the damage [273, 274].

1.3.3.2 The ATR/Chk1 signaling pathway

The ATR/Chk1 axis is essential in mediating the cellular response to DNA replication stress, but it also responds to other genotoxic stressors that lead to the exposure of ssDNA. ATR is recruited to RPA-coated stretches of ssDNA via its partner protein ATRIP (ATR-interacting protein). RPA binds to 3' single-stranded DNA overhangs in the course of DSB end resection; since the resection can be promoted by ATM, ATR signaling may also be activated in a ATM-dependent fashion, providing an important example of cross-talk between the ATM- and ATR-mediated checkpoint signaling (Figure 5) [275, 276]. After being recruited to the site of damage, ATR is activated by TopBP1 (topoisomerase binding protein 1) that needs to establish many different interactions in order to stimulate ATR kinase activity: It contacts both ATR and ATRIP, but also interacts with the RAD9 subunit of the RAD9-RAD1-HUS1 (9-1-1) complex, a ring-shaped heterotrimer that assembles at RPA-ssDNA/dsDNA junctions [277, 278].

A key role of ATR in the DNA damage response is to phosphorylate and activate Chk1 through the mediator protein Claspin [279]. The ATR/Chk1 and ATM/Chk2 pathways have overlapping and redundant functions in controlling cell cycle arrest/progression and apoptosis via Cdc25A/C and p53 but their contribution seems to differ in different phases of the cell cycle (Figure 5) [280]. DSB end resection is mainly active during the S phase, as the phosphorylation of CtIP depends on the activity of CDKs. The activation of the ATR/Chk1 signaling by resected ends would then be prominent in S/G_2, therefore the G_1/S checkpoint is believed to be regulated mainly by the ATM/Chk2 axis. Both checkpoint signaling pathways would equally contribute to the establishment and maintenance of the G_2/M checkpoint, even though a recent study has shown that the G_2-checkpoint in S-phase irradiated cells is dependent on ATR [281, 282].

Chk1 plays an important role in promoting HR by phosphorylating Rad51 and BRCA2, therefore facilitating the BRCA2-mediated replacement of RPA with Rad51 [238]. In addition to the functions in regulating cell cycle arrest, apoptosis and DNA repair, Chk1 has multiple functions during DNA replication upon replication stress [283]. It can prevent the activation of new replication factories and activate dormant origins adjacent to stalled replication forks instead, so to guarantee that proper replication at the site of damage is accomplished before initiation of replication from new origins [284]. Chk1 inhibits origin firing by interfering with the assembly of the replicative helicase CMG (Cdc45-Mcm2-7-GINS), therefore preventing its activation and polymerase loading [285]. The mechanism through which Chk1 is able to redirect replication factors to dormant origins adjacent to replication stalling sites is yet unknown and under investigation. Very speculative is also the hypothesis that Chk1 may regulate the activity of the CMG helicase to prevent dissociation of the replisome and fork

collapse at sites of replication stress [286]. Increasing amounts of evidence link the activation of Chk1 upon replication stress to the facilitation of TLS. It has been observed that Polη can be recruited to the chromatin in a Chk1-dependent manner upon UV irradiation and that Chk1 can potentiate UV-induced PCNA monoubiquitination, therefore avoiding prolonged stalling of replication forks at the site of damage and ensuring fork stability [287-289].

1.4 Aim of the work

The processes of secondary Ig diversification via SHM and CSR rely on the targeted AID-mediated deamination of cytosines in the Ig genes and on the subsequent error-prone repair of the AID-induced lesions. The reasons why faithful DNA repair mechanisms are subverted at the Ig loci are still unclear and under investigation; a differential orchestration of those repair pathways during the DDR may be responsible for the observed phenomenon. Interestingly, hypermutating GC B cells attenuate the DDR by transcriptional repression of ATR, Chk1, p53, and p21 operated by the master regulator of the GC program Bcl-6 [169-172]. The attenuation of the DDR via the ATR/Chk1 axis may be necessary in B cells undergoing AID-induced damage to allow for a better tolerance to the damage and to prevent death by apoptosis, thus ensuring survival and allowing mutations to be passed on by clonal expansion. In addition to those functions, we have previously shown that the downregulation of the checkpoint signaling via Chk1 facilitates the accumulation of mutations during SHM *in vitro*, therefore suggesting a role for Chk1 signaling attenuation in regulating the relative activity of the repair pathways in hypermutating B cells [290]. Nevertheless, the scenario in which the same effect would be recapitulated *in vivo* remained uncertain. With the aim to investigate this possibility, we generated an *in vivo* mouse model that allows for a conditional downregulation of Chk1 in B cells and investigated the role of Chk1 signaling attenuation on the humoral response.

It has been contemplated that B cells could temporally restrict the mechanisms of secondary Ig diversification during the cell cycle to minimize the threat posed to the genome. The role of the cell cycle in the regulation of the error-prone DNA repair of AID-induced lesions has been explored in recent years. Collectively, these studies suggest a model in which uracil removal by UNG and IgGC would mainly occur in G_1, DSBs would be generated in G_1 as well so that CSR would be accomplished in the early S phase, mutations at A:T base pairs in the course of SHM would arise in G_1, while C/G mutagenesis may be efficiently achieved throughout the cell cycle [150, 291-295]. However, the mechanisms behind this model are still elusive; in

particular, AID activity in S/G$_2$ has not been observed, nor efficiently induced so far, therefore it is possible that the mechanisms of repair acting in S/G$_2$ may have been overlooked due to the paucity of AID-induced uracils. The question whether the observed restriction of some mechanisms of diversification to G$_1$ is rather due to S/G$_2$-specific suppression of error-prone repair still stands. Therefore, we used AID-fusion proteins that allow for a cell cycle-specific restriction of AID activity in different *in vitro* and *ex vivo* systems and compared the efficiency of SHM, CSR and IgGC upon lesions introduced by AID specifically in G$_1$ or S/G$_2$.

2 Results

2.1 Effects of Chk1 signaling attenuation on secondary Ig diversification

In order to investigate whether and how the attenuation of the signaling mediated by Chk1 in GC B cells has an impact on the activity of error-prone DNA repair mechanisms during secondary Ig diversification, we generated mice with conditional downregulation of Chk1 specifically in B cells. The complete deletion of Chk1 in B cells has been shown to be incompatible with their survival: Loss of Chk1 during B cell development prevents B cell differentiation, and its complete deletion in mature B cells that have been committed to the GC program results in B cell loss and in a dampened humoral response [296, 297]. Given the dependency of B cells on Chk1 activity, we used mice that undergo a B cell-specific deletion of only one *Chek1* allele during the B cell development and investigated the effects of the decreased expression of Chk1 on their humoral response.

2.1.1 Generation of B cell-specific *Chek1* heterozygous (Chk1^{Bhet}) mice

To obtain conditional downregulation of Chk1 in B cells, we made use of mice in which exon 2 of one *Chek1* allele can be deleted by Cre-mediated recombination of loxP sites resulting in the inactivation of Chk1 (Figure 6A-B) [298]. We crossed *Chek1*-floxed (Chk1$^{fl/+}$) mice with *Mb1*-Cre (Mb1$^{Cre/+}$) mice in which the *Cre* gene is integrated into the *Mb1* gene locus, which encodes the Ig-α signaling subunit of the B cell receptor expressed specifically in B cells [299]. We investigated the effects of Chk1 downregulation in Chk1$^{fl/+}$Mb1$^{Cre/+}$ mice, henceforth referred to as Chk1^{Bhet}, and used Chk1^{BWT} mice (Chk1$^{+/+}$Mb1$^{Cre/+}$ or Chk1$^{fl/+}$Mb1$^{+/+}$) as controls in the experiments.

We verified the proper B cell-specific deletion of one *Chek1* allele in Chk1^{Bhet} mice by PCR. A combination of three primers was used in order to discriminate among the *Chek1^{WT}*, the *Chek1^{fl}*, and the *Chek1*-deleted (*Chek1^{del}*) alleles (amplification of a 358bp, 420bp, and 720bp product, respectively) (Figure 6B-C). We isolated genomic DNA either from tail clips or sorted B cells and confirmed that the deletion of the floxed exon 2 occurred efficiently in B cells of Chk1^{Bhet} mice (Figure 6C); Cre-mediated recombination was virtually 100% effective as no amplification of the *Chek1^{fl}* allele in Chk1^{Bhet} mice was obtained. We analyzed the levels of the Chk1 protein in B cells of Chk1^{Bhet} mice and confirmed that the deletion resulted in the detection of approximately half the amount of Chk1 in comparison to the Chk1^{BWT} controls (Figure 6D-E).
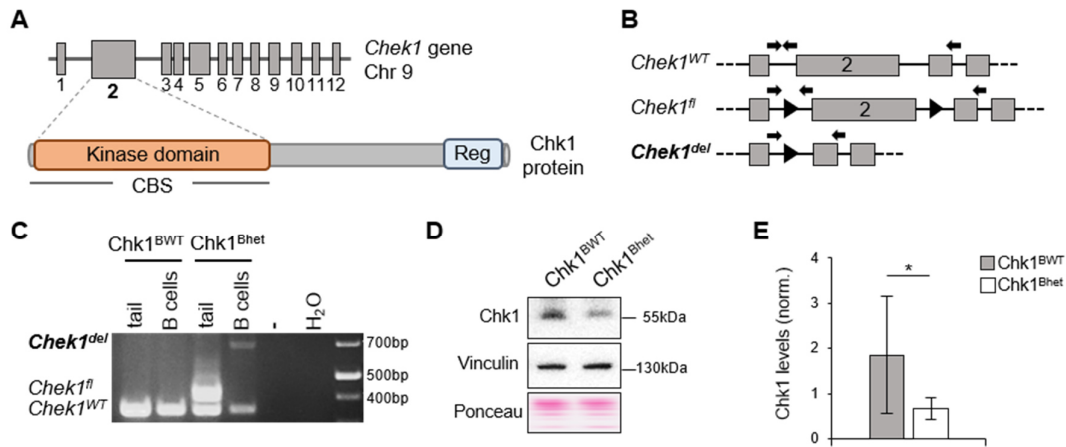
Figure 6: Efficient B cell-specific Chk1 downregulation in Chk1[Bhet] mice.
A) Scheme of the mouse *Chek1* gene and of the protein domains of the mouse Chk1 protein. The grey boxes represent the exons. The kinase domain overlaps with the claspin binding site (CBS) (Reg: regulatory domain). **B)** PCR strategy used to confirm the Cre-mediated deletion at the *Chek1* locus. Grey boxes represent the exons, loxP sites are indicated with black triangles, and the arrows represent the primer binding sites. At the *Chek1[WT]* and *Chek1[fl]* loci, only the smaller PCR product is amplified, as the PCR strategy was designed to prevent amplification of the larger product, which would exceed 2000bp. **C)** Agarose gel electrophoresis of PCR products amplified as in B) from genomic DNA extracted from tails or sorted B cells (in this picture the Chk1[BWT] has a Chk1^{+/+}Mb1[Cre/+] genotype). One representative pair of mice out of four is shown. **D)** Western Blot showing the Chk1 protein levels, the housekeeping protein vinculin, and the protein staining with Ponceau solution in B cells isolated from spleens of Chk1[BWT] and Chk1[Bhet] mice. One representative pair of mice out of six is shown. **E)** Quantification of Chk1 protein levels measured in D) as band intensity normalized to the housekeeping protein vinculin in B cells from Chk1[BWT] and Chk1[Bhet] mice. Mean values ± SD were determined for six mice per genotype (*$p \leq 0.05$; two-sided ratio paired *t* test).

The *Mb1* gene is expressed at the pro- to pre-B cell transition stage, therefore Chk1 deletion in Chk1[Bhet] mice occurs early during B cell development [300]. At this stage of development, B cells undergo V(D)J recombination of their Ig genes, a process that involves the generation of DSBs and subsequent joining of DNA ends by NHEJ. We asked whether the downregulation of Chk1 in B cells undergoing V(D)J recombination could have an impact on their survival, thus preventing B cell maturation and differentiation. We measured the relative percentage of B cell precursors in the bone marrow (pro-B, pre-B, immature, and mature B cells; Figure 7A-B) and of mature B cell populations in the spleen, namely marginal and follicular zone (MZ and FZ, respectively) B cells (Figure 7C-D). We found that the proportion of each subset was comparable to the controls, indicating proper B cell development in Chk1[Bhet] mice (Figure 7A-D). We also asked whether Chk1 downregulation could affect the overall generation of B cells instead of one specific stage of development and/or differentiation. Therefore, we measured the relative proportion of B and T cell populations in the spleen and we did not detect any alterations of the T/B cell ratio between Chk1[Bhet] and Chk1[BWT] mice (Figure 7E-F), concluding that Chk1[Bhet] mice are a suitable model to study the effects of Chk1 signaling attenuation on the humoral B cell responses.
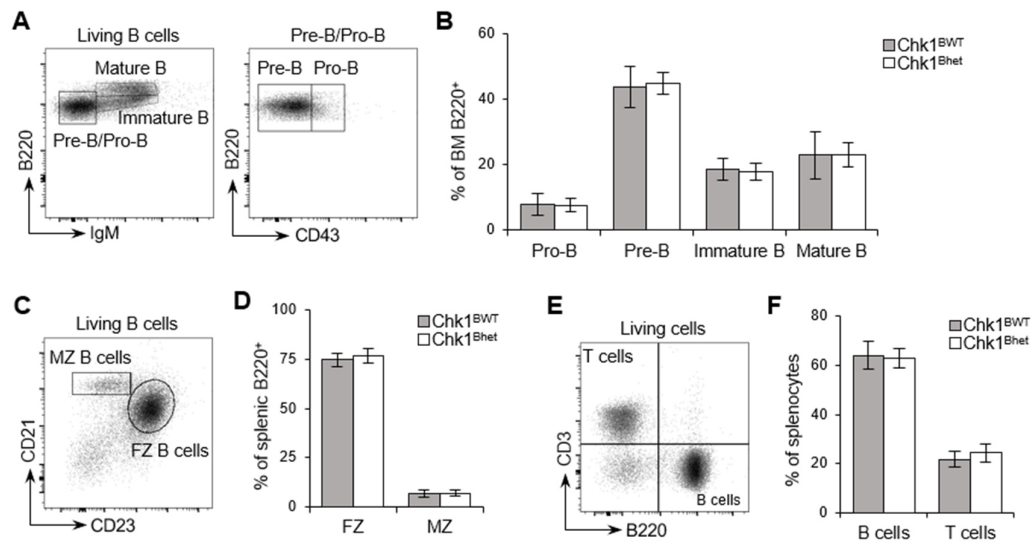
Figure 7: Normal B cell development and differentiation in Chk1^Bhet mice.
A) Gating strategy used to assess B cell subsets in the bone marrow (BM) by flow cytometry. Living B cells gated as DAPI⁻B220⁺. **B)** Percentages of the indicated B cell subsets measured as in A). Mean values ± SD were determined for more than five mice per genotype. **C)** Gating strategy used to assess MZ and FZ B cell populations in the spleen by flow cytometry. Living B cells gated as in A). **D)** Percentages of the indicated B cell populations measured as in C). Mean values ± SD were determined for more than five mice per genotype. **E)** Gating strategy used to assess B and T cell populations in the spleen by flow cytometry. Living cells gated as DAPI⁻. **F)** Percentages of the indicated cell populations measured as in E). Mean values ± SD were determined for more than fifteen mice per genotype.
In B), D), and F) a two-sided Student's *t* test was performed and no significant differences were observed.

2.1.2 Effects of Chk1 downregulation on B cell responses *in vitro*

Upon activation, B cells start proliferating massively, they upregulate AID expression and may undergo CSR and SHM. We first assessed the influence of *Chek1* heterozygosity on the ability of B cells to survive, proliferate and perform CSR by *in vitro* stimulation of *ex vivo*-isolated primary B cells from Chk1^Bhet mice in comparison to the control Chk1^BWT mice. SHM is hardly achieved by *in vitro*-cultured primary B cells, therefore it has been investigated *in vivo*.

We isolated primary B cells from spleens of 8- to 16-week-old mice and stimulate them either with α-CD40, in order to mimic a T cell-dependent activation of the B cells, or with lipopolisaccaride (LPS), for a T cell-independent B cell response via TLR4, in the presence of IL-4, which induces CSR from IgM to IgG1 (Figure 8A).

We observed that the percentage of living B cells from Chk1^Bhet and Chk1^BWT mice was comparable after 72- (Figure 8B) and 96-hour-culture (data not shown) upon both T cell-dependent and -independent stimulation. The staining via CFSE showed no differences in the proliferation ability of B cells from Chk1^Bhet mice in comparison to the controls (Figure 8C).

Furthermore, no differences were detected in the percentage of IgG1$^+$ cells among the B cells isolated from mice of both genotypes (Figure 8D-E).

It seems that the downregulation of Chk1 does not affect B cell responses *in vitro*, as B cells from Chk1^{Bhet} and Chk1^{BWT} mice were found to be equally viable, to proliferate at the same pace and to efficiently perform CSR to IgG1. The presence of one functional *Chek1* allele may masks possible effects of the Chk1 signaling attenuation on the analyzed processes.
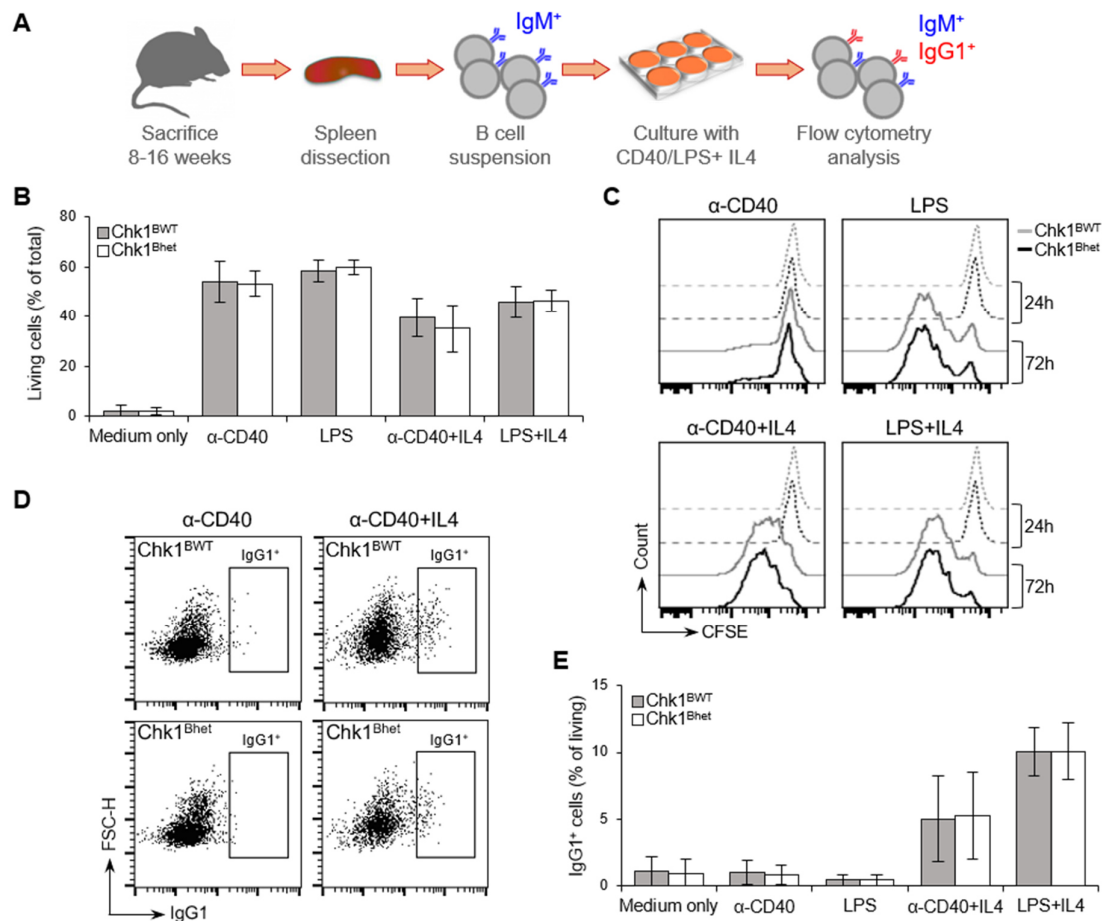
Figure 8: Normal survival, proliferation and CSR of *in vitro*-cultured splenic B cells from Chk1^{Bhet} mice.
A) The representation of the experimental setup is shown. After spleen dissection, the B cells were purified from the splenic single cell suspension by depletion of the CD43$^+$ cells via magnetic-associated cell sorting (MACS). Survival, proliferation and CSR to IgG1 were assessed by flow cytometry. **B)** Survival of splenic B cells cultured for 72 hours in medium only or in the presence of the indicated stimulants. Living cells are expressed as percentage of Fixable Viability Staining (FVS) 780-negative cells out of total events. Mean values ± SD were determined for four mice per genotype. **C)** Proliferation was assessed via CFSE staining: The graphs show living (FVS780$^-$) CFSE-stained splenic B cells after 24- and 72-hour-culture in the presence of the indicated stimulants. One representative experiment out of three is shown. **D)** CSR analysis on splenic B cells cultured for 72 hours in the presence of the indicated stimulants. CSR is measured as percentage of IgG1$^+$ cells out of all living cells (in the plots gated FVS780$^-$ cells are shown). One representative experiment out of four is shown. **E)** Percentages of IgG1$^+$ cells measured as in D). Mean values ± SD were determined for four mice per genotype.
In B) and D) a two-sided Student's *t* test was performed and no significant differences were observed.

2.1.3 *In vivo* B cell responses of Chk1^{Bhet} mice upon immunization

In the attempt to investigate the effects of Chk1 signaling attenuation on the B cell responses in the course of an immune reaction *in vivo*, we immunized Chk1^{Bhet} and Chk1^{BWT} mice with alum-precipitated nitrophenylacetyl chicken γ globulin (NP-CGG). The B cell response to the NP hapten has been widely characterized and the immunization with NP-CGG induces a strong T cell-dependent B cell activation resulting in the efficient formation and maturation of GCs in the secondary lymphoid organs within 10-14 days post-immunization, and in a strong antibody response [301, 302]. This has been analyzed as described in Figure 9A. To avoid possible effects of different Igα levels on the B cell responses, only Chk1$^{+/+}$Mb1$^{Cre/+}$ mice (and not Chk1$^{fl/+}$Mb1$^{+/+}$) were used as Chk1^{BWT} controls in the immunization experiments.

We monitored the levels of NP-binding antibodies and examined the maturation of their affinity for the NP hapten over the course of the immune reaction by ELISA (enzyme-linked immuno-sorbent assay). We coated the plates with NP$_{15}$- or NP$_3$-BSA molecules (15 or 3 NP molecules conjugated to 1 bovine serum albumin) in order to differentiate between α-NP antibodies of all affinities (high and low) and α-NP antibodies of high affinity, respectively. We collected blood samples at day 7 and day 14 post-immunization and measured the levels of the total (all affinities) and high affinity NP-binding class switched IgG1 in the serum of immunized mice (non-immunized mice were used as negative controls). We did not detect any differences in the titers of NP-binding IgG1, suggesting that Chk1^{Bhet} mice were able to produce similar amounts of α-NP antibodies in comparison to the Chk1^{BWT} controls (Figure 9B). These results also showed that Chk1 downregulation does not seem to affect the process of CSR to IgG1 *in vivo*, as previously observed *in vitro* (Figure 8D-E).

Antibody affinity maturation is commonly assessed via the affinity maturation index measured as the ratio between the titers of α-NP$_3$- and α-NP$_{15}$-binding antibodies. The ratios were found to be similar in Chk1^{Bhet} and Chk1^{BWT} mice, therefore it can be assumed that affinity maturation was effectively achieved in Chk1^{Bhet} mice (Figure 9C).

At day 14 post-immunization, the mice were sacrificed in order to sort GC and non-GC B cells for the analysis of SHM by sequencing of the Ig genes (described in chapters 2.1.3.1-3).

We determined the percentages of splenic GC B cells of immunized and nonimmunized (n.i.) mice: No differences were found between Chk1^{Bhet} and Chk1^{BWT} immunized mice and no proper GC formation was observed in the n.i. controls (Figure 9D-E). We conclude that the B cell-specific *Chek1* heterozygosity does not seem to impair the GC reaction and the antibody response upon immunization with NP-CGG, as Chk1^{Bhet} mice were found to be able to mount a response comparable to the controls.
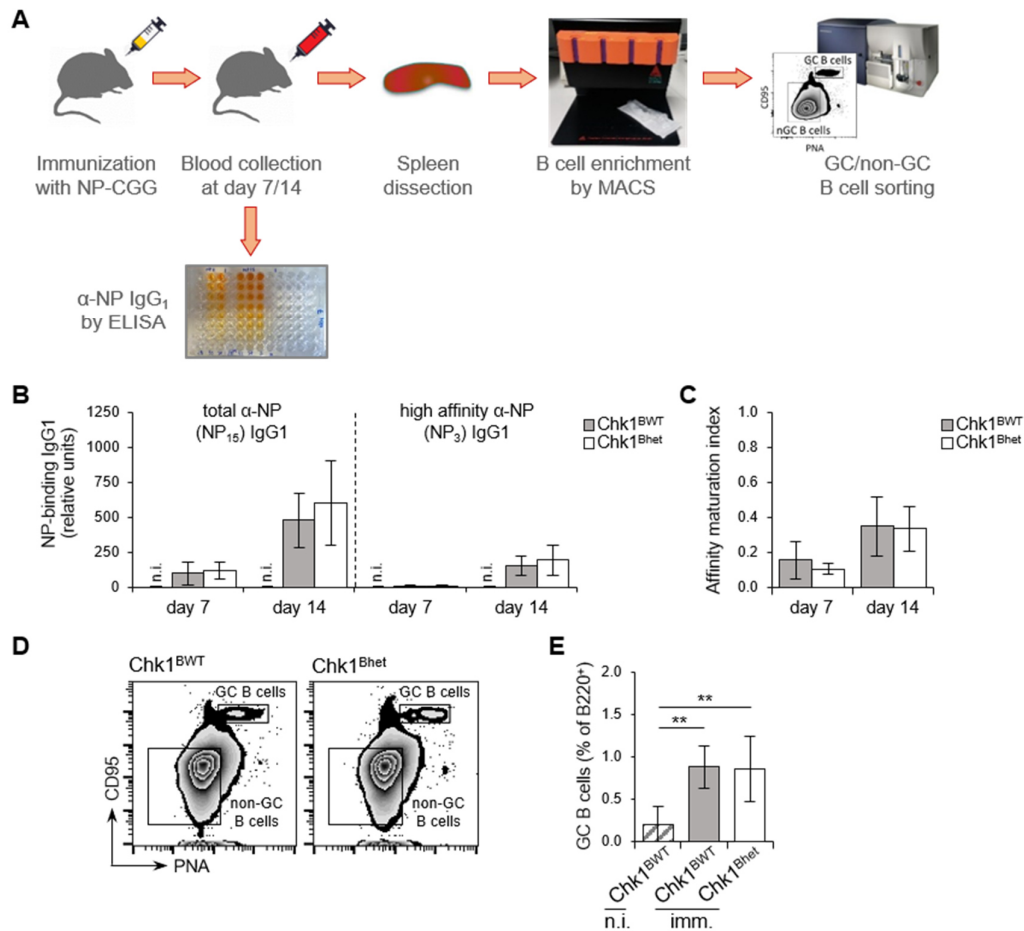
Figure 9: Immunization with NP-CGG induces adequate B cell responses in Chk1^{Bhet} mice.
A) Representation of the experimental setup. Chk1^{Bhet} and Chk1^{BWT} mice were immunized (imm.) by intraperitoneal injection of NP-CGG; nonimmunized (n.i.) mice were used as negative controls. At day 7 and 14 post-immunization, blood samples were harvested from the *vena facialis*. **B)** Titers of α-NP$_{15}$ and α-NP$_3$ IgG1 in the sera of n.i. and imm. mice measured by ELISA. Values are expressed as relative units (relative to an arbitrary unit given to the NP-binding IgG1 titer of a pooled serum control from NP-CGG imm. mice). No NP-binding IgG1 were detected in the n.i. controls. Mean values ± SD were determined for five mice per genotype (two-sided Student's t test). **C)** Affinity maturation index is calculated as ratio between NP$_3$- and NP$_{15}$-binding IgG1 titers measured as in B). Mean values ± SD were determined for five mice per genotype (two-sided Student's t test). **D)** GC formation in the spleen of Chk1^{BWT} and Chk1^{Bhet} mice at day 14 post-immunization with NP-CGG by FACS. In the plots, living B cells (gated as DAPI$^-$B220$^+$ cells) are shown. The strategy for sorting GC and non-GC B cells is depicted. The plots are representative of five analyzed pairs. **E)** Percentages of GC B cells measured as in D) in imm. mice versus n.i. controls. Mean values ± SD were determined for five n.i. mice and five imm. mice per genotype (**$p \leq 0.01$; RM one-way ANOVA and Tukey's post-hoc correction test).

2.1.3.1 Influence of Chk1 signaling attenuation on SHM at the J$_H$4 intron

With the purpose to investigate whether Chk1 signaling attenuation could affect the process of SHM and influence the relative activity of the error-prone DNA repair pathways involved, we amplified and sequenced the *IgH* locus of sorted GC B cells. The observation that hypermutation extends in the intronic region at the 3'-side of the rearranged VDJ gene segment

has facilitated the investigation of SHM. The J_H intronic regions have been frequently used as surrogate markers for SHM in the variable regions avoiding the intrinsic diversity between the VDJ rearrangements of clones responsive to the same/different antigen/antigens. Additionally, the analysis of the hypermutation at the J_H introns avoids the bias due to the selection process undergone by mutations in the exon regions.

The B cell response to the NP hapten in mice has been extensively characterized: In the study by Cumano and Rajewsky, this response was found to be dominated by the V186.2-D-J_H4 rearrangement [303]. With a PCR strategy similar to the one developed by Jolly *et al.* [304], we amplified a portion of the *IgH* locus as shown in Figure 10A from GC B cells (and non-GC B cells as control) sorted 14 days post-immunization as shown in Figure 9D. We used a primer pair where the forward primer binds ~70bp upstream of the V186.2 exon and the reverse primer binds in the J_H4 intronic region; we isolated and purified the products of approximately 1kbp, which is the expected length of products amplified from an *IgH* locus that has undergone a productive V186.2-D-J_H4 rearrangement. We cloned the pool of sequences into a plasmid for transformation and amplification in *E.coli*; assuming that only one copy of plasmid DNA is taken up by each bacterial cell during the transformation, we performed sequencing on the plasmid DNA extracted from individual *E.coli* colonies so to ensure that each sequence obtained represents one individual B cell clone.
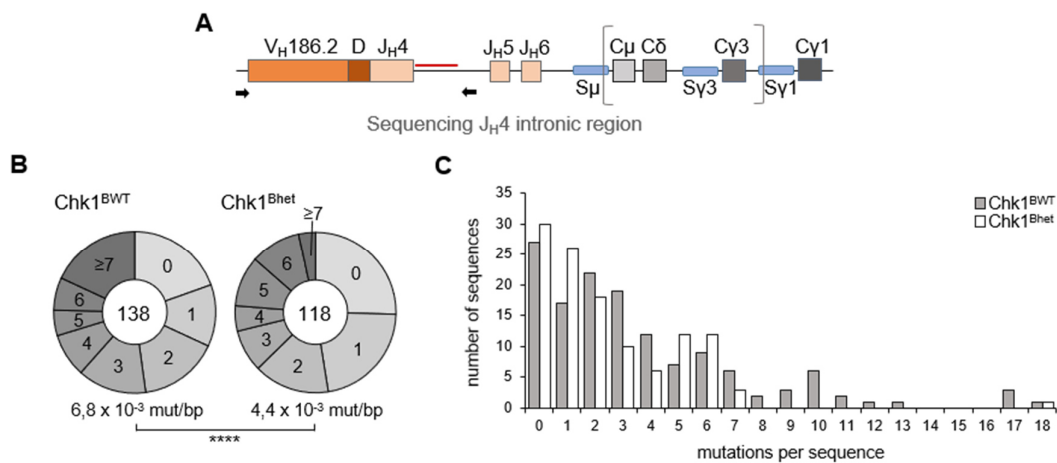
Figure 10: Chk1 downregulation reduces the overall mutation frequency at the J_H4 intronic region.
A) Representation of the PCR strategy at the rearranged *IgH* locus dominating the B cell response to NP. Black arrows represent the primer binding sites. The red line represents the sequenced J_H4 intronic region. The brackets represent the possibility of amplification from a clone that has successfully achieved CSR to IgG1. **B)** The pie charts show the relative fraction of sequences out of total sequences analyzed (in the middle of the charts) presenting the indicated number of non-unique mutations. Each pie chart shows pooled data from three mice. The mutation frequency was determined as mutated bases divided by all analyzed bases. The *p* value for differences among mutation frequencies was calculated with the two-sided χ^2 test with Yates correction for a 2 X 2 contingency table comparing for each genotype the number of mutations versus the number of unmutated bases (****$p \leq 0.0001$). **C)** Representation of the number of sequences analyzed in B) presenting the indicated number of mutations.

To ensure optimal quality of the sequencing results, we performed Sanger sequencing for all sequencing analyses performed in this study. We confirmed the high quality of the sequencing data by analyzing samples from sorted non-GC B cells in parallel, which rarely show mutations (data not shown). We sequenced a 550bp long portion of the J_H4 intron and analyzed the total number of mutations found in the sequences obtained from sorted GC B cells of Chk1[Bhet] and Chk1[BWT] mice. We excluded identical mutated sequences from the analysis to avoid the overrepresentation of mutations that may derive from the same B cell clone.

We found that the overall mutation frequency was significantly reduced in Chk1[Bhet] mice in comparison to the controls (Figure 10B). These results were unexpected as they are at odds with previous findings from our group on the chicken lymphoma B cell line DT40 and the human Burkitt lymphoma cell line RAMOS, where Chk1 downregulation was found to be beneficial for the accumulation of mutations [290]. Since B cells accumulate mutations in progressive rounds of proliferation upon positive selection, proliferation and/or survival defects may account for the observed effects *in vivo*, while lymphoma cells may better tolerate the attenuation of the signaling via Chk1. In support to this argument, we found that the decreased mutation frequency observed in Chk1[Bhet] mice was mostly due to the paucity of highly mutated clones, as we did not obtain sequences presenting more than 7 mutations, besides one exception (Figure 10C). These data show that proper Chk1 dosage *in vivo* is needed for efficient SHM to occur as the overall mutation frequency at the J_H4 intron was found reduced in Chk1[Bhet] mice.

2.1.3.2 Analysis of the mutational pattern at the J_H4 intron

To tackle the question of whether Chk1 signaling attenuation has any effect on the activity of the error-prone repair pathways during SHM, we analyzed the pattern of mutations arising in the J_H4 intron in immunized Chk1[BWT] and Chk1[Bhet] mice. For the analysis of the mutational pattern, we focused our investigation on the unique mutations, namely mutations that occur only once in each particular position in the sequences analyzed. This strategy avoids the overrepresentation of mutations that occur more than once at a particular position (non-unique mutations, also referred to as clonal mutations) as a result of positive selection and expansion of the B cell clone initially bearing the observed mutation.

The absolute numbers of all types of unique mutations found in the sequences analyzed are displayed in Figure 11A; these data are elaborated more comprehensively in Figure 11B. In Figure 11B, the mutations are displayed according to the main repair pathways that are responsible for their occurrence (according to Di Noia and Neuberger [70], Figure 4): TSs at C:G base pairs are mainly the result of replication across uracils that have escaped the detection

A

Chk1^BWT

# mutations from \ to	G	C	A	T	Σ
G		23	48	18	89
C	8		11	40	59
A	75	30		42	147
T	10	32	24		66
					361

Chk1^Bhet

# mutations from \ to	G	C	A	T	Σ
G		10	30	8	48
C	8		8	13	29
A	50	25		29	104
T	11	32	21		64
					245

B

mutation frequency (×10⁻³ mut/bp) — Overall: p=**; Chk1^BWT, Chk1^Bhet; TSs, TVs (C:G); C:G, A:T (all); ** and ***

C

Chk1^BWT

% mutations from \ to	G	C	A	T	Σ	
G		6.4	13.3	5.0	24.7	41
C	2.2		3.0	11.1	16.3	
A	20.8	8.3		11.6	40.7	59
T	2.8	8.9	6.6		18.3	
					100	

Chk1^Bhet

% mutations from \ to	G	C	A	T	Σ	
G		4.1	12.2	3.3	19.6	31.5
C	3.3		3.3	5.3	11.8	
A	20.4	10.2		11.8	42.4	68.5
T	4.5	13.1	8.6		26.1	
					100	

D

relative mutations (%): C:G TSs vs TVs | all C:G vs A:T; TSs C:G, TVs C:G, all C:G, all A:T; Chk1^BWT, Chk1^Bhet; *

Figure 11: Chk1 downregulation allows for more A/T mutagenesis during SHM, mainly at the expense of TSs at C:G base pairs.
A) The tables show the absolute numbers of unique mutations found in the sequences analyzed in Figure 10B. Σ represents the sum of mutations at G, C, A, T bases, and the overall sum in the square on the bottom right. **B)** Frequency of the indicated types of mutations (TSs: transitions; TVs: transversions) determined from data shown in A) as number of mutated bases divided by all analyzed bases. The two-sided χ^2 test with Yates correction for a 2 X 2 contingency table was used to calculate the significant differences: the p value for differences between overall mutation frequencies was calculated as in Figure 10B; the p values for the differences between individual types of mutations were calculated comparing for each genotype the number of a certain type of base substitution, i.e. TSs at C/G bases, versus the cumulative number of all other events occurring at the corresponding type of bases, i.e. TVs at C/G bases plus unmutated C/G bases (**$p \leq 0.01$, ***$p \leq 0.001$). **C)** Percentages of the indicated types of mutation out of the total mutations calculated from data shown in A). **D)** Representation of data shown in C). The two-sided Fisher exact test for 2 X 2 contingency table was used to calculate the significant differences: The p values were calculated comparing the number of a certain type of base substitution versus all other mutations, i.e. all mutations at C/G bases versus all other mutations, namely mutations at A/T bases or TSs at C/G bases versus TVs at C/G bases (*$p \leq 0.05$).

by UNG; TVs at C:G are mainly generated by TLS across non-instructive abasic sites generated upon UNG-mediated uracil removal; mutations at A:T arise upon Polη-mediated gap-filling during repair by ncMMR. We observed a significant reduction in the overall frequency of unique mutations in Chk1^Bhet mice in comparison to the controls and found that, interestingly, a significant decrease of mutagenesis at C:G but not at A:T base pairs accounts for the observed effect (Figure 11B). Furthermore, among mutations at C:G base pairs, we observed a significantly lower frequency of TSs in Chk1^Bhet mice in comparison to the controls, while TVs were not significantly reduced (Figure 11B).

To achieve a broader understanding of the effects of Chk1 downregulation on the relative activity of individual error-prone repair pathways, we calculated the occurrence of each type of mutation as a percentage of total mutations, overcoming the limitations due to the overall decreased mutation frequency (Figure 11C-D). In accordance with many previously published

mutational patterns at the J_H4 intron, we found that, in both Chk1[Bhet] and Chk1[BWT] mice, mutations at A:T base pairs represent more than 50% of the total mutations and we could also observe the typical A/T bias with mutations at A occurring more frequently than at T bases [305] (Figure 11C). Strikingly, we observed that in Chk1[Bhet] mice A/T mutagenesis was significantly higher than mutagenesis at C:G base pairs (more than 2-fold higher) in comparison to the controls (Figure 11D). Even though we found a strongly reduced frequency of TSs at C:G base pairs (Figure 11B), we observed relatively small variations in percentage terms (24,4% in Chk1[BWT] and 17,5% in Chk1[Bhet] mice, Figure 11C-D) as the overall percentage of mutations at C:G base pairs was found to be reduced 1.3-fold in comparison to the controls (Figure 11C-D). We conclude that the attenuation of the DDR via Chk1 in hypermutating B cells leads to a relatively higher activity of the ncMMR via Polη, therefore to a higher A/T mutagenesis at the expense of mutations at C:G base pairs and more specifically to a marked reduction of TSs.

Even though we found a reduced mutation frequency during SHM, we observed that Chk1[Bhet] and Chk1[BWT] mice were equally able to undergo antibody affinity maturation measured by ELISA (Figure 9B-C). It is known that the conversion from tryptophan (W) to leucine (L) in position 33 (W33L) in the variable region leads to about 10-fold increase in the NP-binding affinity [306]. This conversion is mainly due to a G>T TV mutation that determines the codon change from TGG to TTG. We observed that the frequency of TVs at C:G was not greatly affected by Chk1 downregulation, possibly explaining how the reduction of the overall mutation frequency does not result in a reduced affinity maturation for the NP hapten. We confirmed this hypothesis by measuring the proportion of productive V186.2 sequences (where no premature stop codons were detected) presenting the W33L conversion and we found it to be comparable between Chk1[BWT] and Chk1[Bhet] mice (55,6% and 48,5%, respectively).

2.1.3.3 Effects of Chk1 downregulation on mutagenesis at the pre-Sμ region

The activity of AID at the switch (S) regions aims at the generation of DSBs for the achievement of CSR. However, not all the lesions induced by AID in these regions share this fate, since some rather lead to the accumulation of mutations as during SHM [307]. Mutagenesis at the S regions is studied on the portion of DNA flanking the 5' of the Sμ region (pre-Sμ), as the occurrence of PCR artifacts due to high G content in the S regions would complicate the analysis. The relative activity of the error-prone repair pathways to the mutagenesis at the pre-Sμ was found to be intrinsically different than at the J_H4 intronic region, as the typical bias towards A/T over C/G mutagenesis was found to be reverted, indicating a minor contribution of ncMMR/Polη in the generation of point mutations upon AID activity at the S regions [122, 146, 165]. We asked

whether Chk1 downregulation plays a role comparable to that played at the J_H4 intron on the regulation of the repair pathway choice in the course of mutagenesis at the pre-Sµ region.

We amplified the pre-Sµ region from genomic DNA of GC (and non-GC) B cells sorted as previously described for the analysis of SHM at the J_H4 intron. The amplification was performed with the PCR strategy illustrated in Figure 12A: The primer pair used allows amplification from all sorted GC B cells, since it does not discriminate between different VDJ rearrangements. As we did not observe proper GC formation in non-immunized control mice (Figure 9E), we could ensure that virtually all GC B cells sorted as in Figure 9D responded to the immunization with NP-CGG.

We found that the overall frequency of mutations in Chk1^{Bhet} mice in comparison to the controls was reduced to the same extent (~1.5-fold) as for the J_H4 intronic region (Figure 12B), but that Chk1 downregulation did not affect the repair pathway choice in the course of mutagenesis at the pre-Sµ region (Figure 12C-D), as no differences were observed in the mutational pattern.
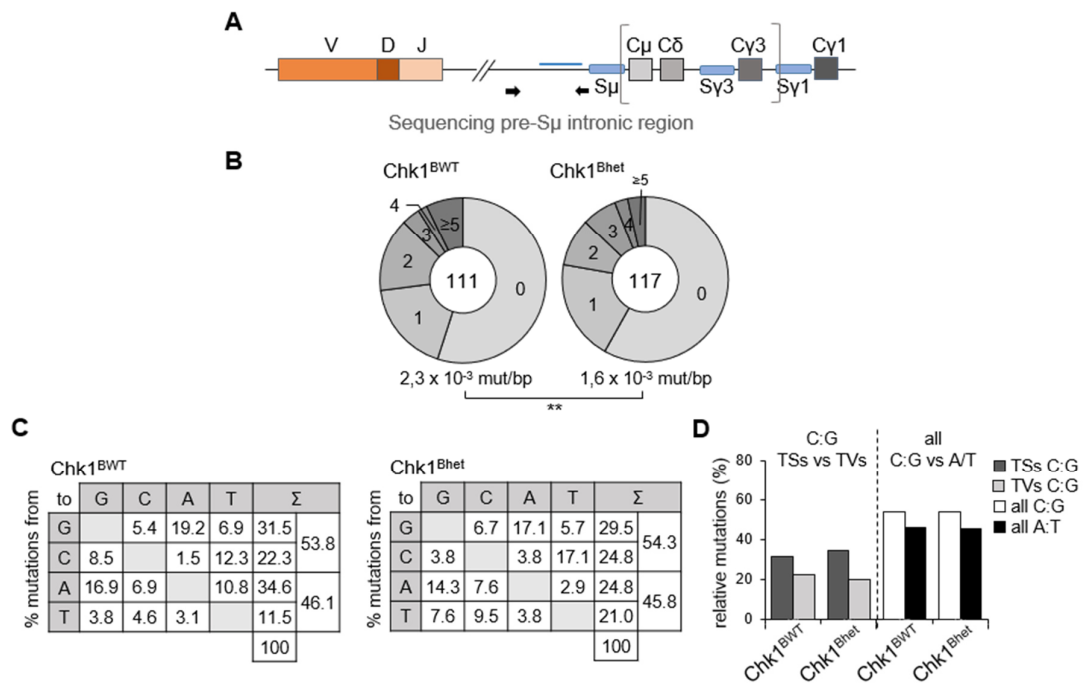
Figure 12: Chk1^{Bhet} mice show reduced mutagenesis and no alteration of the mutational pattern at the pre-Sµ region.
A) Representation of the PCR strategy used. Black arrows represent the primer binding sites; the amplification product is approximately 900bp long. The blue line represents the analyzed pre-Sµ region (587bp). The brackets represent the possibility of amplification from an IgG1-expressing B cell clone. **B)** The pie charts show the relative fraction of sequences out of total sequences analyzed (number in the middle of the charts) presenting the indicated number of non-unique mutations. Each pie chart shows pooled data from three mice. The mutation frequency was determined as mutated bases divided by all analyzed bases (**$p \leq 0.01$; two-sided χ^2 test). **C)** Percentages of the indicated types of unique mutation out of the total unique mutations found in the sequences analyzed in B). **D)** Representation of data shown in C). TSs: transitions; TVs: transversions (two-sided Fisher exact test).

2.1.4 Functions of Chk1 in chronic GCs in the Peyer's patches

In Chk1[Bhet] mice we found that the mutation frequency at both the J_H4 intron and the pre-Sμ region in splenic GC B cells was significantly reduced ~1.5-fold in comparison to the Chk1[BWT] mice and that the paucity of highly mutated sequences most likely accounts for the observed effects (Figure 10B-C and Figure 12B). We speculate that proliferation and/or survival defects may arise in the GCs of Chk1[Bhet] mice while the B cells recirculate and accumulate DNA damage at every hypermutation round. Splenic GCs generated upon immunization are referred to as acute, since they are transient structures that disappear within few weeks from the first immunization [57]. In acute GCs analyzed two weeks post-immunization with NP-CGG, we
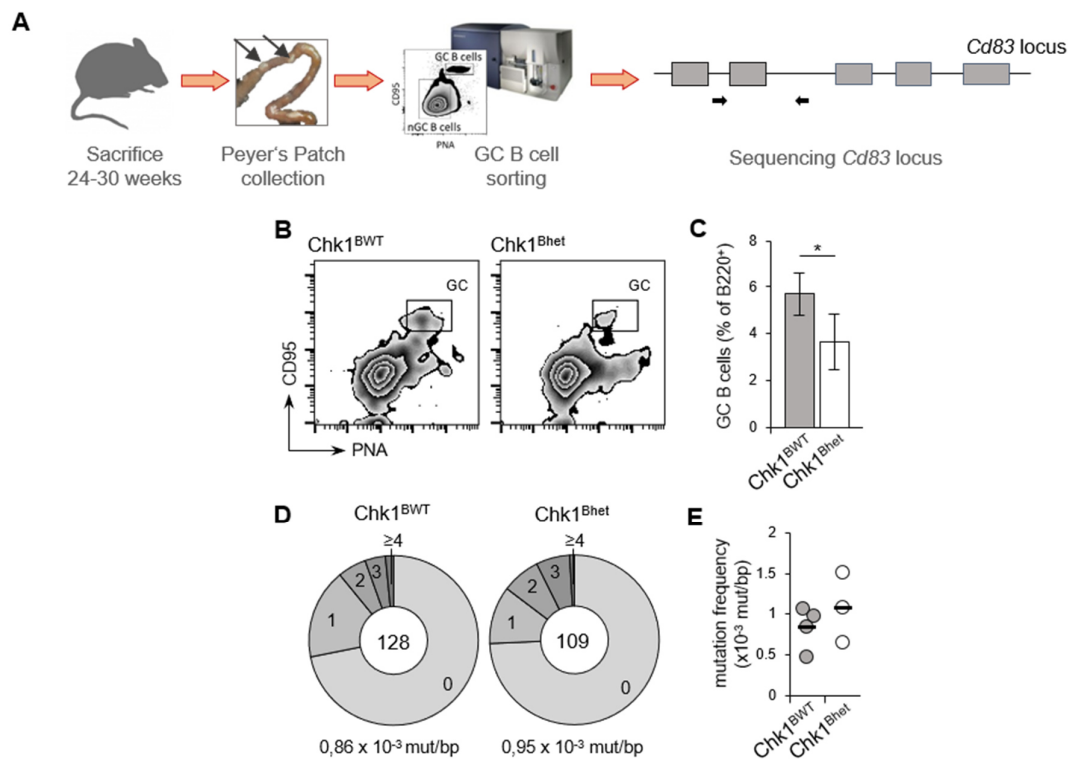
Figure 13: Chk1 downregulation impairs the survival of chronic GCs and allows for sustained off-target mutagenesis.
A) Representation of the experimental setup. 24- to 30-week-old mice were sacrificed for Peyer's patch (PP) collection. The whole length of the intestinal tract was scrutinized. GC B cells were sorted for sequencing of the *Cd83* locus portion amplified with the primer pair indicated by the black arrows. A 570bp long portion has been analyzed. **B)** GC formation in the PPs of Chk1[BWT] and Chk1[Bhet] mice analyzed by FACS. In the plots, living B cells (gated as DAPI⁻B220⁺ cells) are shown. The plots are representative of one out of five analyzed pairs. **C)** Percentages of GC B cells measured as in B). Mean values ± SD were determined for five mice per genotype (*$p \leq 0.5$; two-sided Student's t test). **D)** The pie charts show the relative fraction of sequences out of total sequences analyzed (number in the middle of the charts) presenting the indicated number of non-unique mutations. The pie charts show pooled data from four Chk1[BWT] and three Chk1[Bhet] mice. The mutation frequency was determined as mutated bases divided by all analyzed bases (two-sided χ2 test). **E)** Frequency of non-unique mutations calculated for each individual mouse. Black bars represent average values (two-sided Student's t test).

did not observe survival defects in Chk1[Bhet] mice and we explain the reduced mutation frequency as a consequence of possible alteration in the cell cycle progression. Acute GCs may not be suitable to investigate the long-term impact of *Chek1* heterozygosity on the B cell survival given the transitional nature of their persistence. Therefore, we analyzed the effects of Chk1 downregulation on chronic GCs in the Peyer's patches (PP). PPs consist of lymphoid follicles within the gut-associated lymphoid tissues; here the B cells are continuously exposed to mucosa-derived antigens (from food and microorganisms of the gut flora) and therefore long-living (chronic) GCs can be found within these structures [308]. GC B cells isolated from PPs also represent the main source for the investigation of non-Ig mutagenesis at AID off-targets. The Ig genes are AID's main targets but ~300 genes have been found mutated in B cells upon AID activity. The frequency of mutation, though, is much lower than at the Ig genes, therefore the analysis of non-Ig mutagenesis is performed on PP GC B cells where the mutation frequency at non-Ig genes is higher than in B cells from acute GCs, given their protracted state of activation [309]. We investigated the effects of Chk1 downregulation on the B cell survival and on the non-Ig mutagenesis in chronic GCs from PPs as illustrated in Figure 13A.

We observed a significant reduction in the percentage of GC B cells in Chk1[Bhet] mice in comparison to the Chk1[BWT] controls (Figure 13B-C) and these results support our hypothesis on the role of Chk1 in promoting the survival of B cells as they proliferate and accumulate extensive DNA damage. The presence of one functional *Chek1* allele may delay the manifestation of survival defects to later stages of the GC reaction, so that they are evident in long-lasting but not in short-lived GCs.

To study the influence of Chk1 downregulation on the non-Ig mutagenesis, we sequenced a portion of the AID off-target gene *Cd83* amplified from PP GC B cells sorted as in Figure 13B. As shown in Figure 13D-E, the mutation frequency was not found to be affected, but rather amounted to a similar degree in Chk1[Bhet] and Chk1[BWT] mice irrespective of Chk1 dosage.

Altogether, our data show that Chk1 signaling attenuation influences the repair pathway choice during the process of SHM allowing for more A/T mutagenesis at the variable region of the Ig locus, but limits the overall accumulation of mutations, likely due to proliferation defects in acute GCs. Chk1 downregulation impairs the longevity of PP GC B cells as the DNA damage accumulates and allows for sustained mutagenesis at the AID off-target gene Cd83.

2.2 Regulation of secondary Ig diversification by the cell cycle

In farm animals like chickens and rabbits the secondary Ig diversification via Ig gene conversion (IgGC) relies on the activity of homologous recombination (HR). Conversely, in mice and humans the repair of AID-induced lesions at the Ig genes is mainly carried out by error-prone DNA mechanisms, whose activity exceeds or, presumably, precedes that of faithful mechanisms of repair, such as HR.

It has been shown that in mouse B cells AID acts almost exclusively in the G_1 phase of the cell cycle and that in chicken cells AID localizes in the nucleus predominantly in G_1 [85, 131]. The cell cycle-mediated restriction of the AID activity to G_1 could protect the replicating genome in S/G_2 from the occurrence of forms of genomic instability, such as translocations, in particular upon attenuation of the DDR via the ATR/Chk1 signaling pathway. This theory, though, is entirely speculative and the mechanisms behind such regulation are still elusive. An efficient activity of AID in S/G_2 has not been observed and there are no proofs it has been effectively induced, therefore it has not been possible so far to determine what would be the fate of cells accumulating mutations in S/G_2. Furthermore, we believe that the limitation presented by the paucity of AID-induced uracils in S/G_2 has prevented the investigation of the S/G_2-mediated regulation of error-prone DNA repair mechanisms acting in the course of secondary Ig diversification.

To address these issues, we used a strategy that allows to restrict the activity of AID specifically to the G_1 or to the S/G_2 phase of the cell cycle by fusing the sequence coding for the human AID protein with the probes developed by A. Sakaue-Sawano *et al*. [310]. These probes have been developed with the purpose to facilitate the investigation of cell cycle-related processes by visualizing the different phases of the cell cycle with different colors. Two fluorescent proteins, namely mKO2 (fast folding variant of the monomeric version of Kusabira Orange) and mAG (the monomeric version of Azami Green) emitting in orange and green, respectively, were fused with protein tags, also referred to as "degrons", to mediate the degradation of the whole fusion protein in specific cell cycle phases. The DNA replication factor Cdt1 is a licensing factor required for the assembly of the pre-replication complex (pre-RC); the expression of Cdt1 is regulated during the cell cycle by ubiquitin-mediated proteolysis via the complex SCF^{Skp2} that marks Cdt1 for degradation during the S and the G_2 phases to prevent re-replication (Figure 14A). Inversely, the protein Geminin (Gem) inhibits DNA replication by preventing the incorporation of the MCM (minichromosome maintenance) complex into the pre-RC complex and it is marked for degradation by the APC^{Cdh1} complex during the late mitotic phase of the cell cycle or in the very early G_1 to prevent aberrant replication (Figure 14A). The fusion of the fluorescent proteins mKO2 and mAG with the tag portions of the human Cdt1 (hCdt1) and the human Gem (hGem)
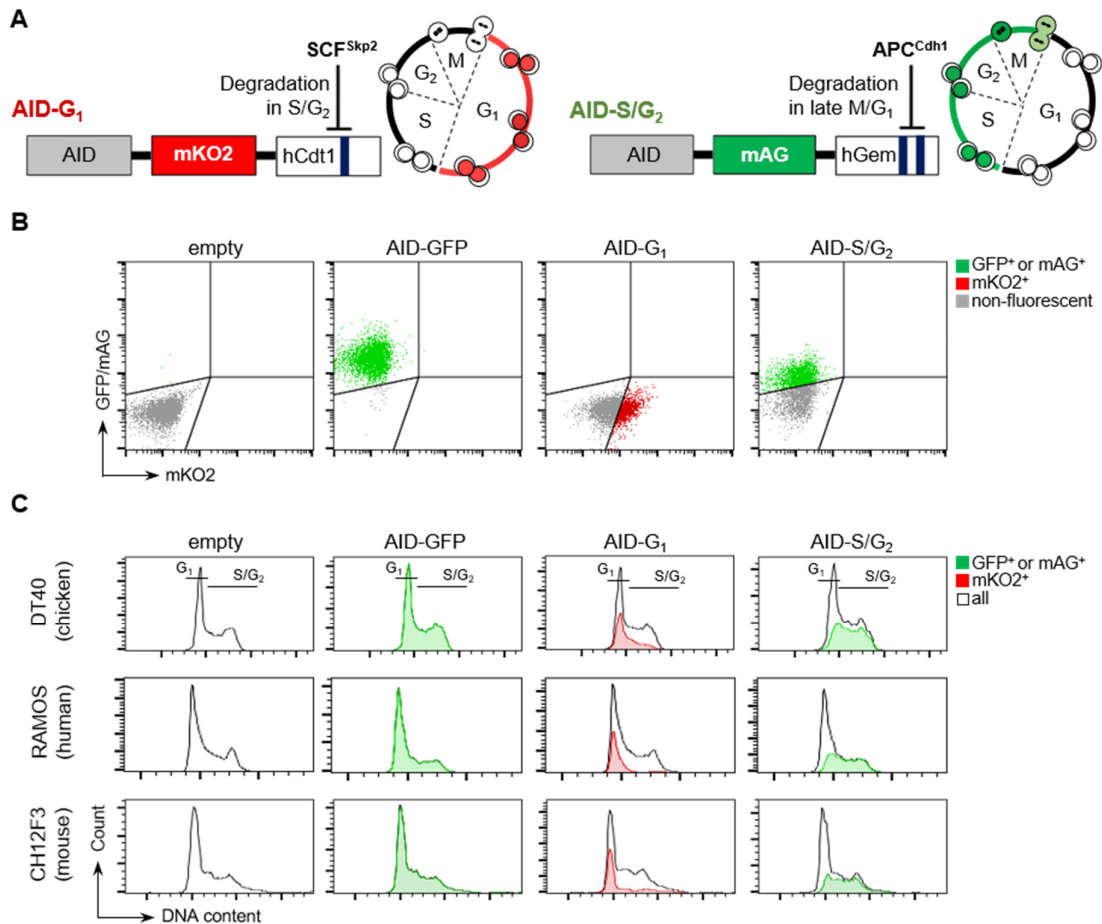
Figure 14: Efficient restriction of AID to G$_1$ or S/G$_2$ in different cell culture systems.
A) Representation of the AID-Fucci fusion proteins and their expression during the cell cycle. Cells expressing the AID-G$_1$ fusion protein emit red fluorescence via mKO2 in G$_1$ and are non-fluorescent in the S/G$_2$/M phases of the cell cycle. Inversely, cells expressing the AID-S/G$_2$ fusion protein, emit green fluorescence via mAG in S/G$_2$/M and are non-fluorescent in G$_1$. Blue portions represent the nuclear localization signals (NLS) of the Fucci tags. **B)** Gating strategy used to identify non-fluorescent, GFP$^+$, mKO2$^+$ or mAG$^+$ cells among single cell clonal populations either transfected with the empty vector or expressing AID-GFP, AID-G$_1$ or AID-S/G$_2$, respectively. In the representative plots, DT40 transfected cells are shown; living cells (FVS780$^-$ cells) are displayed. Each plot is representative of more than six clonal populations. **C)** The graphs show the cell cycle profiles of the entire clonal population (all living cells; grey line), in combination with the cell cycle profile of GFP$^+$, mKO2$^+$ or mAG$^+$ cells gated as in B). Each plot is representative of more than six clonal populations.

proteins, respectively, allows to visualize G$_1$-phase cells in orange (displayed in red in the figures) and S/G$_2$-phase cells in green (Figure 14A). This system has been named "Fucci" from "fluorescent, ubiquitination-based cell cycle indicator".

We exploited the Fucci system to restrict the activity of AID specifically to G$_1$ or S/G$_2$ in different lymphoma B cell lines and in primary B cells in order to investigate the cell cycle-mediated regulation of all processes of secondary Ig diversification.

2.2.1 Restriction of AID activity to the G_1 or S/G_2 phase of the cell cycle

The *in vitro* investigation of the cell cycle-mediated regulation of all mechanisms of Ig diversification has required the handling of different cell culture systems. The diversification via IgGC is traditionally studied in the DT40 cell line, which is a chicken bursal lymphoma cell line induced by the avian leukosis virus (ALV) [311]. The investigation of SHM was performed on the naturally hypermutating RAMOS cell line, which is a human p53-negative Burkitt lymphoma cell line characterized by the typical IgH/c-Myc translocation [312]. For the *in vitro* analysis of CSR, we used mouse primary B cells cultured in the presence of α-CD40 and IL-4 to induce CSR from IgM to IgG1, as previously shown (Figure 8A).

We generated AID-Fucci fusion proteins as shown in Figure 14A: The sequence coding for the human AID was either fused with the Fucci probe mKO2-hCdt1 to restrict the activity of AID specifically to the G_1 phase of the cell cycle (referred to as AID-G_1) or with the probe mAG-hGem for a S/G_2-specific restriction of AID activity (AID-S/G_2). In all the experiments, the positive control is represented by the HA-tagged version of AID fused with GFP (henceforth referred to simply as AID-GFP) for a constitutive expression of AID throughout the cell cycle, while cells transfected with the empty vector represent the negative controls.

We expressed the AID-Fucci proteins in the DT40, RAMOS and CH12F3 (mouse B lymphocyte) cell lines to verify the proper functionality of the constructs across the avian, human and murine cell culture systems, respectively, by flow cytometry. We performed stable transfections of the different cell lines and isolated individual clonal populations expressing the empty vector, AID-GFP, AID-G_1, or AID-S/G_2. We stained the cell populations for their DNA content in order to analyze their cell cycle profile: We confirmed that the red fluorescence emitted by AID-G_1 was detected predominantly in G_1-cells, the green fluorescence of AID-S/G_2 was mainly detected in S/G_2-cells, while the green fluorescence emitted by AID-GFP was detected throughout the cell cycle, in all the cell culture systems analyzed (Figure 14B-C). The plots in Figure 14C show that among cells expressing AID-G_1, a considerable fraction of G_1-cells appears non-fluorescent. The reason for this discrepancy is that among AID-G_1-expressing cells, a clear distinction between mKO2$^+$ and mKO2$^-$ populations is not achievable due to a rather dull fluorescence of mKO2; in Figure 14B, mKO2^{high} cells have been gated to verify G_1-specific expression of AID-G_1. No consistent alterations in the cell cycle profile of the AID-Fucci-expressing cells was observed in comparison to the empty vector- or AID-GFP-expressing cells.

2.2.2 Subcellular localization of the AID-Fucci proteins

One important mechanism that allows limiting the harmful effects of AID activity on the genome is the regulation of its subcellular localization: AID localizes predominantly in the cytoplasm and its nuclear accumulation is regulated by the presence of a nuclear localization signal (NLS) and a nuclear export signal (NES) at the N-terminus and the C-terminus, respectively [112, 113]. The potential role of the cell cycle in regulating AID subcellular localization has been investigated and AID has been found to accumulate in the nucleus in G_1 in different experimental setups [85, 130, 131]. A recent study, though, has revealed by live-cell imaging that AID entry in the nucleus occurs in brief pulses and in a cell cycle-unrelated fashion [132]. This observation has been challenged and defined as "provocative" in a recent review [313] with the argument that the study has been carried out on non-B cells (i.e. human fibrosarcoma and fibroblast lines) and, therefore, the pulses of the overexpressed AID-GFP in the nucleus could not be correlated with mechanisms of Ig diversification.
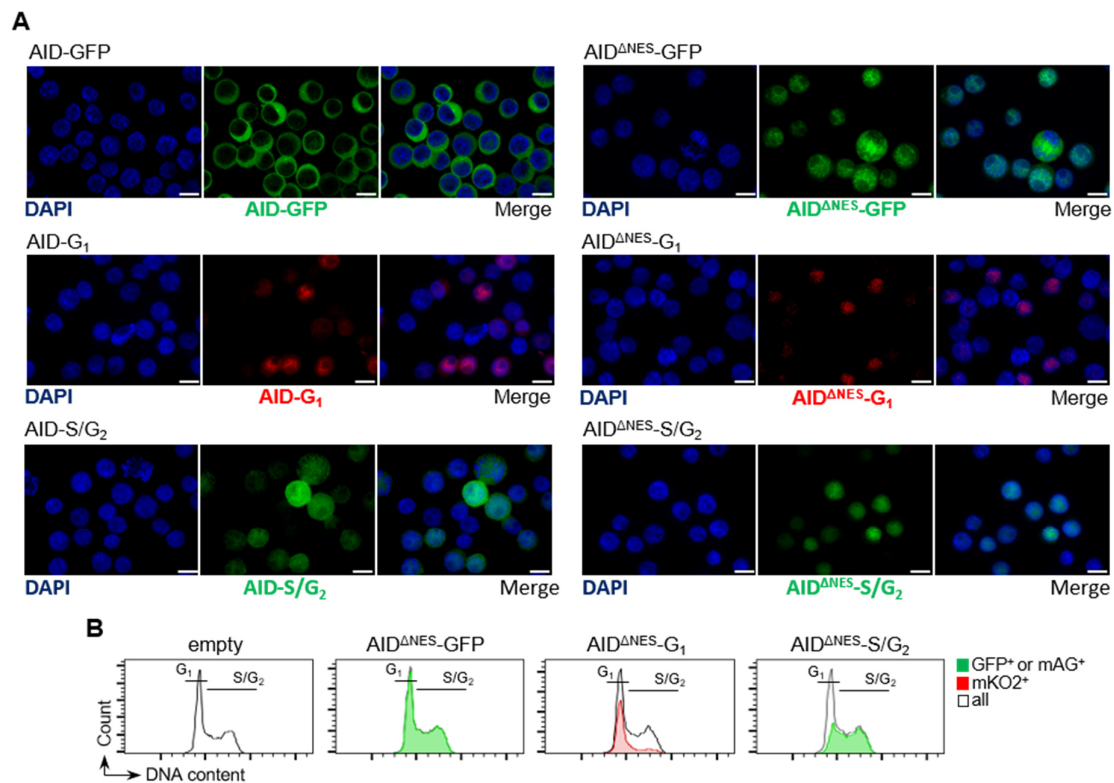
Figure 15: Subcellular localization of AID/AID$^{\Delta NES}$-Fucci proteins and efficient restriction of AID$^{\Delta NES}$-Fucci during the cell cycle.
A) Subcellular localization of AID/AID$^{\Delta NES}$-GFP, AID/AID$^{\Delta NES}$-G$_1$ and AID/AID$^{\Delta NES}$-S/G$_2$ expressed in DT40 cells. Scale bar for all images is 10 µm. Each panel is representative of three clonal populations.
B) The graphs show the cell cycle profiles of the entire clonal population (all living cells; grey line) of DT40 cells expressing the indicated proteins or the empty vector, in combination with the cell cycle profile of GFP$^+$, mKO2$^+$ or mAG$^+$ cells gated as in Figure 14B. Each plot is representative of more than six clonal populations.

We analyzed the subcellular localization of AID-G_1 and -S/G_2 in the attempt to shed light on this controversial issue. In accordance with previous observations in B cells, we found that AID-G_1 shows a distinct nuclear accumulation, while the AID-S/G_2 counterpart seems to allocate uniformly outside and inside the nucleus and this may indicate a relatively more active nuclear export and/or a reduced import in the S/G_2 phase of the cell cycle (Figure 15A, left panels). However, the presence of NLSs in the Fucci probes [310] (Figure 14A, blue boxes) seems to affect the localization of the AID-Fucci proteins, as they both (AID-G_1 and -S/G_2) show a much more pronounced nuclear accumulation in comparison to the AID-GFP control (Figure 15A, left panels).

To rule out possible influences of the cell cycle on the subcellular localization of AID in further experiments where a comparable activity of AID in G_1 and S/G_2 is desirable, we fused the nuclear version of AID (AID$^{\Delta NES}$ lacks the last 14 amino acids at the C-terminus that specify for the NES) with the Fucci probes generating the AID$^{\Delta NES}$-G_1 and AID$^{\Delta NES}$-S/G_2 fusion proteins. As expected, both AID$^{\Delta NES}$-Fucci proteins showed exclusive nuclear accumulation (Figure 15A, right panels) and an effective cell cycle restriction (Figure 15B).

2.2.3 Activity of AID during the cell cycle

After verifying their proper functionality (cell cycle restriction), we measured the activity of the AID-Fucci proteins at the Ig loci. The raw activity of AID is traditionally measured in systems lacking UNG and MSH2/MSH6 because the absence of these factors inhibits all downstream processing of U:G mismatches generated upon AID-mediated deamination, leading to the accumulation of TS mutations (C>T and G>A) at the targeted base pairs as a result of replication across the uracils (Figure 4) [135, 137]. We measured the activity of the AID-Fucci proteins in UNG-deficient DT40 cells: In these cells, the lack of UNG results in the impediment to accomplishing IgGC and in the almost exclusive accumulation of TSs at C:G base pairs, as the A/T mutator is not active in DT40 cells [314]. TSs at C:G base pairs may introduce premature stop codons in the Ig loci or may lead to aberrant conformational changes, thereby the activity of AID can be rapidly assessed via flow cytometry by measuring the proportion of cells that have lost the expression of surface IgM (sIgM) upon AID-mediated deamination (Figure 16A-B). We stably transfected sIgM$^+$ AID$^{-/-}$UNG$^{-/-}$ DT40 cells and cultured individual clonal populations expressing the AID/AID$^{\Delta NES}$-Fucci proteins or the relative controls in order to measure the percentage of sIgM$^-$ cells within each clonal population. As shown in Figure 16C, we found no significant differences in the appearance of sIgM$^-$ cells between AID-G_1- and -S/G_2-expressing cells, nor for their AID$^{\Delta NES}$ counterparts.

Strikingly, these findings show that AID can act throughout the cell cycle and that, even though AID was shown to be active exclusively in G_1, there are no other barriers to its activity at the Ig locus in S/G_2 other than, eventually, its accessibility to the nucleus.

We found that AID-G_1 and -S/G_2 were significantly more active than the AID-GFP controls; this was not due to higher levels of the AID-Fucci proteins, which were found reduced, as expected, due to cell cycle-specific degradation (Figure 16D), but rather reflects a more pronounced nuclear accumulation (Figure 15A, left panels). For the same reason, the lack of the NES results in a higher activity of each of the three AID$^{\Delta NES}$ constructs in comparison to their AID counterparts (p < 0,0001, two-sided Mann-Whitney's test).

However, a faster sIgM-loss was observed for the AID$^{\Delta NES}$-Fucci proteins in comparison to the AID$^{\Delta NES}$-GFP control, likely due to the presence of additional NLSs on the Fucci degrons
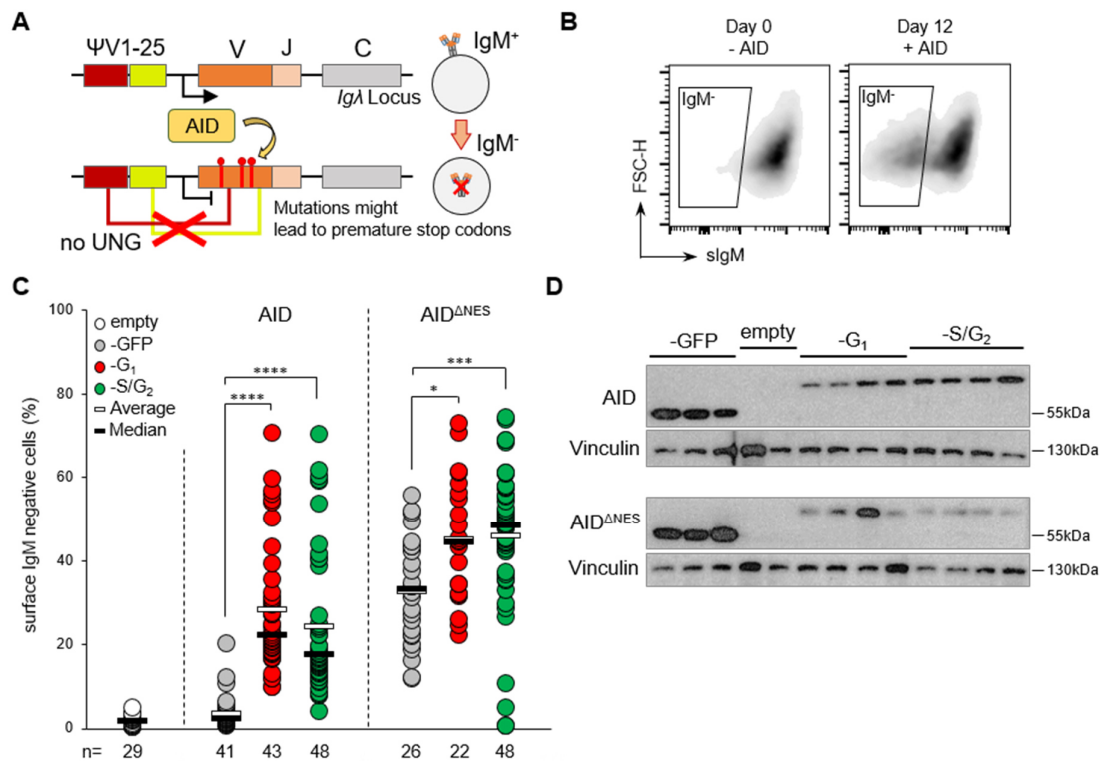
Figure 16: AID- and AID$^{\Delta NES}$-Fucci proteins show comparable activity and expression levels.
A) Schematic representation of the sIgM-loss assay performed in AID$^{-/-}$UNG$^{-/-}$ DT40 cells by flow cytometry. Figure adapted from Arakawa *et al.* [315]. **B)** Representative plots showing the loss of sIgM by AID$^{-/-}$UNG$^{-/-}$ DT40 cells after 12 days in culture in presence of AID. Living cells (FVS780$^-$) are shown. **C)** sIgM-loss in AID$^{-/-}$UNG$^{-/-}$ DT40 cells expressing AID/AID$^{\Delta NES}$-GFP and -Fucci fusion proteins (or the empty vector as negative control) analyzed 12 days post-transfection. Each dot represents the percentage of sIgM$^-$ cells among one individual clonal population measured as in B). The number of clonal populations analyzed (n) is displayed at the bottom of the graph. The data represent more than two independent experiments (*$p \leq 0.05$, ***$p \leq 0.001$, ****$p \leq 0.0001$; Kruskal-Wallis with Dunn's post-hoc correction test). **D)** Levels of the indicated AID/AID$^{\Delta NES}$ fusion proteins and the housekeeping protein vinculin in representative clonal populations. The data represent more than two independent experiments.

(Figure 16C). The random integration of the expressing vectors into the genome upon stable transfection may lead to differences in the levels of the desired exogenous proteins between different clonal populations; we did not observe consistent variation between AID-G_1 and -S/G_2 levels nor for their AID$^{\Delta NES}$ counterparts (Figure 16D).

We wished to confirm the results of the sIgM-loss assay in Figure 16C by sequencing the *IgL* locus (*Igλ*) of selected clonal populations: Within each set, we selected six representative populations as the ones whose percentage of sIgM$^-$ cells was the closest to the median value calculated from all the clonal populations of the set. The sIgM expression on these clones was further assessed twice or three times at later time points (2-3 days apart) and the ones with the steadiest values of sIgM-loss were selected for sequencing analysis. We sequenced a portion of the *Igλ* locus covering the whole variable region (Figure 17A) and calculated the number of unique (non-clonal) mutations found in cells expressing AID/AID$^{\Delta NES}$-GFP, -G_1, -S/G_2 and the negative control (Figure 17B). As expected, we found almost exclusively TS mutations at C:G base pairs and only rarely other types of mutations (including at A:T base pairs, data not shown). We measured the overall frequency of the mutations arising in the chosen clonal populations and we confirmed the results in Figure 16C showing that AID can act throughout the cell cycle at the *Igλ* locus (Figure 17C). We also proved that our AID/AID$^{\Delta NES}$-Fucci proteins are a suitable tool for the investigation of the cell cycle-mediated regulation of the processes of
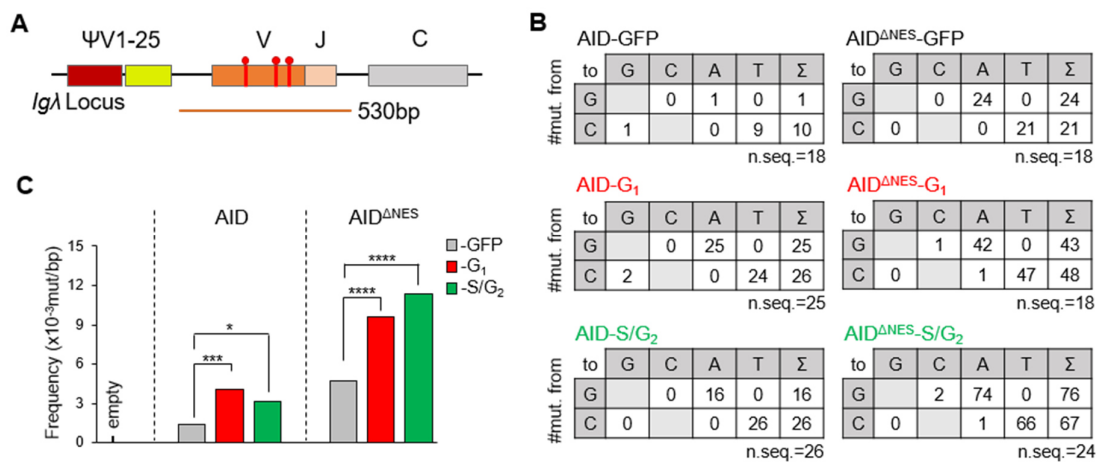
Figure 17: Efficient induction of comparable U:G lesions in G_1 and S/G_2.
A) Schematic representation of the *Igλ* locus; in orange, the portion of the locus that has been sequenced. **B)** The tables show the absolute numbers of unique mutations at C:G base pairs found in the sequences amplified from clonal populations expressing the indicated fusion proteins 13 days after transfection. Each table shows pooled data from two individual clonal populations. The number of analyzed sequences is shown. **C)** Frequency of all unique mutations found in the sequences amplified from two clonal populations expressing the indicated fusion proteins (cells transfected with the empty vector didn't show any mutation); the mutation frequency was determined as mutated bases divided by all analyzed bases (*$p \leq 0.05$, ***$p \leq 0.001$, ****$p \leq 0.0001$; two-sided $\chi2$ test).

secondary Ig diversification, as a comparable activity of AID/AID$^{\Delta NES}$ in G$_1$ and S/G$_2$ could be efficiently induced.

2.2.4 Ig diversification in chicken DT40 cells during the cell cycle

In the chicken B cell line DT40 the predominant mechanism of Ig diversification is the templated mutagenesis via IgGC mediated by HR, even though some AID-induced lesions may be converted into point mutations, as during SHM [315]. We investigated the cell cycle-mediated regulation of IgGC in AID-deficient DT40 cells in which the expression of sIgM is prevented by a frameshift mutation in the variable region of the Igλ chain but it can be restored upon AID-induced templated recombination with pseudogenes (ψV) via IgGC (Figure 18A-B) [316]. In these cells, the gene targeting has been facilitated by stable integration of an inducible cre-recombinase gene, therefore they will be henceforth referred to as DT40^{Cre1} cells [316]. We performed stable transfection of AID$^{-/-}$DT40^{Cre1} cells and generated individual clonal populations that express the AID/AID$^{\Delta NES}$-G$_1$ or -S/G$_2$ proteins or the relative controls; we performed a sIgM-gain assay by flow cytometry measuring the percentage of revertant sIgM$^+$ cells within each clonal population. In comparison to the reversion assay from Arakawa *et al.* [88], we observed low percentages of revertant sIgM$^+$ cells (median values $\leq$ 3%): In cells expressing the AID fusion proteins, the levels of sIgM$^+$ cells were found to be only slightly above the background levels of detection, while relatively higher values could be observed within cells expressing the AID$^{\Delta NES}$ fusion proteins (Figure 18C), due to the more pronounced nuclear accumulation, as observed previously. Nevertheless, the appearance of sIgM$^+$ revertant cells occurred faster in AID/AID$^{\Delta NES}$-G$_1$-expressing populations in comparison to the ones expressing AID/AID$^{\Delta NES}$ in S/G$_2$ (Figure 18C). We selected six representative populations (as described previously in chapter 2.2.3) and we assessed the levels of sIgM$^+$ cells within each of them over time, confirming that the rescue of the sIgM expression via IgGC is more efficient upon activity of both AID and AID$^{\Delta NES}$ in G$_1$ than in S/G$_2$ (Figure 18D).

The sIgM-gain assay provides a rapid but partial evaluation of the IgGC efficiency as it is limited to the detection of the IgGC events that have led to the rescue of the sIgM expression. We sequenced the *Igλ* locus of representative populations as shown in Figure 19A, we aligned each sequence obtained to the sequences of the 25 ΨV genes and classified all the detected events of diversification in accordance with previous studies [82, 317]: an IgGC track was considered to comprise more than one mutation (insertion, deletion and nucleotide substitution) deriving from a donor pseudogene and a minimum of 8 base pairs of homology with the donor; a potential IgGC tract presenting 8 base pairs of homology but a single pseudogene-templated
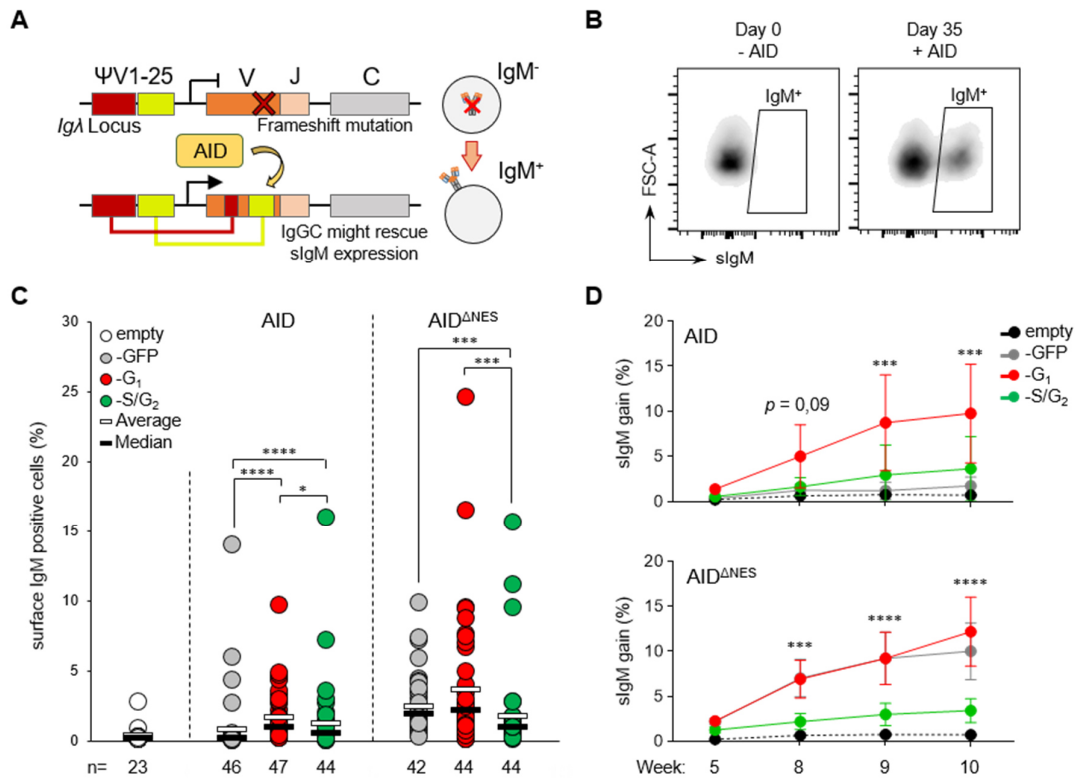
Figure 18: AID activity in G_1 leads to a faster appearance of sIgM$^+$ revertant cells upon IgGC.
A) Schematic representation of the sIgM-gain assay performed in AID$^{-/-}$ DT40^{Cre1} cells by flow cytometry. Figure adapted from Arakawa *et al.* [315]. **B)** Representative plots showing the gain of sIgM by AID$^{-/-}$ DT40^{Cre1} cells after 35 days in culture in presence of AID. Living cells (FVS780$^-$) are shown. **C)** sIgM-gain in AID$^{-/-}$ DT40^{Cre1} cells expressing AID/AID^{ΔNES}-GFP and -Fucci fusion proteins (or the empty vector as negative control) analyzed 35 days post-transfection. Each dot represents the percentage of sIgM$^+$ cells among one individual clonal population measured as in B). The number of clonal populations analyzed (n) is displayed at the bottom of the graph. One representative experiment is shown; due to the low efficiency of the AID fusion proteins, the experiment has been repeated three times with the AID^{ΔNES} fusion proteins (*$p ≤ 0.05$, ***$p ≤ 0.001$, ****$p ≤ 0.0001$; Kruskal-Wallis with Dunn's post-hoc correction test). **D)** Expression of sIgM over time in representative populations chosen according to the data shown in C); each dot represents the mean values ± SD of sIgM-gain among six representative clones. One representative experiment is shown; data referring to the AID^{ΔNES} fusion proteins have been reproduced three times (***$p ≤ 0.001$, ****$p ≤ 0.0001$; RM two-way ANOVA with Tukey's post-hoc correction test; only significant differences between AID/AID^{ΔNES}-G_1 and -S/G_2 are shown).

mutation was considered a "putative IgGC track"; any other non-templated mutation was considered a hypermutation event of diversification. We focused our investigation on the effects of AID^{ΔNES} fusion proteins as a rather lower number of events was detected in cells expressing the AID fusion proteins showing similar results (data not shown). We detected a comparable number of total events in AID^{ΔNES}-G_1- and -S/G_2-expressing cells and the AID^{ΔNES}-Fucci proteins were both found to be more active than the AID^{ΔNES}-GFP control (Figure 19B), as previously observed by sequencing analysis (Figure 17C). We calculated the relative proportion of each event of diversification among the total events detected; even though we found no differences in the percentages of IgGC tracks between AID^{ΔNES}-G_1- and -S/G_2-expressing

populations, we found a significantly higher proportion of putative tracks upon AID$^{\Delta NES}$ activity in G$_1$ than in S/G$_2$ (Figure 19C). Interestingly, significantly more point mutations were generated upon activity of AID$^{\Delta NES}$ in S/G$_2$ than in G$_1$ (Figure 19C). We asked whether the cell cycle could regulate the quality of IgGC by measuring the maximum and the minimum length of all the IgGC tracks detected and no differences could be observed (Figure 19D). Given the impossibility to distinguish between potential IgGC tracks from discrete point mutations, the sequencing data do not confirm that IgGC is more efficient upon lesions introduced by AID in G$_1$ but they rather suggest that it can be achieved throughout the cell cycle, even though uracils in S/G$_2$ seem to be more likely to be converted into point mutations.

We wished to confirm the latter observation, therefore we expressed AID$^{\Delta NES}$-Fucci and -GFP proteins in AID$^{-/-}$ DT40 cells in which the diversification at the $Ig\lambda$ locus via IgGC is prevented
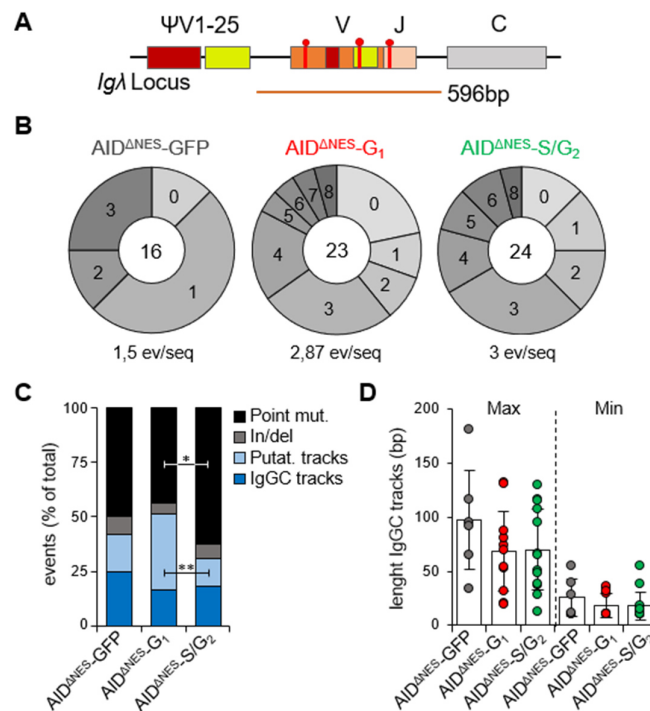
Figure 19: IgGC can be achieved throughout the cell cycle while point mutations are more likely to accumulate in S/G$_2$.
A) Schematic representation of the $Ig\lambda$ locus; in orange, the portion of the locus that has been sequenced. **B)** The pie charts show the relative fraction of sequences out of total sequences analyzed (number in the middle of the charts) presenting the indicated number of total events. The average number of events per sequence analyzed is displayed below the charts. Each pie chart shows pooled data from two representative clonal populations isolated 35 days after transfection. No events were detected in empty vector-expressing cells (data not shown). **C)** Percentage of each of the indicated events out of total detected in the sequences analyzed in B) (Point mut.: point mutations; In/del: insertions/deletions; Putat. tracks: putative IgGC tracks). The two-sided Fisher exact test for 2 X 2 contingency table was used to calculate the significant differences: The p values were calculated comparing the number of a certain type of event versus the cumulative number of the all other types of events (*$p \leq 0.05$; **$p \leq 0.01$; two-sided Fisher exact test). **D)** Maximum and minimum length of IgGC tracks was measured for each IgGC track identified in the sequences analyzed in B) as maximum and minimum number of bp homologous to the donor pseudogene (dots in the graph). Bars indicate mean values ± SD (Kruskal-Wallis test).

by the deletion of the 25 ΨV genes from the $Ig\lambda$ locus (AID$^{-/-}$ ΨV^- DT40); in these cells the activity of AID at the $Ig\lambda$ locus leads to the accumulation of point mutations via hypermutation (Figure 20A) [316]. We stably transfected AID$^{-/-}$ ΨV^- DT40 cells and we cultured individual clonal populations expressing the AID$^{\Delta NES}$-Fucci or the relative controls in order to perform a sIgM-loss assay via flow cytometry and to sequence the variable region of the $Ig\lambda$ locus for analysis of the mutation frequency. We found higher sIgM-loss upon AID$^{\Delta NES}$ activity in S/G$_2$ than in G$_1$ (Figure 20B) and the sequencing data confirmed these results (Figure 20C).

Hence, our data support the following model of diversification in DT40 cells: IgGC could potentially be achieved throughout the cell cycle, even though the activity of AID in G$_1$ leads to a faster appearance of revertant sIgM$^+$ cells, while uracils in S/G$_2$ are more likely to generate point mutations.
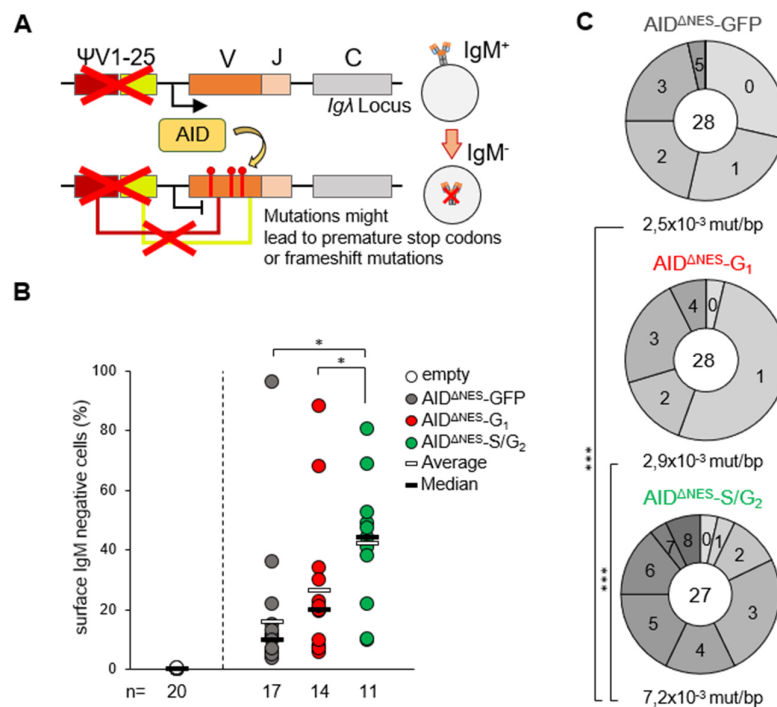
Figure 20: Hypermutation in DT40 cells is favored upon AID$^{\Delta NES}$ activity in S/G$_2$.
A) Schematic representation of the sIgM-loss assay performed in AID$^{-/-}$ ΨV^- DT40 cells by flow cytometry. Figure adapted from Arakawa *et al.* [315]. **B)** sIgM-loss in AID$^{-/-}$ ΨV^- DT40 cells expressing AID$^{\Delta NES}$-GFP and -Fucci fusion proteins (or the empty vector as negative control) analyzed 15 days post-transfection. Each dot represents the percentage of sIgM$^-$ cells among one individual clonal population measured as in Figure 16B. The number of clonal populations analyzed (n) is displayed at the bottom of the graph. The data represent two independent experiments (*$p \leq 0.05$, Kruskal-Wallis with Dunn's post-hoc correction test). **C)** The pie charts show the relative fraction of sequences out of total sequences analyzed (number in the middle of the charts) presenting the indicated number of non-unique mutations. The mutation frequency was determined as mutated bases divided by all analyzed bases. Each pie chart shows pooled data from two representative clonal populations isolated 20 days after transfection. Only rare mutations were detected in the empty vector-expressing cells (2 mutations in 12 analyzed sequences) (***$p \leq 0.001$; two-sided $\chi 2$ test).

2.2.5 Regulation of SHM by the cell cycle in human RAMOS cells

To explore the role of the cell cycle in regulating all error-prone repair mechanisms acting during SHM according to Di Noia and Neuberger [70] (Figure 4), we made use of the natural hypermutating Burkitt B-cell lymphoma RAMOS line. It has been shown that RAMOS cells in culture constitutively mutate the variable region of their IgH and that different clonal populations are characterized by different hypermutation rates, which were found to correlate with the expression levels of AID [318, 319]. We wished to overexpress the AID-Fucci fusion proteins and the relative controls in RAMOS clones with very low expression of the endogenous AID (AID^{low}) so to ensure a minimal influence on the rates of SHM induced by the exogenous AID fusion proteins. We generated different clonal populations and assessed the levels of the endogenous AID protein: We found that some clones showed almost undetectable levels of the endogenous AID via Western Blot (Figure 21A). We stably transfected a clonal population chosen among the ones with the lowest detectable levels of AID and investigated the SHM rate in terms of sIgM-loss in sub-clonal populations expressing the AID$^{\Delta NES}$-Fucci proteins and the relative controls. Since we could not undoubtedly expect that the activity of the AID fusion proteins would lead to the loss of sIgM at levels detectable above the naturally occurring hypermutation, we initially carried out our investigation with the AID$^{\Delta NES}$ fusion proteins, as they showed relatively higher activity in comparison to the AID counterparts. As shown in Figure 21B, we found appreciable levels of sIgM-loss in cells expressing AID$^{\Delta NES}$-Fucci and -GFP proteins in comparison to the negative controls. Interestingly, the sIgM-loss levels
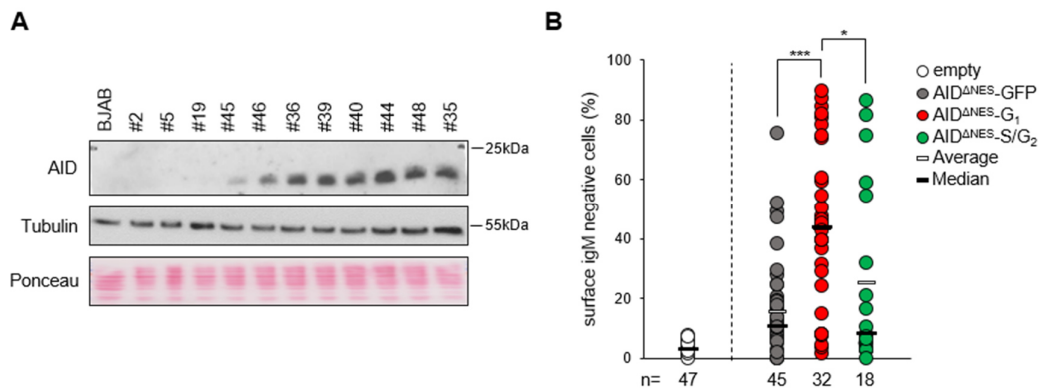
Figure 21: The activity of AID$^{\Delta NES}$ in G$_1$ leads to a faster sIgM-loss than in S/G$_2$.
A) Western Blot showing the levels of the endogenous AID protein, the housekeeping protein tubulin and the protein staining with Ponceau solution in different RAMOS clonal populations. The human B-cell lymphoma line BJAB served as negative control, as it does not express AID mRNA [319]. **B)** sIgM-loss in AID^{low} RAMOS cells (clone #2 in A)) expressing AID$^{\Delta NES}$-GFP or -Fucci fusion proteins, or the empty vector as negative control, analyzed 34 days post-transfection. Each dot represents the percentage of sIgM$^-$ cells among one individual clonal population. The number of clonal populations analyzed (n) is displayed at the bottom of the graph. One experiment is shown (*$p \leq 0.05$, ***$p \leq 0.001$; Kruskal-Wallis with Dunn's post-hoc correction test).

were found to be higher upon $AID^{\Delta NES}$ activity in the G_1 rather than in S/G_2 (Figure 21B). We sequenced the variable region of the *IGH* locus with the aim to determine the influence of the cell cycle on the mutational pattern and, consistently, on the DNA repair mechanisms acting during SHM; unfortunately, the background level of the hypermutation induced by the endogenous AID (measured in the population expressing the empty vector) was found to be too high for our purposes (data not shown), therefore we generated AID^{KO} RAMOS cells for further investigations.

2.2.5.1 Generation of AID^{KO} RAMOS cells

We knocked out the expression of the endogenous AID in RAMOS cells using the CRISPR-Cas9 technology [321, 322]. We transiently transfected RAMOS cells with a commercially available pool of three plasmids each encoding the Cas9 nuclease, a 20-nucleotide long AID-specific guide RNA (gRNA) designed for a maximum knockout efficiency and a minimum off-target activity, and the GFP protein used as reporter (Figure 22A). After a 24-hour culture post-transfection, we sorted the $sIgM^+$ GFP^+ cells and cultured them as single-cell/well in order to isolate individual clonal populations; we assessed the AID

Figure 22: AID knockout in RAMOS cells via the CRISPR/Cas9 system.
A) Representation of the experimental setup. Each of the three plasmids encodes a different gRNA (in orange, red and blue respectively), the Cas9 protein (in purple) and the GFP protein (in green). The pool of plasmid was obtained purified and ready to use (AID CRISPR/Cas9 KO Plasmids, manufactured by Santa Cruz Biotechnology). In order to perform sIgM-loss assays, $sIgM^+$ GFP^+ cells were sorted. **B)** Western Blot showing the levels of the endogenous AID protein, the housekeeping protein tubulin and the protein staining with Ponceau solution in different RAMOS clonal populations. The clones #4 and #7 were detected as putative AID^{KO}. **C)** Above, the PCR strategy used to amplify the *AICDA* locus; the rectangles represent the exons, the arrows represent the primer binding sites. The position of the sequences targeted by the three different gRNAs is shown. Below, the amplification products in two biological replicates for each sample are shown. **D)** Representation of the deleted portions on both alleles of the *AICDA* locus amplified from the clone #7.

protein levels within each population via Western Blot and we identified two of them as putative AID^{KO} as they showed undetectable levels of AID (Figure 22B). We confirmed the efficient AID knockout in the putative AID^{KO} clonal populations by PCR: We amplified the *AICDA* locus with the PCR strategy illustrated in Figure 22C and observed that the two putative AID^{KO} clones showed a much smaller amplification product in comparison to the AID$^+$ cells (~1500bp and ~9250bp, respectively; Figure 22C). The size of the products obtained by PCR suggested that, on both alleles, DSBs were generated by the Cas9 nuclease in correspondence of the exons 1 and 3 of the *AICDA* locus and that the subsequent end joining led to the loss of the intervening portion of DNA. We confirmed this hypothesis by sequencing the amplification products and, for one clonal population, we could identify the deletion of approximately 7500bp from both alleles (Figure 22D). We could not detect any event of sIgM-loss within the AID^{KO} population in comparison to an AID$^+$ control after ~4 weeks in culture (Figure 23A).

2.2.5.2 Cell cycle-mediated regulation of SHM in AID^{KO} RAMOS cells

We stably transfected AID^{KO} RAMOS cells and isolated individual clonal populations expressing the AID/AID$^{\Delta NES}$-G$_1$ or -S/G$_2$ fusion proteins or the respective controls. We performed a sIgM-loss assay and we found that sIgM$^-$ cells appeared faster upon the activity of AID$^{\Delta NES}$ in G$_1$ than in S/G$_2$, as previously observed (Figure 21B); interestingly, the presence of the NES partially rescued the ability of AID-S/G$_2$-expressing cells to perform SHM (Figure 23A). It has been shown that the C-terminus of AID (comprising the NES) is necessary for CSR to occur but is dispensable for SHM [161], therefore we exclude direct effects of the C-terminus on the process of SHM; we observed that an appreciable portion of clonal populations expressing the AID$^{\Delta NES}$-S/G$_2$ protein had either repressed the expression of AID$^{\Delta NES}$, as they had lost their fluorescence over time (mAG fluorescence), or were found to be impaired in their clonal expansion (the number of viable events detected by flow cytometry was found to be below the set threshold, even though all clones had been seeded at comparable cell densities two days before the analysis; Figure 23B). Therefore, we suggest that the active export towards the cytoplasm via the NES may either protect AID from a more pronounced nuclear degradation in S/G$_2$, as previously observed in RAMOS cells [130], and/or prevent excessive toxicity upon AID activity in this phase of the cell cycle, but further experiments are needed to confirm this hypothesis.

We sequenced the VDJ region of the *IGH* locus in representative clonal populations and we could confirm a significantly higher mutation frequency upon AID$^{\Delta NES}$ activity in G$_1$ than in S/G$_2$, but not between AID-G$_1$- and -S/G$_2$-expressing clones (Figure 23C). Altogether, these
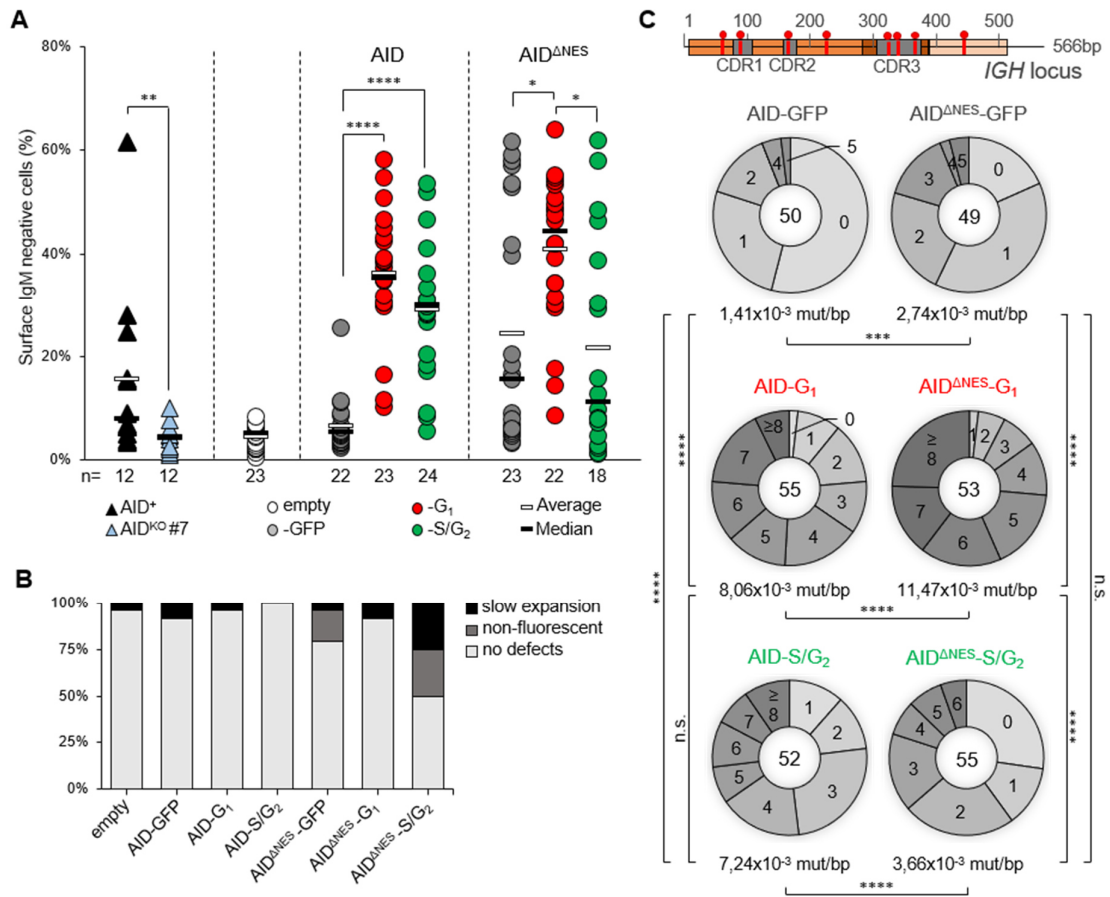
Figure 23: SHM in AID^{KO} RAMOS cells is favored upon AID nuclear accumulation in G$_1$.
A) sIgM-loss in AID$^+$ and AID^{KO} RAMOS cells (clone #7 in Figure 22), and in AID^{KO} RAMOS cells (clone #7) expressing AID/AID$^{\Delta NES}$-GFP or -Fucci fusion proteins, or the empty vector as negative control, analyzed 27 days post-transfection. Each dot represents the percentage of sIgM$^-$ cells among one individual clonal population. The number of clonal populations analyzed (n) is displayed at the bottom of the graph. One experiment is shown (*$p \leq 0.05$, **$p \leq 0.01$, ***$p \leq 0.001$, ****$p \leq 0.0001$; two-sided Mann-Whitney's test for comparison between non-transfected cells, Kruskal-Wallis with Dunn's post-hoc correction test for comparison between AID/AID$^{\Delta NES}$-expressing cells). **B)** Percentage of clonal populations showing expansion defects, no fluorescence or no evident defects in the analysis performed in A). **C)** Above, schematic representation of the 566bp-long portion of the *IGH* locus sequenced from representative clonal populations. The V, D, and J regions are represented in orange, dark brown and light brown, respectively (CDR: complementary determining region). Below, the pie charts show the relative fraction of sequences out of total sequences analyzed (number in the middle of the charts) presenting the indicated number of non-unique mutations. The mutation frequency was determined as mutated bases divided by all analyzed bases. Each pie chart shows pooled data from two representative clonal populations isolated 28 days after transfection. Only rare mutations were detected in the empty vector-expressing cells (1 mutation in 19 analyzed sequences) (***$p \leq 0.001$, ****$p \leq 0.0001$; two-sided $\chi 2$ test).

results suggest that SHM can be achieved throughout the cell cycle, but the activity of AID may be better tolerated in G$_1$ as excessive nuclear accumulation in S/G$_2$ could possibly result in cellular toxicity and in a limited SHM in RAMOS cells.

To understand how the cell cycle influences the activity of all error-prone DNA repair pathways during SHM, we analyzed the frequency of specific types of mutations arising in representative

populations expressing the AID/AID$^{\Delta NES}$-Fucci proteins (Figure 24A). In accordance with previous observations, we noticed a strong bias towards C/G over A/T mutagenesis, which was found to correlate with the low expression levels of the major A/T mutator Polη in RAMOS cells [318]. Strikingly, we observed that mutations at A:T base pairs were almost completely absent upon the activity of both AID and AID$^{\Delta NES}$ in S/G$_2$ (Figure 24). Probably due to the higher toxicity and/or degradation of AID$^{\Delta NES}$ upon nuclear accumulation in S/G$_2$, we were not surprised to find that the frequency of all types of mutations was affected in clones expressing AID$^{\Delta NES}$ in S/G$_2$ in comparison to AID$^{\Delta NES}$-G$_1$-expressing cells (Figure 24A, right panel). Conversely, the presence of the NES favours the accumulation of mutations in AID-G$_1$- and -S/G$_2$-expressing cells to the same extent and we found that the scarcity of mutations at A:T base pairs was compensated by a higher accumulation of TSs at C:G upon AID activity in S/G$_2$ (Figure 24A, left panel). To overcome the limitations due to the differences of the mutation frequency, we compared the relative proportion of each type of mutation out of total mutations found (Figure 24B). We found that lesions generated by AID and AID$^{\Delta NES}$ in the G$_1$ phase of the cell cycle result in both A/T and C/G mutagenesis and to an equal proportion of TSs and TVs at C:G base pairs, while uracils generated in S/G$_2$ do not sufficiently induce A/T
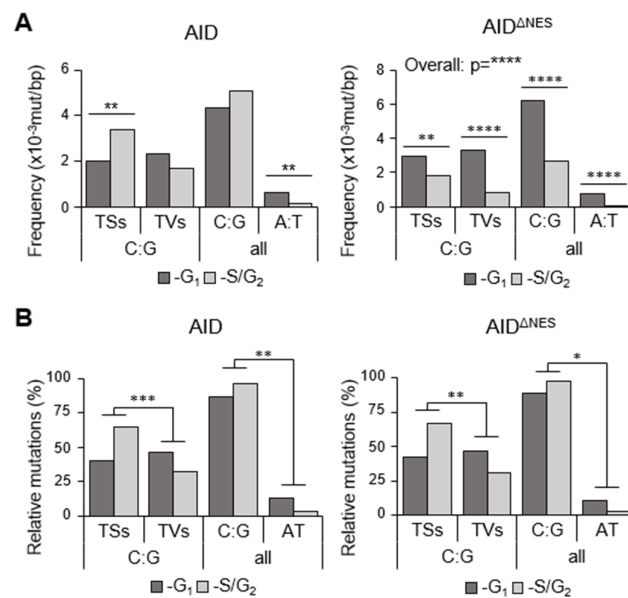
Figure 24: AID activity in G$_1$ but not in S/G$_2$ generates the full spectrum of mutations during SHM
A) Frequency of the indicated types of mutations (unique mutations; TSs: transitions, TVs: transversions) found in the sequences analyzed in Figure 23C expressing the indicated fusion proteins; the mutation frequency was determined as mutated bases divided by all analyzed bases (**$p \leq 0.01$, ****$p \leq 0.0001$; two-sided $\chi 2$ test). **B)** Percentages of the indicated types of mutations out of total (unique mutations) in the sequences analyzed in Figure 23C (*$p \leq 0.05$, **$p \leq 0.01$, ***$p \leq 0.001$; two-sided Fisher exact test).

mutagenesis but lead almost exclusively to the accumulation of mutations at C:G base pairs, especially to TS mutations (Figure 24B, both panels).

These results show that, while A/T mutagenesis via ncMMR/Polη is active almost exclusively in G_1, UNG-mediated mechanisms of repair that result in the accumulation of mutations at C:G base pair can act throughout the cell cycle, even though the replication across uracils in S/G_2 is more likely to generate TS mutations.

2.2.6 Control of CSR during the cell cycle in primary mouse B cells

To explore the role of the cell cycle in the regulation of CSR, we expressed only the AID fusion proteins in primary mouse B cells isolated from AID^{KO} mice, since the C-terminus of AID was found to be necessary for CSR [161]. We transduced proliferating primary B cells in culture with a retroviral system and analyzed the percentage of class switched $IgG1^+$ cells among the living transduced cells by flow cytometry (Figure 25A); efficiently transduced cells could be detected by the expression on their surface of the truncated form of the human nerve growth factor receptor (hNGFR) lacking the intracellular domain [323]. We detected specific events of CSR to IgG1 exclusively upon AID activity in G_1, since putative events of CSR in AID-S/G_2-expressing cells were undistinguishable from the background given by cells transduced with the empty vector (Figure 25B-C). However, the levels of CSR of AID-G_1-expressing cells were found significantly lower than the cells expressing the AID-GFP control (Figure 25B-C); this effect may be due to a higher susceptibility of the AID-Fucci-expressing cells in comparison to the controls (Figure 25D) because of the increased nuclear accumulation of AID-G_1 and -S/G_2 proteins in comparison to AID-GFP, as previously described (Figure 15A, left panel). Another reason that could contribute to the observed effects is the following: AID activity at pre-Sμ region in primary B cells has been observed almost exclusively in the early G_1 phase; in AID-G_1-expressing cells, the levels of AID may be lower than the control AID-GFP in the early G_1 as they have to be restored at every new cell cycle after degradation in S/G_2.

We conclude that CSR is efficiently achieved exclusively upon AID activity in the G_1 phase of the cell cycle, likely due to a more pronounced HR-mediated repair of DSBs generated in S/G_2.

Altogether, our data showed that the S/G_2 phase does not represent a barrier for AID activity per se. We found that IgGC can be achieved throughout the cell cycle, as well as C/G mutagenesis during SHM. However, A/T mutagenesis and CSR could be achieved exclusively upon activity of AID in G_1, suggesting S/G_2-specific suppressive mechanisms.
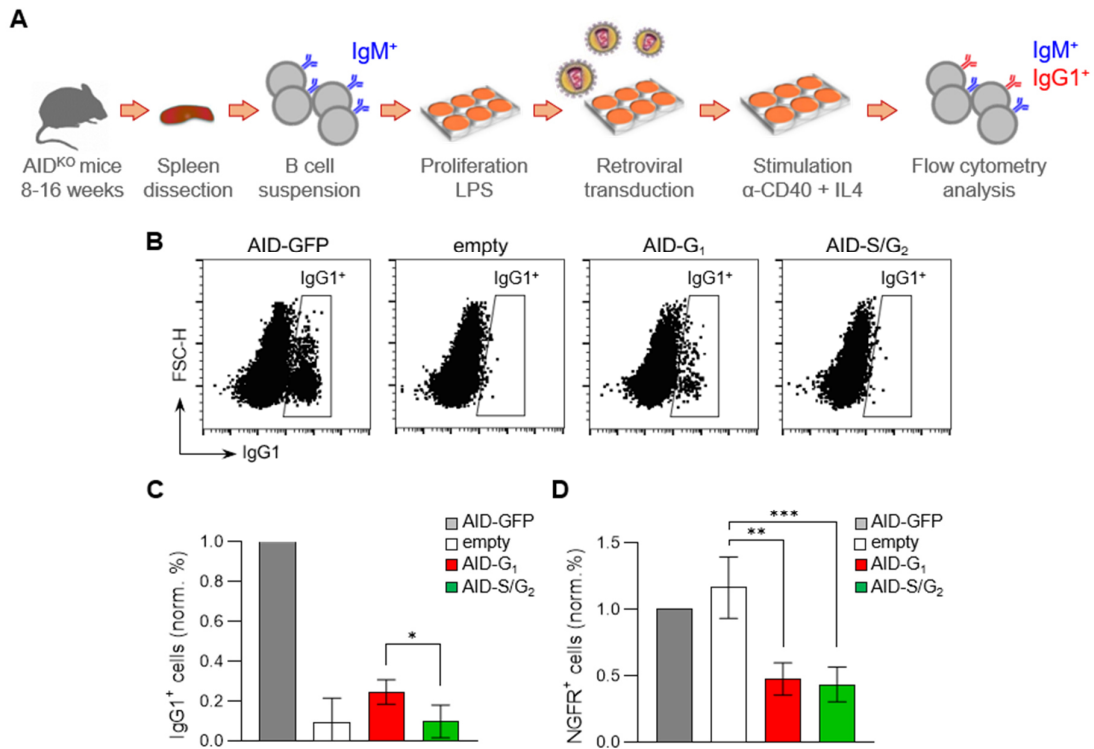
Figure 25: CSR is achieved exclusively upon AID activity in the G$_1$ phase of the cell cycle.
A) Representation of the experimental setup. After spleen dissection, the B cells were purified from the splenic single cell suspension by depletion of the CD43$^+$ cells via MACS. The primary B cells were infected with retroviral particles after 24-hour-proliferation induced by stimulation with LPS. The infected cells were cultivated for 3 days in the presence of α-CD40 and IL-4 to induce CSR to IgG1. **B)** The plots show the percentages of IgG1$^+$ cells among living transduced cells (FVS780$^-$ NGFR$^+$ cells are shown). The plots are representative of five independent experiments. **C)** Percentages of IgG1$^+$ cells measured as in B) normalized to the AID-GFP control. **D)** Percentages of transduced (NGFR$^+$) cells out of all living cells normalized on the AID-GFP control.

In C) and D) mean values ± SD refer to five independent samples per condition (**$p \leq 0.01$, ***$p \leq 0.001$; RM one-way ANOVA with Tukey's post-hoc correction test performed among all conditions but AID-GFP).

3 Discussion

In this thesis we investigated the influence of the checkpoint signaling via Chk1 and the cell cycle on the mechanisms of secondary Ig diversification.

The survival of B cells in the course of development and immune reactions is dependent on the activity of Chk1, therefore we made use of B cell-specific *Chek1* heterozygous mice. The presence of one functional allele may have masked and/or delayed the effects of Chk1 downregulation on some of the B cell responses analyzed in this study. Nevertheless, we found that a proper Chk1 dosage is needed to support the survival of the B cells as they accumulate DNA damage and that adequate levels of Chk1 are crucial for efficient SHM. Even though the overall mutagenesis at the *IgH* locus was reduced, the same was not observed at the AID off-target gene *Cd83* in Chk1[Bhet] mice, suggesting that Chk1 downregulation may allow for sustained mutagenesis outside the Ig genes. Interestingly, we found that reduced levels of Chk1 lead to a higher A/T mutagenesis via ncMMR/Polη in the variable region of the *IgH* locus, mainly at the expense of TSs at C:G base pairs, revealing an additional role for the fine-tuning of the Chk1 dosage on the repair pathway choice during SHM.

A dysfunctional checkpoint signaling represents per se a considerable threat to the genome stability of any cell; in B cells, a temporal restriction during the cell cycle of the mechanisms of secondary Ig diversification could protect the genome from the hazardous consequences of extensive DNA damage, especially upon the attenuation of the ATR/Chk1 signaling pathway.

AID has been shown to act exclusively in G_1 and our data suggest that this temporal restriction is mainly achieved by limiting AID accessibility/accumulation to the nucleus in S/G_2, as no other barriers to its activity in this cell cycle phase have been observed. We found that, while the error-free diversification via IgGC is not restricted during the cell cycle, the error-prone mechanisms acting during SHM and CSR are mainly limited to G_1. Even though C/G mutagenesis via TLS could be achieved throughout the cell cycle, the mutagenesis at A:T base pairs via ncMMR/Polη was found almost entirely restricted to G_1, as well as the accomplishment of CSR via NHEJ-mediated repair of DSBs.

3.1 Effects of Chk1 downregulation on secondary Ig diversification

3.1.1 Limitations posed by the Chk1[Bhet] mouse model

The Chk1 protein is an evolutionary conserved kinase whose role in the context of a functional checkpoint signaling activation is essential for the preservation of genome stability and cell

survival. The exploration of the functions of Chk1 *in vivo* has been limited by the embryonic lethality of Chk1-deficient animals [324, 325]; after the advent of the conditional gene targeting technologies, the complete deletion of Chk1 was found to be incompatible with the cell survival in adult tissues such as mammary glands, thymus and small intestine [298, 326, 327]. The activity of Chk1 was shown to be indispensable for the survival of mouse and human hematopoietic stem and progenitor cells as well as for the B cells during their development [296, 328]. Indeed, in the absence of Chk1, the B cells undergo a block in the differentiation at the pro- to pre-B cell transition stage, likely due to the accumulation of DNA damage during the process of V(D)J recombination [329, 330]. The B cells are dependent on the activity of Chk1 also for the establishment of GCs: The complete deletion of Chk1 in activated B cells upon T cell help (by induction of the cre-mediated recombination upon transcription of the Igγ1 constant region gene segment) was shown to impair the GC formation and resulted in a dampened humoral response [297]. Since a functional Chk1 signaling is needed in activated B cells, we investigated the role of Chk1 signaling attenuation during the GC reaction and on the mechanisms of secondary Ig diversification in Chk1[Bhet] mice whose B cells undergo cre-mediated deletion of only one *Chek1* allele upon the transcription of the *mb1* gene. The presence of one functional *Chek1* allele allows for proper B cell maturation and differentiation and also supports the GC formation upon immunization making the Chk1[Bhet] mouse model suitable for the intended study, but it has also posed some limitations to our investigation.

In our previous study *in vitro* on the murine CH12F3 B cell line, we found that the chemical inhibition of Chk2 resulted in increased levels of Chk1 and in a decreased ability to perform CSR [331]. Chk1 directly promotes DNA repair via HR by phosphorylating the crucial factors Rad51 and BRCA2 [332], therefore increased Chk1 levels would lead to a more efficient HR-mediated repair of AID-induced DSBs and to the observed CSR defects. However, we found that CSR was not facilitated upon complete inactivation of HR: The B cell-specific deletion of BRCA2 leads to profound proliferation and survival defects *in vitro* and *in vivo*, resulting in a compromised ability to successfully achieve CSR [165]. We would have expected similar (potentially milder) results upon Chk1 downregulation but no alteration of the CSR ability was observed in this study. The presence of one functional *Chek1* allele showed to be sufficient to prevent CSR defects *in vitro* and *in vivo*.

In *in vitro*-cultured primary B cells, the ATR/Chk1 axis is supposed to be fully functional: It was shown that the stimulation of primary B cells with different mitogenic agents reduces the levels of Bcl-6 [320] and that the Chk1 mRNA levels of cultured splenic B cells increase upon stimulation with α-CD40 [296]. B cell lines and primary mouse B cells are not sensitive to the

downregulation of Chk1 upon low concentration of Chk1 inhibitors [290, 297]; accordingly, only the full inactivation of Chk1 was shown to induce survival defects and alterations of the cell cycle progression in unperturbed DT40 cells [333].

In vivo, the total B cell-specific deletion of Chk1 leads to a block of B cell differentiation at the pro- to pre-B cell transition stage; the presence of only one *Chek1* allele was shown to be sufficient to completely rescue this phenotype [296]. If the block would be due to DSB-induced cell death during V(D)J recombination, it would imply that Chk1 is indispensable to support the survival of the B cells in the presence of DSBs. This would lead to the assumption that, in a similar way, the B cells are dependent on the activity of Chk1 during CSR for their survival. A recent study has shown that CSR is infrequently achieved in established GC but is more likely to occur at earlier stages [58]: The temporal separation between CSR and the establishment of the Bcl-6-mediated transcriptional repression of the ATR/Chk1 axis in the GCs could provide another evidence in support of the dependence of the B cells undergoing CSR on a functional Chk1 signaling.

As explained in the next chapters, Chk1 downregulation *in vivo* does eventually affect the survival of hypermutating B cells, but the presence of one functional *Chek1* allele delays the manifestation of those to later stages of the GC reaction, therefore Chk1^{Bhet} mice are able to form acute GCs and to mount an adequate humoral response upon immunization with NP-CGG but they show a compromised persistence of B cells in chronic GCs.

Additionally, we believe that eventual effects of Chk1 downregulation on the mutagenesis at the pre-Sμ region may also be masked in Chk1^{Bhet} mice, as discussed in chapter 3.1.4.

3.1.2 Chk1 is required for efficient SHM *in vivo*

The mutation frequency at the *IgH* locus of splenic GC B cells generated upon immunization with NP-CGG was found to be ~1.5-fold lower in Chk1^{Bhet} mice in comparison to the controls. At first, these results were surprising as they contradict previous findings from our group. In the hypermutating ΨV$^-$ DT40 cell line, the partial depletion of two out of four *Chek1* alleles (due to chromosomal duplication) leads to higher SHM and this was confirmed also upon chemical inhibition of Chk1 in the Ramos cell line [290]. Consistently, the depletion and the chemical inhibition of Chk2 showed opposing effects on SHM due to an increased ATM-dependent Chk1 activation upon Chk2 downregulation [331].

In lymphoma cells, the overexpression of the proto-oncogene c-*myc* sustains proliferation and the lack of p53 desensitizes the cells to DNA damage-induced apoptosis [334-337]. For this reasons, the downregulation of Chk1 is well tolerated by lymphoma cells and a reduced Chk1-mediated

repair via HR was found to facilitate SHM. *In vivo*, the B cells may be more sensitive to the attenuation of the checkpoint signaling via Chk1. In this study we show that the downregulation of Chk1 beyond the levels dictated by the Bcl-6-mediated transcriptional repression is not beneficial for SHM *in vivo*.

The overall reduced mutation frequency at the Ig locus observed in Chk1^{Bhet} mice in comparison to the controls was due to the almost complete loss of highly mutated clones. It has been estimated that GC B cells accumulate ~1 mutation per cell division in their variable region, therefore the accumulation of mutations depends on their ability to keep proliferating and recirculating in the GC upon positive selection [338-341]. The scarcity of highly mutated clones can be due to a progressive slowdown of proliferation or to the loss of cells as a consequence of the accumulation of excessive DNA damage in multiple rounds of hypermutation. We did not find differences in the percentage of GC B cells between Chk1^{Bhet} and Chk1^{BWT} mice upon immunization, therefore it is conceivable that defects in the cell cycle progression more than in the survival may account for the observed effects in acute GCs. However, further experiments in this direction are needed to confirm this hypothesis.

B cells proliferate at an exceptionally higher rate in comparison to other mammalian cells: the length of a complete cell cycle of activated B cells in culture can be as short as 9 hours [342] while in the DZ of the GC the average cell cycle duration is of 7 hours [343] and is independent on the affinity of the BCR [344]. Consequently, even a moderate arrest may lead to a reduced accumulation of mutations, given the remarkably short duration of the overall cell cycle.

It was observed that Chk1-deficient DT40 cultures were moderately enriched in G_1- and S/G_2-phase cells at the expense of S-phase cells [333]. An arrest in G_2/M may still be achieved via an alternative Chk1-independent checkpoint, which has been observed in Chk1-deficient fibroblasts: It relies on the cytoplasmic retention of cyclin B1, which is responsible for the G_2/M transition [345]. The extent to which this would contribute in the presence of one functional *Chek1* allele remains to be verified nonetheless. Cells bearing unrepaired DNA damage, such as DSBs that have bypassed the G_2/M checkpoint and have successfully completed a mitotic division escaping cell death, may be arrested at the subsequent G_1/S border upon the activation of the ATM/Chk2 signaling pathway. A recent publication has unveiled the possibility that broken chromosome ends can be "tethered" during mitosis until they can be repaired in the following G_1 phase [346].

The activation of ATM upon genotoxic stress may contribute to the loss of highly mutated clones observed in the acute GCs of Chk1^{Bhet} mice also in ways other than by establishing G_1/S cell cycle arrest. The signaling via ATM can lead to the ubiquitin-mediated degradation of the

crucial GC factor Bcl-6 [173], therefore to the loss of the GC phenotype. Additionally, the ATM-mediated degradation of Bcl-6 may alleviate the repression of the DDR via ATR/Chk1 and restore a normal p53-dependent and -independent apoptosis.

3.1.3 Chk1 signaling aids the longevity of GC B cells in the Peyer's Patches

In acute GCs, the DNA damage accumulated by hypermutating B cells does not seem to exceed the threshold of damage tolerance dictated by the Chk1 dosage, as no survival defects were observed 2 weeks post-immunization. In chronic GCs in the Peyer's patches, though, the effects of the Chk1 downregulation on the survival of hypermutating B cells were noticeable, as observed also by another group in Cγ1-cre Chk1$^{fl/+}$ mice [297]. It is reasonable that the survival defects are due to the essential role played by Chk1 in promoting repair via HR and in establishing the intra-S- and the G$_2$/M-checkpoint in cells accumulating DNA damage.

The B cell-specific inactivation of HR *in vivo* impairs GC formation, leads to CSR defects and a to decreased SHM, mainly by affecting viability and proliferation capacities [165]. HR is the main DSB repair pathway in the S/G$_2$ phase of the cell cycle; it was shown that DSBs generated upon AID activity in G$_1$ do not strongly induce the G$_1$/S checkpoint, therefore B cells bearing unrepaired DSBs often enter into the S phase [167]. Experiments with X-ray irradiated cells have shown that the G$_1$/S checkpoint is activated in a dose-dependent manner above 1 Gy [347]; AID induces a relatively lower DNA damage that was found to be comparable to 0,5 Gy [167]. Furthermore, it appears that the activation of the G$_1$/S checkpoint upon DSB generation also depends on the timing of the DNA damage induction: When the cells were irradiated in the middle or late G$_1$ phase, even extremely high doses of IR failed to abolish S-phase entry, while this was not the case for early G$_1$-phase irradiated cells [347]. AID was shown to act in early G$_1$ [85] but the generation of DSBs may occur at a later time point in G$_1$ as it is dependent on the activity of UNG [159] whose expression levels progressively increase, reaching their peak in the S phase [228].

Chk1 plays an essential role in stabilizing replication forks and/or in promoting intra-S-arrest by preventing new origin firing upon replication stress [283]. The DNA damage induced by AID, such as SSBs and abasic sites, can lead to replication stress in the S phase [348]; Chk1 downregulation may result in an aberrant S-phase progression and in generation of DSBs as a result of replication fork instability and collapse [349, 350]. Importantly, Chk1 inactivation results in a dysfunctional G$_2$/M checkpoint [324]. If cells with under-replicated DNA and/or unrepaired DSBs enter into mitosis, this could lead to aberrant chromosomal segregation, loss of genetic material and cell death by "mitotic catastrophe" [351]. For all these reasons, the

inhibition of ATR and/or Chk1 is a strategy that is currently being exploited to increase the sensibility to the chemotherapy and the radiotherapy of tumor cells with defective G_1/S checkpoint due, for example, to the loss of p53 [352].

Therefore, even though the attenuation of the DDR via Chk1 mediated by Bcl-6 in GC B cells allows for a better tolerance to the undergoing DNA damage and for evading cell death by apoptosis [169, 170], our results suggest that the downregulation of Chk1 is not tolerated beyond a certain threshold of DNA damage, as observed in chronically activated B cells in the Peyer's patches, resulting in a decreased survival.

3.1.4 Chk1 downregulation facilitates A/T mutagenesis in the J_H4 intron

A comprehensive view of the role played by Chk1 in the regulation of the DNA repair pathways acting in the course of SHM could not be provided by our previous studies carried out *in vitro* on lymphoma B cell lines [290, 331] due to the limitations posed by the low efficiency of the A/T mutator in *in vitro* systems [314, 318]. The analysis of the pattern of mutations arising in the J_H4 intron *in vivo* provides a widely accepted tool for the investigation of the error-prone mechanisms of DNA repair involved in the resolution of AID-induced lesions during SHM [304]. When we compared the frequency of the different types of mutations according to Di Noia and Neuberger [70], we found that the downregulation of Chk1 significantly limits the accumulation of mutations specifically at C:G base pairs as the mutation frequency at A:T base pairs was found not impaired in Chk1[Bhet] mice. The interpretation of these results cannot disregard the fact that the overall mutation frequency at the *IgH* locus was found to be significantly reduced upon Chk1 downregulation. To overcome this limitation, the occurrence of all types of mutations has also been evaluated as the percentage of each type of mutation out of total mutations found; this analysis elucidates the relative contribution of each repair pathway during SHM. Interestingly, we observed that A/T mutagenesis is significantly favored over C/G mutagenesis in Chk1[Bhet] mice in comparison to the controls, indicating that the attenuation of the signaling via Chk1 facilitates the activity of the ncMMR/Polη pathway.

At first, these results seemed at odds with previous findings showing that Chk1 promotes TLS via Polη either via direct recruitment or by potentiating PCNA monoubiquitination [287-289]; in these studies, the activities of Chk1 observed upon treatment with hydroxyurea and/or UV irradiation are intrinsically linked to the process of lesion bypass during DNA replication. In this thesis we have shown that the ncMMR via Polη is active almost exclusively in the G_1 phase, therefore the different cell cycle phases in which these processes take place may account for the observed discrepancies.

We propose two complementary mechanisms by which the attenuation of the signaling via Chk1 can result in an increased A/T mutagenesis. As discussed in the previous chapters, Chk1 downregulation may lead to an ATM/Chk2-dependent cell cycle arrest at the G_1/S border in cells with persisting DNA damage; if this was proven to be the case, the uracils generated upon AID activity in the early G_1 phase would have more time to be detected and repaired by ncMMR/Polη and less uracils would persist till S/G_2. We found that uracils in S/G_2 are more likely to be replicated over and to be converted into TSs; consistently, the mutation frequency of TS mutations at C:G base pairs was found to be significantly lower in Chk1[Bhet] mice in comparison to the controls. The second hypothesis is that the ssDNA gaps generated in the course of repair via the ncMMR can be sensed by the ATR/Chk1 axis and this could limit the gap-filling via Polη. It was reported that the ATR/Chk1 axis can be activated by the MSH2-MSH6 mismatch recognition complex [353] and Chk1 itself has been found in a complex with MSH2 [354]. Furthermore, the ATR/Chk1 axis can sense and mitigate the replication stress accumulated in the course of the MMR-dependent processing of the DNA damage induced by alkylating agents [355]. Thus, the ssDNA stretches generated upon the ncMMR activity in hypermutating B cells can activate the signaling via ATR/Chk1, which could either initiate cell cycle arrest and apoptosis or mark the lesions for faithful repair via HR in the subsequent S phase of the cell cycle. In support to the hypothesis that a reduced Chk1-initiated apoptosis could contribute to the shown effects on the mutational pattern there are data from our group (unpublished data) showing that the deficiency of p53 leads to an increased A/T mutagenesis; another group reported higher mutations specifically at A in the absence of p53 [356]. In relation to the effects that Chk1 downregulation could have via HR, we found that the damage generated by the A/T mutator poses a high threat to the survival of hypermutating B cells in the absence of BRCA2 *in vivo* and since HR is limited to S/G_2, the ssDNA gaps must have access to this phase of the cell cycle [165]. We conclude that the attenuation of the signaling via Chk1 may favour A/T mutagenesis by prolonging the G_1 phase via ATM/Chk2 in cells carrying DNA damage and by increasing the tolerance of hypermutating B cells to the ncMMR-mediated damage (ssDNA intermediates) in G_1, therefore limiting the accessibility of those lesions to S/G_2 and their HR-mediated repair.

The same effects of Chk1 downregulation on the mutagenesis at A:T base pairs observed in the J_H4 intron were not recapitulated in the pre-Sμ region. It is known that in this region the ncMMR/Polη pathway contributes to a lesser extent to the mutagenesis than at the J_H4 intron. The typical bias observed at the J_H4 intron is reverted at the pre-Sμ region showing that mutations at A/T represent only ~45% of the total mutations [122, 146, 165]. It was reported

that the depletion of MSH6 or Polη significantly reduces the overall mutation frequency in the J_H4 intron but not in the pre-Sμ region where the C/G mutagenesis seems to compensate for the reduced mutations at A:T [146, 357]. Consistently, mutagenesis at A/T was not found to compensate for the reduced mutation frequency at C:G base pairs observed in UNG$^{-/-}$ mice at the pre-Sμ region [122].

Many reasons could account for the reduced activity of the A/T mutator at the pre-Sμ regions. The targeting of AID at the switch regions seems to be an early event upon B cell activation as it was shown that CSR is achieved even before the formation of the GC [58]. The expression levels of Polη may be low at this stage as they gradually increase following B cell activation reaching their peak in the DZ of mature GCs [57]. In the switch regions, the presence of overlapping, highly repetitive and palindromic motifs 5'-AGCT-3' facilitates the generation of R-loops during transcription and it has been suggested that this could limit the activity of the MSH2-MSH6 complex [122]. Additionally, it is reasonable that the processing of U:G mismatches by MMR at the switch regions may facilitate CSR over A/T mutagenesis: MMR excises nucleotides on one strand of the DNA and, as soon as the exonuclease would reach a nick on the opposite strand, its activity would terminate creating DSBs [160].

In light of the reduced contribution of the A/T mutator to the mutagenesis at the pre-Sμ regions, we believe that the effects of Chk1 downregulation may be masked by the presence of one functional *Chek1* allele.

3.1.5 Off-target mutagenesis is sustained in Chk1^{Bhet} mice

AID has been found to associate with thousands of genes outside the Ig loci and the mutagenesis in these off-targets is associated with oncogenic transformation and lymphomagenesis [358, 359]. The factors that determine AID occupancy on those off-targets are the same that recruit AID on the Ig genes, among which there is the accessibility of ssDNA exposed upon high levels of transcription and RNAPII stalling [124, 125]. However, among all genes AID can associate with, ~300 have been found mutated in normal B cells and the mutation frequency at these off-targets is much lower than at the Ig loci [133]. It was observed that the protection mediated by the error-free BER and MMR repair pathways is more effective at the off-targets than at the Ig loci [134] but the mechanisms behind the differential regulation of the repair pathway choice at different loci remain elusive.

We have proposed that a reduced proliferation and/or survival of GC B cells upon Chk1 downregulation may account for the reduced mutation frequency observed in the J_H4 intron and the pre-Sμ region. Interestingly, we found that the mutation frequency at the AID off-target

gene *Cd83* amplified from GC B cells in the PPs was not reduced in Chk1[Bhet] mice but was rather found to be comparable to the controls. If Chk1 did not have any additional role on the AID-induced mutagenesis at non-Ig genes, we may have observed a comparable reduction of the mutation frequency, given the significantly reduced survival of the B cells in chronic GCs upon Chk1 downregulation. Therefore, we speculate that Chk1 signaling attenuation may allow for higher mutagenesis at AID off-targets; this argument remains speculative, though, as we did not see a significant increase of the mutation frequency at the *Cd83* locus in Chk1[Bhet] mice and they did not develop lymphomas during the 5-6 months observation period.

Chk1 promotes the repair via HR and a reduced activation of HR via Chk1 may allow for higher mutagenesis at AID off-target genes, since HR contributes to the repair of DNA damage outside the Ig genes [167]. The increased cell death in the GCs from the PPs may have led to the loss of those clones showing an increased accumulation of mutations. In a comparable way, we found that the mutation frequency at the *Cd83* and *Bcl-6* loci was not perturbed in GC B cells upon inactivation of HR [165]. Due to the limitations posed by the reduced viability, a way to verify whether the inactivation of HR and the downregulation of Chk1 could truly increase off-target mutagenesis would be to compare the mutation frequency at the *Cd83* locus and/or other off-target genes to the mutation frequency at the variable region of the Ig loci from PP GC B cells but this kind of analysis is complicated by the multiclonality of the Ig rearrangements in B cells that respond to a variety of different antigens in the PPs.

3.1.6 Regulation of the ATR/Chk1 axis in the GC

The master regulator of the GC program Bcl-6 has been shown to control the expression of more than one thousand genes in GC B cells, modulating a multitude of functions including activation, proliferation, cell cycle arrest, DDR and differentiation [360]. The Bcl-6 gene represents a classical AID off-target [361]; the deregulation of its functions due to the accumulation of mutations or gene translocations is associated with the malignant transformation of the B cells leading to various forms of non-Hodgkin's lymphoma [362]. Given its role in the attenuation of the DDR, the aberrant expression of Bcl-6 may lead to a persistent tolerance of the DNA damage and may support the accumulation of additional oncogenic mutations, therefore the inhibition of Bcl-6 has recently emerged as an attractive therapeutic strategy for lymphoma [363].

In the LZ of the GC, the B cells recognize their cognate antigen retained on the surface of the FDCs and internalize it through the BCR for further presentation to the T_{FH} cells, which then provide survival signals likely proportional to the amount of antigen captured, depending on

the affinity of the BCR [51]. The signaling via the BCR has been shown to lead to a MAP kinase-mediated phosphorylation and degradation of the Bcl-6 transcription factor [364] and the activation of the CD40 signaling on the B cells activates the NF-κB pathway, which in turn leads to the disruption of the repression complex formed by Bcl-6 and the corepressor SMRT [365]. Therefore, in the LZ, the transcriptional repression mediated by Bcl-6 would be mitigated and this could lead to a restoration of the expression and the functions of the ATR/Chk1 axis. The reasons why the dependence of the B cells on the ATR/Chk1 signaling pathway would oscillate as the cells migrate from the DZ to the LZ of the GC are still unclear. For a long time, CSR was believed to occur in the LZ [366] and this could have explained the need for a functional DDR via Chk1, as discussed in 3.1.1, but due to the recent observation that CSR occurs infrequently in the GCs [58], this theory does no longer stand. We found that Chk1 signaling is activated by ssDNA stretches generated as intermediates for A/T mutagenesis; Polη is expressed at high levels in the DZ [57], therefore a DZ-specific downregulation of Chk1 would facilitate Polη activity. Another hypothesis is that a functional signaling via Chk1 in B cells that have been positively selected in the LZ could prevent the GC exit (as memory B cells or plasmablasts) of cells bearing DNA damage. In support to this argument, plasmablasts/plasma cells were found to express the highest levels of Chk1 when compared to immature, mature naïve, FZ/MZ and GC B cells [297].

Even though the signaling via the BCR and CD40 in the LZ is supposed to release the transcriptional repression of Chk1 mediated by Bcl-6, the transcriptional profile of centroblasts (DZ B cells) and centrocytes (LZ B cells) does not show differences in Chk1 expression between the two compartments and this is consistent across different studies [57, 367, 368]. The reasons for this discrepancy have not been discussed in the literature so far; the alleviation of the Chk1 transcriptional repression may be a transitional feature associated with an "intermediate phenotype" typical of intrazonal migrants or cells that are programmed to leave the GC. The results in this study suggest that a peculiar fine-tuning of the expression of Chk1 may be crucial to keep the Chk1 levels in check as the attenuation of the DDR allows for a better tolerance to the undergoing DNA damage but at the same time represents a threat to the survival of hypermutating B cells and may lead to malignant transformation.

3.2 Cell cycle-mediated regulation of secondary Ig diversification

3.2.1 Previous use of the Fucci system

The hypothesis that the mechanisms of secondary Ig diversification could be temporally regulated during the cell cycle has raised great interest in the scientific community and in the recent years different strategies have been used to shed light on this issue.

In the context of secondary Ig diversification, the Fucci system has been used for the first time in order to restrict the activity of UNG in the G_1 or the S/G_2 phase [291]; specifically, the GFP-conjugated uracil glycosylase inhibitor (ugi) was fused with the sequences encoding the degradation tags of the RAG2 and the hCdt1 proteins for a G_1-specific inhibition of UNG, and with the degradation tag of the mouse cyclin B2 to inhibit UNG activity in S/G_2. This strategy led to the observation that UNG excises AID-induced uracils predominantly in G_1 as the CSR ability and the frequency of TV mutations at C:G base pairs were found significantly reduced only upon UNG inhibition in G_1 [291]. As discussed in the next chapter, a later study has shown that uracils at the Ig loci accumulate predominantly in G_1 [85]; we believe that the paucity of AID-induced uracils in S/G_2 has limited the exploration of the activity of UNG in this phase of the cell cycle and may account for the observed effects.

In the study by Le *at al.*, the mCherry-conjugated AID was fused with the Cdt1 and Gem tags for the cell cycle-specific restriction of the activity of AID in G_1 or S/G_2, respectively, as performed in our study [130]. The authors expressed the AID fusion proteins in RAMOS cells and in primary mouse B cells and show that SHM and CSR are more efficient upon G_1-restriction of AID activity. The most critical points of this study are the following: The cell cycle-restricted AID proteins were expressed in the presence of the endogenous AID and the authors do not show whether the unrestricted AID-mCherry and the S/G_2-restricted AID proteins were able to induce SHM and CSR at levels higher than the ones induced by the endogenous AID, therefore there are no pieces of evidence that AID in combination with mCherry-hGem is actually functional. When the same S/G_2-restricted AID fusion protein was used by Zubani *et al.*, the construct was proven to have little or no detectable activity [150]. Despite the lack of proofs, these findings corroborated the idea that the activity of AID in the S/G_2 phase is negatively regulated and/or totally prevented, possibly due to the threat to the genome stability that the AID-induced DNA damage would pose during DNA replication.

In our study, the full-length AID and the $AID^{\Delta NES}$ proteins were fused with the original Fucci proteins developed by Sakaue-Sawano *et al.*, as the modification of the fluorescent protein in combination with the hCdt1 and hGem degrons was shown to affect the functionality of the

constructs [310]. Our G_1- and S/G_2-restricted AID and AID$^{\Delta NES}$ proteins showed a comparable activity in DT40 cells, they induced detectable levels of SHM above the used controls in RAMOS cells and were shown to equally affect the survival of primary mouse B cells. Our findings have the important implication that AID could potentially act throughout the cell cycle and that the S/G_2 phase does not represent, per se, a barrier to its activity, therefore other mechanisms must be responsible for the limited activity observed in S/G_2 in other studies, such as the regulation of AID subcellular localization, as discussed in the next chapter.

Even though the activity of AID outside G_1 does not seem to be a physiological event, the generation of uracils specifically in S/G_2 allows for the investigation of the cell cycle-mediated regulation of the downstream pathways of DNA repair leading to IgGC, SHM and CSR.

3.2.2 Activity and subcellular localization of AID

The first evidence that suggested a cell cycle-mediated regulation of the activity of AID was provided by the observation that in the hypermutating BL2 Burkitt's lymphoma cell line, the induction of IgM cross-linking initiates mutagenesis as a "single wave" event that could be detected not before 90 min from the stimulation [369]. In the attempt to clarify whether this time frame had any biological meaning, the authors sorted cells in different phases of the cell cycle, stimulated and analyzed them separately; they found that the process of hypermutation was initiated in G_1- and G_2/M-cells, but not in S-phase cells, and that the mutations were maintained only in G_1-stimulated cells, suggesting that the hypermutation is achieved in this phase of the cell cycle [369].

AID was found to be transcribed throughout the cell cycle [110]; its ability to detect and deaminate ssDNA is dependent on its association with RPA [115], which requires PKA-mediated phosphorylation of AID at the residue S38 [126]. Despite the essential role of RPA in protecting ssDNA during DNA replication, the hypermutation was not detected in S-phase-stimulated cells and the underlying mechanisms became of great interest.

More recently, the activity of AID at the Ig loci was measured by the detection of raw uracils in *in vitro*-cultured UNG-deficient primary B cells in different phases of the cell cycle, confirming that the G_1 phase is the main window for the activity of AID [85]. In line with previous studies [130, 131, 292], Wang *et al.* showed by time-lapse imaging that AID accumulates in the nucleus exclusively in G_1 and they propose that the breakdown of the nuclear membrane during the cell division enables AID, which is mainly present in the cytoplasm, to access the genome in mitosis, cytokinesis and shortly in the early G_1 phase, after which AID would be actively transported back to the cytoplasm [85]. The authors suggest that the

condensation of the chromatin would protect the DNA from AID attacking during mitosis, resulting in efficient AID targeting only in G_1. We and others [313] are sceptical that the proposed mechanism can alone explain the increased nuclear accumulation in G_1 because it leaves the open question of why a nuclear import mechanism for AID would have evolved if the accessibility to the nucleus may be granted by the dissolution of the nuclear membrane.

We measured the raw activity of AID in UNG$^{-/-}$ DT40 cells in which the only fate of AID-induced uracils is being replicated over generating TS mutations, since the lack of UNG prevents the diversification via IgGC and the A/T mutator is not active in this cell line [314]. The accumulation of TSs may lead to the generation of premature stop codons or induce aberrant conformational changes, which would result in the loss of the expression of sIgM. This event would normally result in B cell death [370, 371] but myc-driven lymphomas are able to induce a constitutive activation of the signaling downstream the BCR via PI3K, which abolishes the dependency on a functional BCR for their survival [372].

Both AID-G_1 and -S/G_2 proteins showed a much more pronounced nuclear accumulation (likely due to the presence of additional NLS on the Fucci degrons) than the AID-GFP control, which accumulates predominantly in the cytoplasm; the AID-G_1 and -S/G_2 constructs showed comparable activity both in terms of sIgM-loss and as mutation frequency at the $Ig\lambda$ locus and their activity was found to be higher than the AID-GFP control. Though, the activity of AID-G_1 was not found to be higher than the AID-S/G_2 counterpart even though the former almost completely localized in the nucleus while the latter seemed to uniformly distribute in both cytoplasmic/nuclear compartments; this may be due to modest differences in the catalytic activity of AID in combination with the Fucci probes. The activity of all AID$^{\Delta NES}$ proteins was higher than the relative full-length AID counterparts, as expected, and recapitulated the same findings. Our data show that AID can potentially act throughout the cell cycle and that its activity in S/G_2 is not prevented by mechanisms other than, eventually, the limitation of its nuclear accumulation.

Another process that could limit AID accumulation in the nucleus besides its active import/export is the degradation via the proteasome: the RING finger protein 126 was shown to be able to ubiquitylate AID [373] but no specific lysine residues could be linked to this degradation [110]. It has been shown that in RAMOS cells AID undergoes a faster nuclear degradation in S/G_2, possibly as a mechanism to prevent the higher threat to genome stability that its nuclear accumulation would pose during DNA replication [130]. Accordingly, we speculated that the sensibility of RAMOS cells to the DNA-damage may be higher upon nuclear accumulation of AID$^{\Delta NES}$ in S/G_2 as a consistent fraction of clonal populations analyzed had

either repressed the expression of AID$^{\Delta NES}$ or were found to be impaired in their clonal expansion; these data, though, certainly require a more thorough investigation.

3.2.3 IgGC is favored by recombination *in cis* initiated in G$_1$

The chicken lymphoma DT40 cells constitutively diversify their Ig genes in culture; the predominant mechanism of diversification is IgGC mediated by HR [374], even though some AID-induced lesion may lead to the generation of point mutations as during SHM [315].

HR is known to be limited to S/G$_2$ because of the availability of the sister chromatid, but other reasons account for the limitation of HR during the cell cycle: The activity of CDKs, which influences HR initiation, is low until the S phase and a mechanism of suppression of HR outside S/G$_2$ has been reported in the 293T human cell line [207-209]. Nevertheless, previous studies in DT40 have suggested that IgGC is initiated and may even be completed in G$_1$ [131, 292]. This hypothesis derives from indirect evidence among which are the more pronounced nuclear accumulation of AID and the presumed higher UNG activity in G$_1$, as previously discussed, but also the enhanced association of the factors E2A and Polη to the *Igλ* locus in G$_1$ [131, 292]. The transcription factor E2A was shown to stimulate IgGC in ways other than by promoting the transcription of the *Igλ* locus [102, 375]; Polη, which is the major contributor to the A/T mutagenesis during SHM in mice and humans, is instead required for IgGC in DT40 cells [376] due to its role played during HR in promoting DNA synthesis from strand invasion intermediates [377]. Due to these observations, the Meizels's group suggests that IgGC may be achieved even before the S-phase entry but they do not exclude the possibility that the association of E2A and Polη with the *Igλ* locus in G$_1$ could prepare the locus for events of IgGC that may occur later in the cell cycle [292]. Our data rather support the latter hypothesis.

We restricted the activity of AID and AID$^{\Delta NES}$ in G$_1$ or in S/G$_2$ in a DT40 cell line in which the sIgM expression is prevented by a frameshift mutation in the *Igλ* locus but it may be rescued by IgGC. The sIgM-gain assay revealed that IgGC is successfully triggered by uracils introduced in both phases of the cell cycle, even though it appears to be more efficient upon AID activity in G$_1$ as a faster appearance of revertant sIgM$^+$ was observed among AID/AID$^{\Delta NES}$-G$_1$-expressing cells. Since the sequencing data showed that lesions in both G$_1$ and S/G$_2$ triggered an equal number of "pure" IgGC tracks and HR is known to be active in S/G$_2$, we propose that IgGC is not limited to G$_1$ but is favored when it is initiated in this phase of the cell cycle.

E2A was found to associate with the rearranged but not with the unrearranged *Igλ* locus, therefore stimulating IgGC via a mechanism of recombination *in cis* [292]. If IgGC is initiated

in G_1 and eventually completed in the early S phase before the locus is replicated, an event of recombination with pseudogenes *in cis* would be favored given the absence of the sister chromatid. In support to this theory, there is evidence that the V_H gene sequences in mature mouse B cells replicate late in the S phase [378]. In late-S/G_2, the newly replicated V region could be used as template *in trans* instead of the pseudogenes, thus reducing the chances for an effective diversification. Therefore, we suggest that IgGC is initiated in G_1 and completed in the early S phase: IgGC factors such as E2A and Polη would associate with the *Igλ* locus in G_1 in an AID-independent and -dependent fashion, respectively, for a quick HR-mediated diversification *in cis* in the early S phase.

The fact that uracils generated by AID in S/G_2 can trigger IgGC has also another important implication: Since IgGC is dependent on UNG for the generation of SSBs or DSBs [314] and that Polη association with the *Igλ* locus occurs in an UNG-dependent manner [131], this means that the activity of UNG is not limited to G_1 as previously proposed and it confirms that the scarcity of uracils in S/G_2 in physiological settings has mislead previous interpretations.

Our sequencing results also show that, despite being able to induce IgGC in S/G_2, uracils that would still persist in this phase of the cell cycle are more likely to be converted into discrete mutations than trigger IgGC. We restricted the activity of AID$^{\Delta NES}$ in the hypermutating ΨV⁻ DT40 cells, which are unable to undergo IgGC, therefore they accumulate mutations as during SHM. We confirmed that in DT40 cells the S/G_2 phase represents the main window for the hypermutation mechanisms while error-free repair pathways, such as BER, may compensate for the absence of IgGC in G_1. Collectively, our data support a model in which IgGC is initiated in G_1 and completed in the early S phase via a mechanism of recombination *in cis* and that uracils that have escaped the detection and persist in S/G_2 would rather contribute to increasing the extent of the diversification via hypermutation.

3.2.4 AID activity in G_1 leads to the full spectrum of mutations during SHM

AID activity is limited to G_1 in physiological contexts and previous attempts to induce the activity of AID outside G_1 have not been successful, therefore it hasn't been possible so far to investigate whether and how SHM could be achieved in S/G_2. Nevertheless, the scientific community gathered around the idea of an almost entirely "G_1-phase model for SHM". Besides the presumed restriction to G_1 of the activity of UNG, previously discussed, additional evidence contributed to this theory.

The deoxynucleotide triphosphohydrolase SAMHD1 is an important restrictor of virus replication because of its activity in limiting the dNTP supply specifically in G_1 [379]; it was

shown that the inactivation of SAMHD1 *in vivo* leads to an increased frequency of TVs but not TSs at both A:T and C:G base pairs. Since Polη is referred to as the sole contributor to A/T mutagenesis during SHM [145] and that TVs at C:G are generated via TLS in a UNG-dependent manner, Thientosapol *et al.* concluded that those data provide evidence for the G_1-limited activity of both the A/T mutator via ncMMR/Polη and the C/G mutagenesis via UNG/TLS. We believe that these data are not sufficient to support these conclusions, as no S/G_2-specific events could be investigated in this study. The study from Pilzecker *et al.* has shown that the inactivation of the polymerase PrimPol, which prevents the generation of mutations during DNA replication in correspondence of uninstructive abasic sites [380], leads to a higher frequency of TVs at C:G base pairs [381] observed also by our group upon inactivation of HR [165], providing evidence for the activity of the UNG/TLS pathway in S/G_2.

In DT40 cells, our AID/AID$^{\Delta NES}$-Fucci proteins have shown to be suitable to investigate S/G_2-specific events of Ig diversification, therefore we expressed them in the human lymphoma cell line RAMOS for the investigation of the error-prone repair mechanisms acting in the course of SHM in different phases of the cell cycle. Our results revealed that SHM can be achieved efficiently upon AID activity both in G_1 and S/G_2. When we restricted the activity of AID$^{\Delta NES}$ during the cell cycle, both the sIgM-loss assay and the sequencing data showed that SHM was impaired in S/G_2, likely due to the increased toxicity upon the excessive nuclear accumulation of AID$^{\Delta NES}$ in S/G_2 in RAMOS cells as previously proposed [130].

We investigated the relative contribution of each repair pathway acting during SHM in the different phases of the cell cycle by analysis of the mutational pattern at the *IGH* locus. We found that the mutagenesis at A:T base pairs is almost completely restricted to G_1 while C/G mutagenesis can occur throughout the cell cycle, even though uracils in S/G_2 are more likely to be replicated over and generate TSs at C:G base pairs.

The fact that the activity of the ncMMR/Polη was observed almost exclusively in G_1 may indicate that it is prevented in S/G_2; as discussed in the chapter 3.1.4, the MMR-generated ssDNA intermediates can be sensed by the Chk1 signaling pathway, which could stimulate the repair via HR, therefore it is conceivable that the temporal restriction of the A/T mutagenesis to G_1 is due to suppression by HR in S/G_2. Polη is recruited at sites of replication stress by the monoubiquitinated PCNA; it has been proposed that the source of replication stress in correspondence of the MMR-generated ssDNA stretches could be ascribed to the paucity of dNTPs in G_1 [295].

Even though C/G mutagenesis can be achieved throughout the cell cycle, only the activity of AID in G_1 leads to an equal proportion of TVs and TSs, because in S/G_2 the replication across

the uracils skews the mutation pattern towards TSs over TVs at C:G base pairs; our results in combination with previous observations support the idea that the TLS across abasic sites generated upon UNG/APE activity is not limited during the cell cycle.

We conclude that the nuclear accumulation of AID in G_1 is better tolerated, at least in the human B cell line RAMOS, and that uracils generated in G_1 induce to the full spectrum of mutations observed during SHM, leading to mutations at A:T and to equal TVs and TSs at C:G base pairs.

3.2.5 CSR requires AID activity in G_1

It has been observed that when *in vitro*-cultured mouse B cells are stimulated to perform CSR to IgG1, DSBs at the Sμ region are generated and detected in G_1 [293]. The process of NHEJ, known to be the main mechanism of repair of DSBs in the G_1 phase, seems to accomplish CSR at the G_1/S transition border [294, 342]. The completion of CSR immediately upon S-phase entry may be crucial because the presence of the sister chromatid would allow for an HR-mediated repair, which would prevent the diversification of the Ig heavy chain. In support to this argument, HR carries out the repair at the Ig locus of DSBs that have not been detected in G_1 and that persist till S/G_2 [168]; DSBs at AID off-target genes are also mainly repaired via HR [167].

Nevertheless, the fate of S/G_2-generated DSBs at the Ig locus could not be assessed so far, therefore we wished to investigate whether CSR could still be achieved upon AID activity in S/G_2 or would rather be completely suppressed by HR. We expressed the AID-G_1 and -S/G_2 fusion proteins in primary mouse B cells stimulated *in vitro* to perform CSR to IgG1: We could verify that CSR requires AID activity in G_1, as no specific events of diversification were observed upon AID activity in S/G_2.

An HR-mediated suppression of CSR in S/G_2, though, is not the only reason behind the temporal regulation of CSR during the cell cycle: It has been found that S-phase entry is necessary for CSR to occur as the firing of DNA replication origins in the proximity of recombining switch regions is required for efficient long-range (up to ~200kb) synapsis formed by the interaction of the Eμ and 3'RR enhancers [294]. DSBs generated at the Ig locus post-replication would have less chances to be properly joined as the topological association between the recombining regions may not be properly achieved. The detection of the DSBs in G_1 by NHEJ factors is believed to be indispensable for a quick recombination upon S-phase entry, before the C gene segments are replicated, which was reported to occur early in the S phase [378].

3.3 Secondary Ig diversification: an integrated view

The main findings of the present study are illustrated in Figure 26.

The downregulation of the DDR via Chk1 allows the hypermutating B cells to tolerate the undergoing DNA damage and, in particular, the damage induced in the course of repair via ncMMR/Polη in the G_1 phase of the cell cycle.

The restriction of the activity of AID to G_1 observed in physiological contexts suffices for all the mechanisms of secondary Ig diversification: it facilitates IgGC promoting a mechanism of recombination *in cis*, it leads to the generation of the full spectrum of mutations during SHM and allows for NHEJ-mediated repair during CSR. The temporal restriction of many of the processes of diversification to G_1 or to the early S phase may, on the one hand, allow to circumvent HR-repair at the Ig locus and, on the other hand, give a second chance to unrepaired lesions at the Ig locus and at off-targets to be repaired in an error-free way in S/G_2.
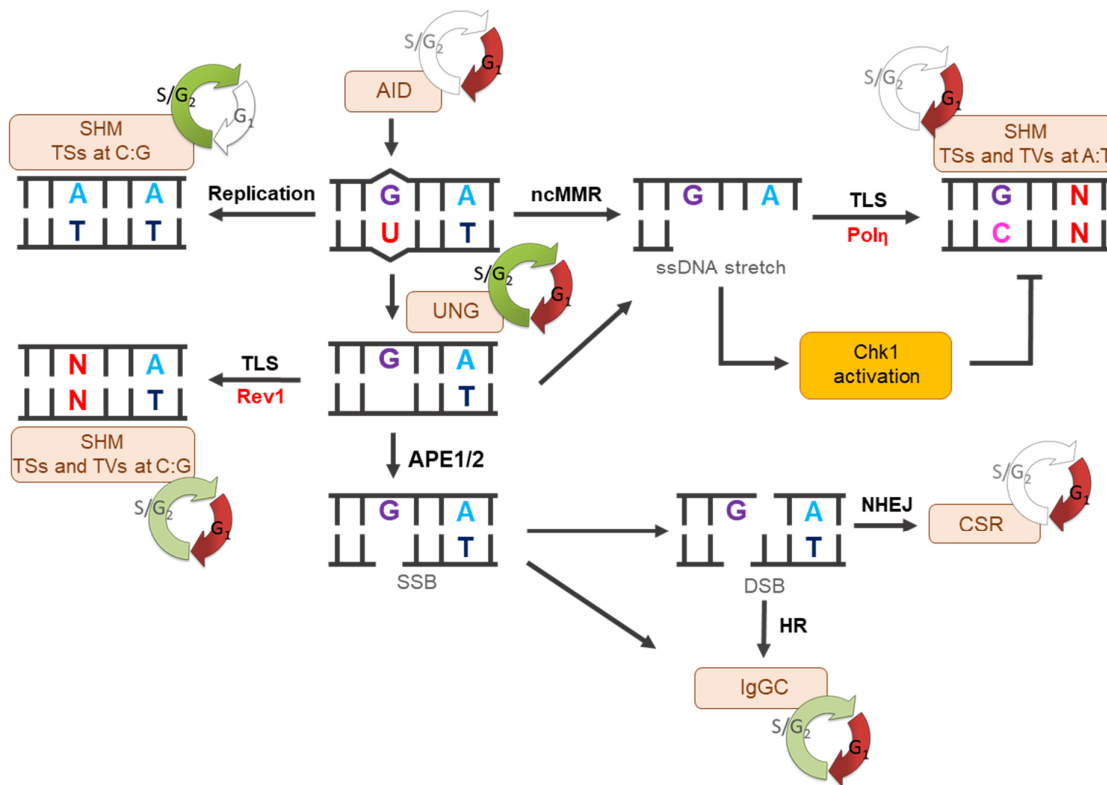
Figure 26: Role of the signaling via Chk1 and the cell cycle during secondary Ig diversification.
Chk1 activation by ssDNA stretches generated in the course of ncMMR activity promotes repair via HR and sensitizes the cells to DNA damage-induced cell cycle arrest and apoptosis, resulting in a decreased A/T mutagenesis.
AID acts exclusively in G_1 in physiological contexts. During SHM, A/T mutagenesis is accomplished in G_1, UNG acts throughout the cell cycle, TLS via Rev1 is not limited during the cell cycle but is more efficient in G_1, TSs at C:G base pairs are associated with the process of replication limited to S/G_2. CSR is initiated in G_1 and completed immediately after the G_1/S transition. IgGC can occur throughout the cell cycle but is facilitated when initiated in G_1.
Figure adapted from Di Noia and Neuberger [70].

3.4 Outlook

The Bcl-6-mediated attenuation of DDR in the GC is supposed to increase the tolerance of the hypermutating B cells to the undergoing DNA damage; we found that a further downregulation of the DDR via Chk1 in not beneficial for the survival of the GC in long terms. In acutely induced GC upon immunization these effects were not as clear as in chronic GCs in the PPs and we speculated that a slowdown of the proliferation due to Chk1-independent cell cycle arrest may justify the reduced accumulation of mutations during SHM. It would be highly interesting to confirm this hypothesis by analyzing the cell cycle profile of the B cells in acute GCs and identify the factors involved for the presumed cell cycle arrest.

The replication stress induced by the processing of AID-induced DNA lesions may be worsened by further downregulation of Chk1; the assessment of the amount of replication fork stalling in the GCs of Chk1^{Bhet} mice could help clarifying the mechanisms underlying the dependence of SHM on an attenuated but still functional Chk1 signaling.

We showed that in the course of the A/T mutagenesis, the Chk1 signaling is activated upon ssDNA stretches generated as intermediates for Polη-mediated gap-filling; Polη reaches its peak of expression in the DZ of the GC [57], therefore an analysis of the architecture of the GC by a staining of the GC DZ/LZ in Chk1^{Bhet} mice could reveal the reasons why the DDR via ATR/Chk1 is supposed to be more strongly repressed in the DZ.

The activity of AID has been shown to be limited to G_1 due to a cell cycle-mediated regulation of its nuclear accumulation. The mechanisms behind the more pronounced active import in G_1 and active export in S/G_2 are yet unknown. The AID-Fucci contructs have proven not to be suitable for the investigation of these mechanisms due to the presence in the Fucci degrons of NLSs that are required for their proper functionality. An analysis of the association of AID during the cell cycle with proteins involved in its nuclear/cytoplasmic shuttle, such as karyopherins and the exportin CRM1, may help address this issue. A possible role mediated by cell-cycle regulated CDKs in these processes could also be explored.

The regulation of AID nuclear accumulation is mediated also by the DNA damage: a study from our group has shown that AID accumulates in the nucleus of lymphoma cells upon the activation of the DNA damage sensor PARP-1 [382]. It would be highly interesting to investigate whether the DNA damage itself could play different roles during the cell cycle in the regulation of AID nuclear accumulation.

In S/G$_2$, a higher nuclear degradation of AID has been observed [130]; our data in RAMOS cells support the theory that an excessive nuclear accumulation of AID in S/G$_2$ is not well tolerated. The AID$^{\Delta NES}$-S/G$_2$ fusion protein could be used to explore the extent and the nature of the DNA damage induced by AID in the course of the DNA replication. A research in this direction may link a deregulation of AID during the cell cycle with the malignant transformation of hypermutating B cells.

4 Materials and Methods

4.1 Mice

4.1.1 Breeding and genotyping

Chk1^{fl} mice were generated in the Jeffrey M. Rosen lab [298] and obtained from the Jackson Laboratory. Mb1^{Cre} mice were obtained from Dr. C. Kosan with permission of M. Reth [299]. Chk1$^{fl/+}$ and Mb1$^{Cre/+}$ are on a C57BL/6 background and were intercrossed to generate Chk1$^{+/+}$Mb1$^{Cre/+}$, Chk1$^{fl/+}$Mb1$^{+/+}$ and Chk1$^{fl/+}$Mb1$^{Cre/+}$ mice for experiments. The genotyping was performed by the amplification of the *Chek1* locus with the primers Chk1^{fl}-fwd and Chk1^{fl}-rev and the amplification of the *Mb1* locus with the primers Mb1-fwd and Mb1-rev. The PCR reactions were performed on genomic DNA isolated from mouse tails. B cell-specific recombination of the *Chek1* locus in Chk1$^{fl/+}$Mb1$^{Cre/+}$ mice was verified on genomic DNA from tails and sorted non-GC splenic B cells (see chapter 4.3.3): the primer Chk1-R3 was used in combination to the genotyping primers in order to detect the Cre-mediated deletion.

AID$^{-/-}$ mouse embryos generated by Tasuku Honjo [26] were obtained from the RIKEN BioResource Center (Tsukuba, Japan) and implanted in C57BL/6 mice in the Forschungszentrm Lobeda (FZL) of the Universitätsklinikum Jena. First generation AID$^{-/-}$ mice were transferred to the Service Unit for Experimental Biomedicine of the Friedrich Schiller University Jena and intercrossed in-house with C57BL/6 mice from Janvier Labs; AID$^{+/-}$ mice were intercrossed to generate AID$^{-/-}$ mice for experiments. The genotyping was performed by the amplification of the *Aicda* locus with the primers mAID-1, mAID-2, mAID-3 and mAID-4 on genomic DNA isolated from tails.

All primer sequences and PCR conditions are illustrated in Table 2 and Table 3, respectively.

All mice were bred in specific pathogen-free conditions in the Service Unit for Experimental Biomedicine of the Friedrich Schiller University Jena. Female and male littermates were used without discrimination in all experiments but the immunization experiments (see chapter 4.1.2). All the breedings and the animal experiments were approved by the Thüringer Landesamt für Verbraucherschutz.

4.1.2 Immunization with NP-CGG and organ collection

Immunization was performed by peritoneal injection of 100µg of NP-CGG; five independent immunization experiments have been performed: In each experiment, two experimental mice (one Chk1$^{+/+}$Mb1$^{Cre/+}$ and one Chk1$^{fl/+}$Mb1$^{Cre/+}$ mouse) were immunized and one Chk1$^{+/+}$Mb1$^{Cre/+}$

mouse was used as nonimmunized (n.i.) control; within each experiment, 8- to 12-week-old mice of the same gender were used and preferably littermates. Blood samples were collected 7- and 14-days post-immunization from immunized and n.i. mice by punctuation of the *vena facialis*. At day 14 post-immunization, the mice were sacrificed by cervical dislocation for spleen collection.

Mice were sacrificed by cervical dislocation at the age of 6- to 18-week-old for bone marrow and spleen collection and at the age of 24- to 30-week-old for Peyer's patches collection. The spleen was placed in PBS after dissection; the gut was inspected from the duodenum to the ceacum for Peyer's patch detections.

4.2 Cell culture methods

4.2.1 Plasmids

Sequences coding for the Fucci probes mKO2-hCdt1 (Fucci-G_1) and mAG-hGem (Fucci-S/G_2) were provided by A. Sakaue-Sawano [310] in the pcDNA3.1 plasmid backbone. The sequence coding for the human AID, in its full length or lacking the last 14 amino acids at the C-terminus (AID$^{\Delta NES}$) were cloned by Voigt S. into the Fucci plasmids generating AID/AID$^{\Delta NES}$-G_1 and AID/AID$^{\Delta NES}$-S/G_2 coding sequences. The pCAGGs vectors [383] containing HA-AID/AID$^{\Delta NES}$-GFP were obtained from J. Bachl.

The Fucci-conjugated AID/AID$^{\Delta NES}$ sequences and/or the HA-AID/AID$^{\Delta NES}$-GFP control sequences were cloned into: i) the pcDNA3.1 vector for expression of the fusion proteins in DT40 and CH12F3 cell lines driven by the CMV promoter; ii) the pCAGGS vector for expression in RAMOS cells driven by the chicken β-actin promoter (CMV promoter is known to be repressed in RAMOS cells); iii) the NGFR retroviral vector [323] for the generation of viral particles from Platinum-E (Plat-E) cells and subsequent infection of mouse primary B cells. Plasmid DNA was amplified and purified with NucleoBond Xtra Maxi Kit.

AID CRISPR/Cas9 KO Plasmid comprises a pool of three plasmids encoding for three different gRNAs and was purchased ready-to-use (Santa Cruz Biotechnology); the plasmid pool was used to knockout the expression of AID in RAMOS cells.

4.2.2 Culture and transfection of lymphocyte B cell lines

The DT40 cell line is an ALV-induced bursal B-cell lymphoma line; AID$^{-/-}$ UNG$^{-/-}$ DT40 cells obtained from H. Saribasak [84], AID$^{-/-}$ DT40^{Cre1} and AID$^{-/-}$ ΨV$^-$ DT40 cells obtained from H.

Arekawa [316] were cultured at 41°C and 5% CO_2 in chicken B cell medium and fed every 2-3 days at a cell density of 2-5x10^5 cells/ml. The CH12F3 is a mouse B lymphocyte cell line. CH12F3 cells were cultured at 37°C and 5% CO_2 in mouse B cell medium and fed every 2-3 days at a cell density of 3-10x10^4 cells/ml. The RAMOS cell line is a human Burkitt's lymphoma cell line. RAMOS cells were cultured at 37°C and 5% CO_2 in human B cell medium and fed every 2-3 days at a cell density of 2-5x10^5 cells/ml.

Individual clonal populations were generated prior to transfection; the cell density was adjusted to 10 cells/ml and the cells were seeded in 96-well plates (100µl/well). The single-cell clones were collected 7- to 14-days after seeding.

DT40, CH12F3 and RAMOS cells were pelleted, washed and resuspended in 500µl of PBS; the DNA was linearized with ScaI for stable transfection, precipitated in 100% EtOH, washed in 70% EtOH and resuspended in 300µl of PBS. The cells and the DNA suspension were mixed and incubated on ice for 10-20 min. The cell/DNA suspension was transferred to certified cuvettes and the transfection was performed by electroporation with a Gene Pulser Xcell™ (Bio-Rad); the electroporated cells were seeded in 96-well plates for the generation of individual subclonal populations (100µl/well) and 24 hours post-transfection the medium was supplemented with the appropriate antibiotic for the selection of the transfected cells. The single-cell subclones were harvested 7- to 18- days post-transfection. The specifications regarding the transfection conditions in the individual cell lines are illustrated in Table 1.

Table 1: Protocols for stable transfection in B lymphocyte cell lines by electroporation

Cell line	Cells	DNA	Vector	µF/V	Selection	Days
DT40	1x10^7	50µg	pcDNA3.1	50/800	Zeocin (300µg/ml)	7 to 10
CH12F3	2x10^6	20µg	pcDNA3.1	400/400	Zeocin (300µg/ml)	10 to 12
RAMOS	1x10^7	50µg	pCAGGS	975/250	Puromycin (0,5µg/ml)	14 to 18

Number of cells and amount of DNA per transfection are indicated. The vector indicates the plasmid backbone used for ectopic expression of AID- and/or AID$^{\Delta NES}$-GFP and -Fucci proteins in each cell line. µF/V indicates the protocol for the electroporation the Gene Pulser Xcell™ electroporation system (µF: capacitance, V: voltage). The final concentration of the antibiotics used for the selection of transfected cells is shown. Single-cell subclones are harvested in the indicated time range post-transfection.

RAMOS cells were transiently transfected with AID CRISPR/Cas9 KO Plasmid using Amaxa® Cell Line Nucleofector® Kit V (Lonza) according to manufacturer instructions for the generation of AID^{KO} RAMOS cells. The cells were cultured for 24 hours and the transfected cells were sorted as described in 4.3.5. After sorting, the cell density was adjusted to 10cells/ml for the generation of individual clonal populations in 96-well plates (100µl/well). The single-cell clones were harvested 10-12 days post-transfection.

The BJAB cell line is a human B lymphoma cell line used in this study as negative control for AID expression in WB analysis. BJAB cells were cultured at 37°C and 5% CO_2 in human B cell medium and fed every 2-3 days at a cell density of $5\text{-}7\times10^5$ cells/ml.

4.2.3 Culture of packaging Plat-E cells and generation of viral particles

Viral particles for retroviral transduction of mouse primary B cells were obtained transfecting the packaging Plat-E cells [384] with NGFR retroviral vectors. Plat-E cells were cultured at 37°C and 5% CO_2 in complete Plat-E medium. Plat-E cells were mechanically released from the plates when 70-80% confluent and were plated at a cell density of $2\text{-}4\times10^5$ cells/ml in 10ml in 100x20mm cell culture dishes every 2-3 days.

For the generation of viral particles, 4×10^6 cells were plated in complete medium in 100x20mm cell culture dishes. 24 hours after plating, the medium was replaced with medium without antibiotics (puromycin and blasticidin) for transient transfection with Bimake DNA Transfection Reagent according to manufacturer instructions. The cells were incubated at 37°C for 4-6 hours prior to changing the medium to mouse B cell medium (12ml per plate). After 48 hours incubation, the medium was collected and the viral particles were concentrated with Amicon® Ultra-15 Centrifugal Filter Devices (30kDa filter device). The samples were centrifuged at 5000xg for 10min (RT) to obtain 500µL of high-titer viral particles, which were subsequently diluted in 2ml mouse B cell medium.

4.2.4 Purification, culture and transduction of splenic primary B cells

To obtain a splenic single cell suspension, the spleens were smashed through 70µm strainers, incubated in red blood cell lysis buffer and filtered again through a 40µm strainer. The B cells were purified from the splenic single cell suspension by MACS depletion with α-CD43 beads according to manufacturer instructions. The cell suspension was applied to LS columns that were placed in a MACS separator; the α-CD43-labelled cells attached to the columns were discarded and the B cells were collected in the flow-through in PBA-E, washed, and resuspended in RPMI. The purity of the B cell population was assessed by flow cytometry staining the cell suspension before and after the MACS depletion (see chapter 4.3.1, T vs B cell staining) and a purity of ~90-95% was achieved in all the experiments.

Splenic primary B cells were cultured at 37°C and 5% CO_2.

B cells from Chk1[BWT] and Chk1[Bhet] mice were seeded at the density of $5x10^5$ cells/ml in mouse B cell medium; LPS (10 µg/ml), α-CD40 (1 µg/ml) and IL-4 (20 ng/ml) were added to the culture medium 1 hour after seeding.

B cells from AID^{-/-} mice were seeded at the density of $1x10^6$ cells/ml in mouse B cell medium. LPS (10 µg/ml) was added to the culture 1 hour after seeding; after 48 hours, the LPS was removed by centrifugation and the B cells were resuspended in half of the initial volume in mouse B cell medium for retroviral transduction by spin infection. The spin infection was performed in 6-well plates: The B cells (1 ml) were infected with viral particles (1 ml) by centrifugation at 1000xg for 90 min (RT). After the infection, 3 ml of mouse B cell medium were added to the cell suspension; the medium was supplemented with α-CD40 (1 µg/ml) and IL-4 (20 ng/ml).

4.3 Flow cytometry and FACS

4.3.1 B cell subsets in Chk1[BWT] and Chk1[Bhet] mice

Bone marrow B cells were obtained from the femur and tibia of both hind legs; the bones were cut behind the joint on both end and the inner cavities were rinsed with RPMI medium with 5% FCS. The cells were pelleted directly and the whole sample was stained for pro-B, pre-B, mature, and immature B cell markers with α-B220-BV786, α-IgM-APC, α-CD43-FITC, and DAPI in PBA-E. The staining of MZ vs FZ B cells in the spleen was performed on 10^6 cells from the splenic single cell suspension (see 4.2.4) with α-B200-BV786, α-CD21-FITC, α-CD23-PE and DAPI in PBA-E. The T vs B cell ratio was assessed on 10^6 cells from the splenic single cell suspension and on 10^6 cells from the B cell suspension after the MACS depletion (see 4.2.4) with α-B220-FITC, α-CD3-PE, and DAPI in PBA-E.

Flow cytometry data were acquired from cells resuspended in PBS 1% BSA with an LSR Fortessa (BD Biosciences) using the FACSDiva software (BD Biosciences); the data were further analyzed with FlowJo (FlowJo, LLC).

4.3.2 CSR and proliferation of *in vitro*-cultured primary B cells

Viability and CSR of *in vitro*-cultured Chk1[BWT] and Chk1[Bhet] mouse B cells were assessed after 72 and 96 hours in culture by staining with α-IgG1-DyLight405 and Fixable Viability Stain 780 (FVS780) in PBS 1% FCS. For the analysis of the proliferation via CFSE staining, the *ex vivo*-isolated splenic B cells ($5x10^6$ cells/ml) were stained with 1µM CFSE and washed in RPMI

before seeding as described in 4.2.4; after 24 and 72 hours in culture, the B cells were stained with α-B220-PE and FVS780 in PBS 1% FCS.

CSR on AID$^{-/-}$ mouse B cells infected with retroviral particles for the expression of AID-GFP, AID-Fucci or the negative control (empty NGFR vector) was measured 72 hours after spin infection; the B cells were stained with α-LNGFR-APC, α-IgG1-DyLight405, and FVS780 in PBS 1% FCS. The fluorescence deriving from the GFP/mAG and mKO2 fluorescent proteins was detected in the FITC and PE channel, respectively.

Flow cytometry data were acquired from cells resuspended in PBS 1% FCS with an LSR Fortessa (BD Biosciences) using the FACSDiva software (BD Biosciences); the data were further analyzed with FlowJo (FlowJo, LLC).

4.3.3 Sorting of GC B cells from Chk1^{BWT} and Chk1^{Bhet} mice

For sorting of splenic GC B cells of immunized mice, the whole B cell suspension obtained by MACS depletion of CD43$^+$ cells from the splenic single cell suspension (see 4.2.4) was stained with α-B220-PerCP, PNA-FITC, α-CD95-PE, and DAPI in PBA-E.

For sorting of GC B cells from Peyer's patches (PP), three to eight patches per mouse were smashed through a 70μm strainer and the cells were resuspended in PBA-E. The whole cell suspension was stained with α-B220-BV786, PNA-FITC, α-CD95-PE and DAPI in PBA-E. Cells resuspended in PBA-E were sorted by the FACS facility staff of the Leibniz Institute on Ageing (Fritz Lipmann Institute) in Jena on a FACSAria (BD Biosciences) using the FACSDiva software (BD Biosciences). The purity of the sorted population was confirmed by re-analyzing the sorted samples; the flow cytometry data were further analyzed with FlowJo (FlowJo, LLC). Sorted GC and, eventually, non-GC B cells were collected in PBS 1% BSA, pelleted and stored at -20°C for sequencing analyses (see chapter 4.6).

4.3.4 Cell cycle profile and sIgM expression of lymphocyte B cell lines

The cell cycle profile of lymphocyte B cell lines (DT40, CH12F3 and RAMOS cells) was analyzed by staining the cells for their DNA content with Hoechst33342 in the respective medium. The cells were washed and resuspended in PBS 1% FCS for flow cytometry analysis. Since Hoechst33342 is incorporated by alive cells, no dead/alive staining was performed. The fluorescence deriving from the GFP/mAG and mKO2 fluorescent proteins was detected in the FITC and PE channel respectively.

The analysis of the sIgM expression of DT40 cells was performed by incubating individual clonal population with α-IgM-biotin in PBS 1% FCS; after washing, the cells were stained with streptavidin-APC and FVS780 in PBS 1% FCS. The analysis of the sIgM expression of RAMOS cells was performed by staining individual clonal populations with α-IgM-APC and FVS780 in PBS 1% FCS.

The fluorescence deriving from the GFP/mAG and mKO2 fluorescent proteins was verified for each clonal population; the subclones transfected with AID/AID$^{\Delta NES}$-GFP and -Fucci that never showed expression of the respective fluorescent proteins were discarded.

Flow cytometry data were acquired from cells resuspended in PBS 1% FCS with an LSR Fortessa (BD Biosciences) and a coupled High Throughput Sampler (BD Biosciences) using the FACSDiva software (BD Biosciences); the data were further analyzed with FlowJo (FlowJo, LLC).

4.3.5 Sorting of RAMOS cells expressing AID CRISPR/Cas9 KO plasmids

RAMOS cells transiently transfected with AID CRISPR/Cas9 KO Plasmid and cultured for 24 hours were collected and stained with α-IgM-APC and DAPI in PBS 1% FCS. The transfected cells were detected by the expression of the GFP fluorescent protein; living (DAPI⁻) sIgM⁺ GFP⁺ RAMOS cells were sorted by the FACS facility staff of the Leibniz Institute on Ageing (Fritz Lipmann Institute) in Jena on a FACSAria (BD Biosciences) using the FACSDiva software (BD Biosciences) and were resuspended in human B cell medium after the sorting.

4.4 Western Blot

The cells (freshly MACS-purified splenic B cells, DT40 or RAMOS cells) were lysed by sonication (Sonicator UW70, Bandelin electronic) in Bäuerle buffer with protease and phosphatase inhibitors. The protein quantification was performed using the Bio-Rad DC Protein Assay. The protein samples (50µg) were denatured in the appropriate amount of sample buffer and then separated by SDS-PAGE (12% acrylamide gel) in Laemmli buffer. The proteins were transferred to PVDF membranes pre-activated in methanol at constant 450 mA for 1h (4°C) in blotting buffer. The efficient protein transfer was visualized using Ponceau S solution. The primary antibodies α-Chk1, α-AID (L7E7), and α-vinculin were diluted in 5% milk TBST and the primary antibody α-tubulin was diluted in 5% milk PBS. The HRP-conjugated α-mouse IgG diluted in 5% milk TBST was used as secondary antibody for the detection of Chk1, AID and vinculin, and the HRP-conjugated α-rabbit IgG diluted in 5% milk TBST was used as secondary

antibody for the detection of tubulin. The proteins were detected by chemoluminescence using ECL™ Western Blotting Reagents and the chemoluminescence was imprinted on X-ray films. The quantification of the band intensities was performed with the ImageJ software [385] (ImageJ developers).

4.5 ELISA

To assess the titers of circulating NP-binding IgG1 in immunized and non-immunized mice, serum was extracted from blood samples collected at day 7 and 14 post-immunization. ELISA plates were coated with NP_3 and NP_{15} diluted in carbonate buffer (5µg/ml). Serum samples were diluted 1:100 (day 7) and 1:500 (day 14) in 1% (powdered) milk PBS. As standard, a pooled serum control from NP-CGG immunized mice (C57BL/6 mice) was used for the detection of NP_{15} and diluted 1:400 in 1% milk PBS. For each sample, serial dilutions 1:2 of the initial dilution were applied to the plates (eight dilutions from 1:1 to 1:128). NP-binding antibodies were detected using an α-IgG_1-biotin primary antibody and streptavidin-HRP diluted in 1% milk PBS, and substrate buffer. The reaction catalysed by HRP was stopped adding 3N HCl and the absorbance was measured at 493 nm in an ELISA plate reader (Tecan Deutschland GmbH).

4.6 Sequencing analyses

4.6.1 Isolation of genomic DNA and PCRs

GC and, eventually, non-GC mouse B cells sorted as in 4.3.3 from spleens (from mice immunized with NP-CGG) and Peyer's patches (from unchallenged mice) were digested with lysis buffer (10mM Tris with 0,5µg/µl proteinase K) at 50°C for 4 hours; the digestion was stopped by incubating the lysates at 95°C for 10 min. The J_H4 intron and pre-Sµ region were amplified from splenic GC and non-GC B cells; the *Cd83* locus was amplified from Peyer's patch GC B cells. The J_H4 intron was amplified with the primers V186.2-fwd and JH4-rev; the pre-Sµ region was amplified with the primers pre-Sµ-fwd and pre-Sµ-rev; the *Cd83* locus was amplified with the primers Cd83-fwd and Cd83-rev. DT40 cells (representative clonal populations chosen as explained in 2.2.3) were digested with lysis buffer (10mM Tris with 0,25µg/µl proteinase K) as for GC and non-GC mouse B cells. The rearranged VJ region of the *Igλ* locus was amplified with the primers λ1 and C2.

The genomic DNA was isolated from RAMOS cells with QIAamp DNA Mini Kit. The *AICDA* locus was amplified from single-cell clones generated after the sorting described in 4.3.5 with the primers AID-Exon1-fwd and AID-Exon5-rev. The rearranged V_HDJ_H region was sequenced with the primers Primer1-f and Intron3-r.

All PCR reactions but the *AICDA* PCR were performed using Phusion High Fidelity DNA Polymerase; the *AICDA* PCR was performed with Expand Long Template PCR System. The primer sequences and the PCR conditions are illustrated in Table 2 and 3, respectively.

4.6.2 Cloning, amplification in *E.coli* and sequencing

The PCR products obtained as in 4.6.1 were resolved by electrophoresis and the bands of the expected size were excised (~1000bp for J_H4, pre-Sμ and Cd83; 1500bp for the chicken VJ region; ~9250bp for the human *AICDA* in AID$^+$ RAMOS cells and ~1500bp from the AID^{KO} RAMOS cells; ~1500bp for the human V_HDJ_H region from RAMOS cells). The amplification products were purified with Nucleo Spin Gel and PCR Clean-Up Kit. A-tailing of the PCR products prior to cloning into the pGEM-T vector was performed by incubation with A-tailing solution at 68°C for 30 min. The A-tailed PCR products were purified and the cloning was performed with the pGEMT vector kit. DH5alpha electro-competent *E. coli* were electroporated with purified ligated products: 100μl of *E.coli* was transformed in certified cuvettes at 2.5 kV, 25 μF and 200 Ω with a Gene Pulser Xcell™ (Bio-Rad). After a short incubation in SOC medium, the bacteria were plated on LB 1,5% Agar plates with 10μg/ml ampicillin, 1mM IPTG and 20μg/ml X-gal for blue/white selection (proper insert integration into pGEM-T). Single white colonies were picked and expanded o.n. in LB medium with 10μg/ml ampicillin. The cells were pelleted, resuspended in E1 buffer and lysed in E2 buffer; the lysates were cleared in E3 buffer. The DNA was precipitated and the dried DNA pellets were resuspended in H_2O for subsequent sequencing analysis.

Sanger sequencing of the DNA samples was performed by Eurofins Genomics (Ebersberg); the DNA and the sequencing primers were diluted in H_2O according to the company's instructions. The primers used for sequencing were: J_H4-rev, Pre-Sμ-rev, Cd83-fwd, λ2, AID-Exon3-rev and VHLeader-Sequ. The sequences obtained were aligned and processed with the software Geneious (Biomatters) and the analysis of mutagenesis was performed using the SHMTool (http://shmtool.montefiore.org/cgi-bin/p1) [386]. The analysis of the W33L mutations in the J_H4 sequences was performed with the IMGT "V-Quest" tool [387] (http://www.imgt.org).

4.7 Fluorescence microscopy

In order to analyze the subcellular localization of GFP- and Fucci-conjugated AID/AID$^{\Delta NES}$ proteins, the cells were seeded on poly-L-lysine-coated glass coverslips. The cells were fixed in 2% PFA PBS, permeabilized in 0,15% Triton-X-100 PBS and stained with DAPI. The coverslips were mounted onto the microscopy slides with Mowiol.

The pictures were captured on a ZEISS ApoTome microscope with a Plan-Apochromat 63×/1.40 Oil DIC M27 objective and processed with ZEN 2.6 Software (Zeiss).

4.8 Statistical analyses

Prior to the analysis, the D'Agostino & Pearson's test was performed to assess whether the values of each data set were normally or non-normally distributed (gaussian distribution) and the F-test was used to assess homoscedasticity and heteroscedasticity, when needed.

The statistical significance of the difference between two data sets was obtained with the following tests: i) two-sided ratio paired t test was performed to assess whether the ratio of paired values was consistent; ii) two-sided Student's t test (parametric test) was performed for sets of normally distributed and homoscedastic values; iii) two-sided Mann-Whitney test (non-parametric test) was performed for sets of non-normally distributed values to compare ranks of distribution.

The statistical significance of the difference between more than two data sets was obtained with the following tests: i) one-way (one variable) or two-way (two variables) ANOVA with Tukey's post-hoc correction test (parametric test) was performed for sets of normally distributed and homoscedastic values; ii) Related measures (RM) one-way or two-way ANOVA with Tukey's post-hoc correction test (parametric test) was performed for sets of normally distributed and homoscedastic values in which each value unequivocally corresponded to one value in each of the other data sets (matched data, obtained at different time points); iii) Kruskal-Wallis with Dunn's post-hoc correction test (non-parametric test) was performed for sets of non-normally distributed values.

The statistical significance of the difference between two values within two conditions (e.g. mutated vs unmutated bases in Chk1^{BWT} vs Chk1^{Bhet} mice) was calculated with a 2x2 contingency table and either a two-sided Fisher's exact test (for small numbers) or a two-sided χ^2 test with Yates correction (for high numbers).

The software programs MS Office Excel (Microsoft) or GraphPad Prism 9 (GraphPad Software) were used to perform the described tests.

4.9 Primers and PCR conditions

Table 2: PCR primers

Locus	Species	Primer name	Primer sequence 5'-3'
Chek1	mouse	Chk1^{fl}-fwd	CGTAGTTACACCCAGCTGCTC
		Chk1^{fl}-rev	GCCATGACTCCAAGCACAG
		Chk1-R3	CCAGCAGCACACACAACGTA
Mb1	mouse	Mb1-fwd	CCCTGTGGATGCCACCTC
		Mb1-rev	GTCCTGGCATCTGTCAGAG
Aicda	mouse	mAID-1	GGGCCAGCTCATTCCTCCACTC
		mAID-2	CCAGGCTTTGAAAGTTCTTTCACG
		mAID-3	GGTCCCAGTCTGAGATGTAGCGTAGG
		mAID-4	CAACGTGGCGTCCAAACAGGCACTTCCG
IgH (J$_H$4)	mouse	V186.2-fwd	CAGTAGCAGGCTTGAGGTCTGGAC
		JH4-rev	CTCCACCAGACCTCTCTAGACAGC
IgH (pre-Sµ)	mouse	pre-Sµ-fwd	GGATACCTCAGTGGTTTTTAATGGTGGGT
		pre-Sµ-rev	GGAATTCCAGTCCAGTGTAGGCAGTAGA
Cd83	mouse	Cd83-fwd	CCTTGCTTACGCCGCTCTGTTTC
		Cd83-rev	AGAAGGCAGTCCCGTGTTTCTTG
Igλ (VJ)	chicken	λ1	TGGGAAATACTGGTGATAGGTGGAT
		C2	CCTCCATTTTTTGACAGCACTTACCTGGACAGCTG
		λ2	GAGCGCAGGGAGTTATTTGCATAG
AICDA	human	AID-Exon1-fwd	CAGGAGCTGCTAGTGCCTGT
		AID-Exon5-rev	GCCAGACCTGTGTTCCTTCT
		AID-Exon3-rev	AATGGCTCAGAGACAAGGCC
IGH (VDJ)	human	Primer1-f	CAGGGTACCCCCAAGGTGAGCCCAAAAGA
		Intron3-r	CGGGATCCCGCATCGGGGCCGACAGCACT
		VHLeader-Sequ	CTCCTGGTGGCAGCTCCCAGA

Table 3: PCR conditions

Locus	Use	PCR program
Chek1	Genotyping	2 min 94°C, [20 s 94°C, 15 s 65°C (-0.5°C per cycle), 10 s 68°C] x10, (15 s 94°C, 15 s 60°C, 10 s 72°C) x35, 2 min 72°C, ∞ 10°C
	Genotyping (Chk1^{del})	2 min 94°C, (15 s 94°C, 30 s 63°C, 45 s 72°C) x35, 5 min 72°C, ∞ 4°C
Mb1	Genotyping	3 min 94°C, (45 s 94°C, 30 s 55°C, 30 s 72°C) x40, 10 min 72°C, ∞ 4°C
Aicda	Genotyping	5 min 94°C, (30 s 94°C, 30 s 60°C, 1.5 min 72°C) x32, 5 min 72°C, ∞ 4°C
J$_H$4	Sequencing	5 min 95°C, (10 s 98°C, 30 s 70°C, 30 s 72°C) x35, 10 min 72°C, ∞ 4°C
pre-Sµ	Sequencing	1 min 98°C, (10 s 98°C, 30 s 58°C, 2 min 72°C) x35, 10 min 72°C, ∞ 4°C
Cd83	Sequencing	1 min 98°C, (10 s 98°C, 30 s 58°C, 2 min 72°C) x35, 10 min 72°C, ∞ 4°C
Igλ	Sequencing	5 min 95°C, (50 s 95°C, 30 s 60°C, 2 min 72°C) x35, 10 min 72°C, ∞ 4°C
AICDA	Sequencing	2 min 94°C, (10 s 94°C, 30 s 64°C, 8.5 min 68°C) x35, 7 min 68°C, ∞ 4°C
IGH	Sequencing	2 min 95°C, (50 s 95°C, 30 s 65°C, 3 min 72°C) x35, 10 min 72°C, ∞ 4°C

4.10 Materials and reagents

Table 4: List of buffers and mediums

Buffer/Medium	Composition
Acrylamide Gel (12%)	3.3ml dH_2O, 4ml 30% Acrylamide, 2.5ml 1M Tris (pH 8.8), 100µl 10% SDS, 100µl 10% APS, 4µl TEMED
Agarose Gel (1%)	350ml TAE buffer, 18µl Ethidium Bromide, 3.5 g Agarose
Bäuerle Buffer	20mM HEPES (pH 7.9), 350mM NaCl, 20% Glycerine, 1mM $MgCl_2$, 0.5mM EDTA, 0.1mM EGTA, 1% NP-40
Blotting Buffer	200mL 10X Blotting Buffer, 400mL Methanol in 2L H_2O
Blotting Buffer (10X)	30.3g Tris Base, 144.2g Glycine in 1L H_2O
Carbonate Buffer	0.2M Na_2CO_3, 0.2M $NaHCO_3$ in H_2O, pH 9.5
Chicken B cell Medium	RPMI, 10% FCS, 1% Chicken Serum, 0.1mM β-mercaptoethanol, 100U/ml Penicillin/Streptomycin, 2mM Glutamine, 1mM Sodium Pyruvate
E1 Buffer	50mM Tris, 10mM EDTA, 100µg/ml Rnase, pH 8.0
E2 Buffer	200mM NaOH, 1% SDS
E3 Buffer	3.1M Potassium Acetate, pH 5.5
Human B cell Medium	RPMI, 10% FCS, 100U/ml Penicillin/Streptomycin, 2mM Glutamine, 1mM Sodium Pyruvate
Laemmli Buffer	200mL 10X Laemmli Buffer in 2L H_2O
Laemmli Buffer (10X)	30.3g Tris Base, 144.2g Glycine, 10g SDS in 1L H_2O
LB Agar	3g Agar in 200ml LB medium
LB medium	25g LB medium powder in 1L H_2O
Mouse B cell Medium	RPMI, 10% FCS, 10mM HEPES, 50mM β-mercaptoethanol, 0.2U/ml Penicillin/Streptomycin
PBA-E	100ml PBS 10X, 6g BSA, 1g Sodium Azide, 4mL 0.5M EDTA in 1L H_2O
PBS	137mM NaCl, 2.7mM KCl, 10mM Na_2HPO_4, 1.76mM KH_2PO_4 in H_2O, pH 7.4
PBS (10X)	80g NaCl, 2g KCl, 26.8g Na_2HPO_4, 2.4g KH_2PO_4 in 1L H_2O
Plat-E Medium	DMEM, 10% FCS, 100U/ml penicillin/streptomycin, 1µg/ml puromycin, 10µg/ml blasticidin
Sample Buffer	120mM Tris (pH 6.8), 4% SDS, 20% Glycerol, 0.1% Bromophenolblue, 0.1M DTT
SOB Medium	2% Tryptone, 0.5% Yeast Extract, 10mM NaCl, 2.5mM KCl in 1L H_2O, pH 7.0
SOC Medium	20mM Glucose, 10mM $MgSO_4$, 10mM $MgCl_2$ in SOB medium
Substrate Buffer	0.2M $Na_2HPO_4x7H_2O$, 0.1M Citric Acid in H_2O, pH 5.0
TAE Buffer	40mM Tris, 20mM Acetic Acid, 1 mM EDTA in H_2O
TBS (10X)	6.05g 50mM Tris, 8.76g 150mM NaCl in 1L H_2O, pH 7,5
TBST	1ml Tween 20 in 1L TBS

Table 5: List of chemicals and reagents

Chemical	Company
Acetic Acid	Carl Roth
Acrylamide	Carl Roth
Agar	Thermo Fisher Scientific

Agarose	VWR
AID CRISPR/Cas9 KO Plasmid	Santa Cruz Biotechnology
Ampicillin	Roche AG
APS	Merck
Bimake DNA transfection reagent	Bimake
Bio-Rad DC Protein Assay	Bio-Rad
Blasticidin	MoBiTec
Bromophenolblue	Carl Roth
BSA	Diagonal
Chicken Serum	VWR
Citric Acid	Sigma
DH5alpha electro-competent *E. coli*	Invitrogen
DMEM	Thermo Fisher Scientific
DTT	Invitrogen
ECL™ Western Blotting Reagents	GE Healthcare
EDTA	AppliChem GmbH
EGTA	Fluka Chemie
Ethanol	Merck
Ethidium Bromide	Merck
FCS	Merck
Glucose	Fluka Chemie
Glycerine	Carl Roth
Glycerol	MP Biomedicals
Glycin	Carl Roth
HCl	Carl Roth
HEPES	Thermo Fisher Scientific
IL-4	eBiosciences
IPTG	Carl Roth
K_2HPO_4	Kmf
KCl	Carl Roth
LB Medium powder	Carl Roth
L-Glutamine	Carl Roth
LPS	Sigma
MACS beads	Miltenyi Biotec
Methanol	Fluka Chemie
$MgCl_2$	Carl Roth
$MgSO_4$	AppliChem
Mowiol	Sigma-Aldrich
Na_2CO_3	Carl Roth
Na_2HPO_4	Carl Roth
$Na_2HPO_4 x 7H_2O$	Carl Roth
NaCl	Carl Roth
$NaHCO_3$	Carl Roth
NaOH	Carl Roth
NP_{15}	BioCat
NP_3	BioCat
NP-40	AppliChem
NP-CGG	Biosearch Technologies

Penicillin/Streptomycin	Invitrogen
PFA	Serva
Poly-L-Lysine	VWR
Ponceau S Solution	Sigma-Aldrich
Potassium Acetate	Carl Roth
Powdered Milk	Carl Roth
Protease and Phosphatase Inhibitors	Roche
Proteinase K	VWR
Puromycin	Carl Roth
Red Blood Cell lysis Buffer	Merck
Rnase	Carl Roth
RPMI	Thermo Fisher Scientific
ScaI	Thermo Fisher Scientific
SDS	Carl Roth
Sodium Azide	Sigma
Sodium Pyruvate	Invitrogen
TEMED	Merck
Tris	Carl Roth
Triton-X-100	Sigma
Tryptone	AppliChem
Tween 20	Merck
X-gal	Carl Roth
Yeast Extract	Carl Roth
Zeocin	Invitrogen
α-CD40	eBiosciences
β-mercaptoethanol	Merck

Table 6: List of antibodies, dyes and detection reagents

Reagent	Reactivity	Use	Company	Art. Number
α-AID (L7E7)	Human	WB	Cell Signaling	#4975
α-B220-BV786	Mouse	Flow cytometry	BioLegend	103246
α-B220-FITC	Mouse	Flow cytometry	BD Biosciences	553088
α-B220-PE	Mouse	Flow cytometry	BD Biosciences	553090
α-B220-PerCP	Mouse	Flow cytometry	BD Biosciences	553093
α-CD21-FITC	Mouse	Flow cytometry	BD Biosciences	561769
α-CD23-PE	Mouse	Flow cytometry	BD Biosciences	561773
α-CD3-PE	Mouse	Flow cytometry	BD Biosciences	553064
α-CD43-FITC	Mouse	Flow cytometry	BD Biosciences	561856
α-CD95-PE	Mouse	Flow cytometry	BD Biosciences	554258
α-Chk1	Mouse	WB	Santa Cruz Biotechnology	SC-8408
α-IgG$_1$-biotin	Mouse	ELISA	BD Biosciences	553441
α-IgG1-DyLight405	Mouse	Flow cytometry	BioLegend	409109
α-IgG-HRP	Mouse	WB	Promega	W402B
α-IgG-HRP	Rabbit	WB	Cell signalling	7074
α-IgM-APC	Mouse	Flow cytometry	BioLegend	406509

α-IgM-APC	Human	Flow cytometry	BD Biosciences	551062
α-IgM-biotin	Chicken	Flow cytometry	Sigma-Aldrich	SAB3700240
α-LNGFR-APC	Human	Flow cytometry	Miltenyi	130-110-078
α-tubulin	Cross-reactivity	WB	abcam	ab 4074
α-vinculin	Cross-reactivity	WB	Biozol	BLZ-03106
PNA-FITC	-	Flow cytometry	Vector Laboratories	FL-1071
DAPI	-	Microscopy	Fluka Chemie	32670
DAPI	-	Flow cytometry	Sigma	D9542
FVS780	-	Flow cytometry	BD Biosciences	565388
Hoechst33342	-	Flow cytometry	VWR	B2261-25MG
streptavidin-APC	Biotin	Flow cytometry	BioLegend	405207
streptavidin-HRP	Biotin	ELISA	Biolegend	405210

Table 7: List of kits

Kit	Company
Amaxa® Cell Line Nucleofector® Kit V	Lonza
Expand Long Template PCR System	Roche
Nucleo Spin Gel and PCR Clean-Up Kit	MACHEREY-NAGEL
NucleoBond Xtra Maxi Kit	MACHEREY-NAGEL
Peqlab Taq Polymerase	VWR
pGEM-T Vector System	Promega
Phusion High Fidelity Pol-ymerase Kit	Thermo Fisher Scientific
PlateSeqKit DNA	Eurofins MWG
QIAamp DNA Mini Kit	Quiagen
Vybrant CFDA SE Cell Tracer Kit	Thermo Fisher Scientific

Table 8: List of laboratory materials

Material	Company
40μm strainers	Greiner Bio-One
70μm strainers	Greiner Bio-One
Amicon® Ultra-15 Centrifugal Filter Devices	Millipore
CEA-RP New 18×24 X-ray films	Christiansen GmbH
Cover slips microscope (18 mm)	Roche
Cuvettes certified for Gene pulser Xcell™	Bio-Rad
MACS LS columns	Miltenyi Biotech
MACS separator	Miltenyi Biotech
Microscope slides (76×26 mm)	Roth
Nunc 96-well ELISA plate	Thermo Fisher Scientific
PVDF membranes	Carl Roth
Whatman Chromatography Paper	VWR

5 Abbreviations

9-1-1	-	RAD9-RAD1-HUS1
53BP1	-	p53 binding protein 1
A	-	Adenine
AID	-	Activation-induced cytidine deaminase
alt-EJ	-	alternative end-joining
ALV	-	Avian leucosis virus
APC	-	Antigen presenting cell
APE	-	Apurinic/apyrimidinic endonuclease
apoB	-	apolipoprotein B
APOBEC	-	Apolipoprotein B mRNA editing catalytic polypeptide-like
APRIL	-	Proliferation-inducing ligand
ATM	-	Ataxia telangiectasia mutated
ATR	-	ATM and Rad3-related
ATRIP	-	ATR-interacting protein
BAFF	-	B cell-activating factor
Bcl-6	-	B cell lymphoma 6
BCR	-	B cell receptor
BER	-	Base excision repair
bp	-	base pair
BRCA	-	Breast cancer-associated gene
BSA	-	Bovine serum albumin
C	-	Constant
C	-	Cytosine
CBS	-	Claspin binding site
Cdc25A/C	-	Cell division control protein 25 homolog A/C
Cdk	-	Cyclin-dependent kinase
CDR	-	Complementary-determining region
CFSE	-	Carboxyfluorescein succin-imidyl ester
Chk1/2	-	Checkpoint kinase 1/2
CMG	-	Cdc45-Mcm2-7-GINS
CRM1	-	Chromosome region maintenance 1
CSR	-	Class switch recombination
CtIP	-	C-terminal-binding protein-interacting protein
CXCR	-	C-X-C chemokine receptor
D	-	Diversity
DAPI	-	4'-6-Diamidino-2-phenylindole
dC	-	deoxycytidine
DC	-	Dentritic cell
DDR	-	DNA damage response
DNA2	-	DNA replication ATP-dependent helicase/nuclease 2
DNAJA1	-	DnaJ homolog subfamily A member 1
DNA-PK	-	DNA-dependent protein kinase
DNA-PKCS	-	DNA-PK catalytic subunit
dNTP	-	deoxyribonucleotide triphosphate
DSB	-	Double-strand break
dsDNA	-	double-stranded DNA
dU	-	deoxyuridine
DZ	-	Dark zone
E.coli	-	*Escherichia coli*
eEF1A	-	translation elongation factor 1A
ELISA	-	Enzyme-linked immuno-sorbent assay
EXO1	-	Exonuclease 1
FACS	-	Fluorescence-activated cell sorting

Fc	-	Fragment crystallizable
FCS	-	Fetal calf serum
FDC	-	Follicular dendritic cell
Fucci	-	Fluorescent ubiquitination-based cell cycle indicator
FVS780	-	Fixable Viability Stain 780
G	-	Guanine
GC	-	Germinal center
GFP	-	Green fluorescent protein
gRNA	-	guide RNA
H2AX	-	H2A histone family member X
hCdt1	-	human Cdt1
hGem	-	human Geminin
HIGM2	-	Hyper-IgM syndrome
hNGFR	-	human nerve growth factor receptor
HR	-	Homologous recombination
HRP	-	Horseradish Peroxidase
HSP90	-	Heat shock protein 90 kDa
Ig	-	Immunoglobulin
IgGC	-	Ig gene conversion
IL	-	Interleukin
IR	-	Ionizing radiation
J	-	Joining
Ku70/80	-	Ku autoantigen protein p70/p80 homolog
LIG1	-	DNA ligase 1
LPS	-	Lipopolisaccaride
LZ	-	Light zone
MACS	-	Magnetic-activated cell sorting
mAG	-	monomeric Azami Green
MCM	-	Minichromosome maintenance
MDC1	-	Mediator of DNA damage checkpoint protein 1
MHC	-	Major histocompatibility complex
mKO	-	monomeric Kusabira Orange
MLH1	-	MutL homolog 1
MMR	-	Mismatch repair
MMS2	-	Methyl methanesulfonate-sensitive 2
MRN	-	Mre11–Rad50–Nbs1
MSH	-	MutS homolog
mut	-	mutation
ncMMR	-	non-canonical MMR
NER	-	Nucleotide excision repair
NES	-	Nuclear export signal
NF-κB	-	Nuclear factor 'kappa-light-chain-enhancer' of activated B cells
NHEJ	-	Non-homologous end-joining
NLS	-	Nuclear localization signal
NP-CGG	-	nitrophenylacetyl chicken γ globulin
o.n.	-	over night
p53	-	tumor protein 53
PARP	-	Poly ADP-ribose polymerase
PAX5	-	Paired box 5
PBS	-	Phosphate-buffered saline
PCNA	-	Proliferating cell nuclear antigen
PI3K	-	Phosphoinositide 3-kinase
PIKK	-	PI3K-related kinases
PKA	-	Protein kinase A
Pol	-	Polymerase
PP	-	Peyer's patch

PRDM1	-	PR domain zinc finger protein 1
pre-RC	-	pre-replication complex
PVDF	-	Polyvinylidene Difluoride
Rad	-	Radiation-sensitive
RAG	-	Recombination-activating genes
RM	-	Related measures
RNAPII	-	RNA pol II
ROS	-	Reactive oxygen species
RPA	-	Replication protein A
RT	-	Room temperature
S	-	Switch
SHM	-	Somatic hypermutation
sIgM	-	surface IgM
SMRT	-	Silencing mediator for retinoid or thyroid-hormone receptors
SOC	-	Super Optimal broth with Catabolite repression
SSA	-	Single strand annealing
SSB	-	Single strand break
ssDNA	-	single-stranded DNA
STAT6	-	Signal transducer and activator of transcription 6
T	-	Thymine
TBS	-	Tris-buffered saline
TCR	-	T cell receptor
TdT	-	Terminal deoxynucleotidyl transferase
TFH	-	T follicular helper
TGF	-	Tumor growth factor
TLR	-	Toll-like receptor
TLS	-	Translesion synthesis
TNF	-	Tumor necrosis factor
TopBP1	-	Topoisomerase binding protein 1
TS	-	Transition
TSS	-	Transcription start site
TV	-	Transversion
U	-	Uracile
UBC13	-	Ubiquitin-conjugating enzyme 13
ugi	-	uracil glycosilase inhibitor
UNG	-	Uracil-DNA glycosylase
UV	-	Ultraviolet light
V	-	Variable
XLF	-	Xrcc4-like factor 1
XRCC	-	X-ray cross complementation
ΨV	-	Pseudo V gene

6 References

1.   Murphy, K., P. Travers, and M. Walport, *Janeway's immunobiology, 9th edition.* Garland Science, 2017.
2.   Hoffmann, J. and S. Akira, *Innate immunity.* Curr Opin Immunol, 2013. **25**(1): p. 1-3.
3.   Yatim, K.M. and F.G. Lakkis, *A brief journey through the immune system.* Clin J Am Soc Nephrol, 2015. **10**(7): p. 1274-81.
4.   Bonilla, F.A. and H.C. Oettgen, *Adaptive immunity.* J Allergy Clin Immunol, 2010. **125**(2 Suppl 2): p. S33-40.
5.   Swain, S.L., *T cell subsets and the recognition of MHC class.* Immunol Rev, 1983. **74**: p. 129-42.
6.   Heesters, B.A., et al., *Antigen Presentation to B Cells.* Trends Immunol, 2016. **37**(12): p. 844-854.
7.   Luckheeram, R.V., et al., *CD4(+)T cells: differentiation and functions.* Clin Dev Immunol, 2012. **2012**: p. 925135.
8.   Kim, T.S. and E.C. Shin, *The activation of bystander CD8(+) T cells and their roles in viral infection.* Exp Mol Med, 2019. **51**(12): p. 1-9.
9.   Zamora, A.E., J.C. Crawford, and P.G. Thomas, *Hitting the Target: How T Cells Detect and Eliminate Tumors.* J Immunol, 2018. **200**(2): p. 392-399.
10. Nutt, S.L., et al., *The generation of antibody-secreting plasma cells.* Nat Rev Immunol, 2015. **15**(3): p. 160-71.
11. Eisen, H.N. and G.W. Siskind, *Variations in Affinities of Antibodies during the Immune Response.* Biochemistry, 1964. **3**: p. 996-1008.
12. Gourley, T.S., et al., *Generation and maintenance of immunological memory.* Semin Immunol, 2004. **16**(5): p. 323-33.
13. Hardy, R.R. and K. Hayakawa, *B cell development pathways.* Annu Rev Immunol, 2001. **19**: p. 595-621.
14. Pleiman, C.M., D. D'Ambrosio, and J.C. Cambier, *The B-cell antigen receptor complex: structure and signal transduction.* Immunol Today, 1994. **15**(9): p. 393-9.
15. Crotty, S., *A brief history of T cell help to B cells.* Nat Rev Immunol, 2015. **15**(3): p. 185-9.
16. Vos, Q., et al., *B-cell activation by T-cell-independent type 2 antigens as an integral part of the humoral immune response to pathogenic microorganisms.* Immunol Rev, 2000. **176**: p. 154-70.
17. Kurosaki, T., K. Kometani, and W. Ise, *Memory B cells.* Nat Rev Immunol, 2015. **15**(3): p. 149-59.
18. Lu, L.L., et al., *Beyond binding: antibody effector functions in infectious diseases.* Nat Rev Immunol, 2018. **18**(1): p. 46-61.
19. D. R. Davies, S.C., *Antibody structure.* Accounts of Chemical Research, 1993. **26**: p. 421-427.
20. Bruggemann, M., et al., *Comparison of the effector functions of human immunoglobulins using a matched set of chimeric antibodies.* J Exp Med, 1987. **166**(5): p. 1351-61.
21. Davies, D.R. and H. Metzger, *Structural basis of antibody function.* Annu Rev Immunol, 1983. **1**: p. 87-117.
22. Rees, A.R., *Understanding the human antibody repertoire.* Mabs, 2020. **12**(1).
23. Schatz, D.G., M.A. Oettinger, and M.S. Schlissel, *V(D)J recombination: molecular biology and regulation.* Annu Rev Immunol, 1992. **10**: p. 359-83.
24. Honjo, T., *Immunoglobulin genes.* Annu Rev Immunol, 1983. **1**: p. 499-528.
25. Nishana, M. and S.C. Raghavan, *Role of recombination activating genes in the generation of antigen receptor diversity and beyond.* Immunology, 2012. **137**(4): p. 271-81.
26. McBlane, J.F., et al., *Cleavage at a V(D)J recombination signal requires only RAG1 and RAG2 proteins and occurs in two steps.* Cell, 1995. **83**(3): p. 387-95.
27. Lieber, M.R., et al., *The mechanism of vertebrate nonhomologous DNA end joining and its role in V(D)J recombination.* DNA Repair (Amst), 2004. **3**(8-9): p. 817-26.
28. Rajewsky, K., *Clonal selection and learning in the antibody system.* Nature, 1996. **381**(6585): p. 751-8.
29. Benedict, C.L., et al., *Terminal deoxynucleotidyl transferase and repertoire development.* Immunol Rev, 2000. **175**: p. 150-7.

30. Victora, G.D. and M.C. Nussenzweig, *Germinal centers.* Annu Rev Immunol, 2012. **30**: p. 429-57.

31. De Silva, N.S. and U. Klein, *Dynamics of B cells in germinal centres.* Nat Rev Immunol, 2015. **15**(3): p. 137-48.

32. Cyster, J.G., *Chemokines and cell migration in secondary lymphoid organs.* Science, 1999. **286**(5447): p. 2098-102.

33. Ansel, K.M., et al., *A chemokine-driven positive feedback loop organizes lymphoid follicles.* Nature, 2000. **406**(6793): p. 309-14.

34. Okada, T., et al., *Antigen-engaged B cells undergo chemotaxis toward the T zone and form motile conjugates with helper T cells.* PLoS Biol, 2005. **3**(6): p. e150.

35. Liu, D., et al., *T-B-cell entanglement and ICOSL-driven feed-forward regulation of germinal centre reaction.* Nature, 2015. **517**(7533): p. 214-8.

36. Adler, L.N., et al., *The Other Function: Class II-Restricted Antigen Presentation by B Cells.* Front Immunol, 2017. **8**: p. 319.

37. . Ledderman S, Y.M., Inghirami G, Lee J, Knowles D, Chess L. , *Molecular interactions mediating T-B lymphocyte collaboration in human lymphoid follicles: Roles of T cell-B cell activating molecule (5c8 antigen) and CD40 in contact-dependent help.* J. Immunol., 1992. **149**: p. 3817-26.

38. Zotos, D. and D.M. Tarlinton, *Determining germinal centre B cell fate.* Trends Immunol, 2012. **33**(6): p. 281-8.

39. Gonzalez, D.G., et al., *Nonredundant Roles of IL-21 and IL-4 in the Phased Initiation of Germinal Center B Cells and Subsequent Self-Renewal Transitions.* J Immunol, 2018. **201**(12): p. 3569-3579.

40. Shih, T.A., et al., *Role of BCR affinity in T cell dependent antibody responses in vivo.* Nat Immunol, 2002. **3**(6): p. 570-5.

41. Wensveen, F.M., et al., *Antigen-affinity controls pre-germinal center B cell selection by promoting Mcl-1 induction through BAFF receptor signaling.* Sci Rep, 2016. **6**: p. 35673.

42. Kerfoot, S.M., et al., *Germinal center B cell and T follicular helper cell development initiates in the interfollicular zone.* Immunity, 2011. **34**(6): p. 947-60.

43. Baumjohann, D., T. Okada, and K.M. Ansel, *Cutting Edge: Distinct waves of BCL6 expression during T follicular helper cell development.* J Immunol, 2011. **187**(5): p. 2089-92.

44. Basso, K. and R. Dalla-Favera, *BCL6: master regulator of the germinal center reaction and key oncogene in B cell lymphomagenesis.* Adv Immunol, 2010. **105**: p. 193-210.

45. Moser, B., *CXCR5, the Defining Marker for Follicular B Helper T (TFH) Cells.* Front Immunol, 2015. **6**: p. 296.

46. Victora, G.D., et al., *Identification of human germinal center light and dark zone cells and their relationship to human B-cell lymphomas.* Blood, 2012. **120**(11): p. 2240-8.

47. Allen, C.D., T. Okada, and J.G. Cyster, *Germinal-center organization and cellular dynamics.* Immunity, 2007. **27**(2): p. 190-202.

48. MacLennan, I.C., *Somatic mutation. From the dark zone to the light.* Curr Biol, 1994. **4**(1): p. 70-2.

49. Allen, C.D., et al., *Germinal center dark and light zone organization is mediated by CXCR4 and CXCR5.* Nat Immunol, 2004. **5**(9): p. 943-52.

50. Imal, Y. and M. Yamakawa, *Morphology, function and pathology of follicular dendritic cells.* Pathol Int, 1996. **46**(11): p. 807-33.

51. Shulman, Z., et al., *Dynamic signaling by T follicular helper cells during germinal center B cell selection.* Science, 2014. **345**(6200): p. 1058-62.

52. Gitlin, A.D., Z. Shulman, and M.C. Nussenzweig, *Clonal selection in the germinal centre by regulated proliferation and hypermutation.* Nature, 2014. **509**(7502): p. 637-40.

53. Cyster, J.G. and C.D.C. Allen, *B Cell Responses: Cell Interaction Dynamics and Decisions.* Cell, 2019. **177**(3): p. 524-540.

54. Hauser, A.E., et al., *Definition of germinal-center B cell migration in vivo reveals predominant intrazonal circulation patterns.* Immunity, 2007. **26**(5): p. 655-67.

55. Palm, A.E. and C. Henry, *Remembrance of Things Past: Long-Term B Cell Memory After Infection and Vaccination.* Front Immunol, 2019. **10**: p. 1787.

56.   Landsverk, O.J., et al., *Antibody-secreting plasma cells persist for decades in human intestine.* J Exp Med, 2017. **214**(2): p. 309-317.

57.   Victora, G.D., et al., *Germinal center dynamics revealed by multiphoton microscopy with a photoactivatable fluorescent reporter.* Cell, 2010. **143**(4): p. 592-605.

58.   Roco, J.A., et al., *Class-Switch Recombination Occurs Infrequently in Germinal Centers.* Immunity, 2019. **51**(2): p. 337-350 e7.

59.   Methot, S.P. and J.M. Di Noia, *Molecular Mechanisms of Somatic Hypermutation and Class Switch Recombination.* Adv Immunol, 2017. **133**: p. 37-87.

60.   Reynaud, C.A., et al., *Formation of the chicken B-cell repertoire: ontogenesis, regulation of Ig gene rearrangement, and diversification by gene conversion.* Adv Immunol, 1994. **57**: p. 353-78.

61.   Knight, K.L. and M.A. Crane, *Generating the antibody repertoire in rabbit.* Adv Immunol, 1994. **56**: p. 179-218.

62.   Wang, J.H., *The role of activation-induced deaminase in antibody diversification and genomic instability.* Immunol Res, 2013. **55**(1-3): p. 287-97.

63.   Tang, E.S. and A. Martin, *Immunoglobulin gene conversion: synthesizing antibody diversification and DNA repair.* DNA Repair (Amst), 2007. **6**(11): p. 1557-71.

64.   Lynch, M., *Rate, molecular spectrum, and consequences of human mutation.* Proc Natl Acad Sci U S A, 2010. **107**(3): p. 961-8.

65.   Peters, A. and U. Storb, *Somatic hypermutation of immunoglobulin genes is linked to transcription initiation.* Immunity, 1996. **4**(1): p. 57-65.

66.   Lebecque, S.G. and P.J. Gearhart, *Boundaries of somatic mutation in rearranged immunoglobulin genes: 5' boundary is near the promoter, and 3' boundary is approximately 1 kb from V(D)J gene.* J Exp Med, 1990. **172**(6): p. 1717-27.

67.   Johnson, G. and T.T. Wu, *Kabat database and its applications: 30 years after the first variability plot.* Nucleic Acids Res, 2000. **28**(1): p. 214-8.

68.   Rogozin, I.B. and N.A. Kolchanov, *Somatic hypermutagenesis in immunoglobulin genes. II. Influence of neighbouring base sequences on mutagenesis.* Biochim Biophys Acta, 1992. **1171**(1): p. 11-8.

69.   Rogozin, I.B. and M. Diaz, *Cutting edge: DGYW/WRCH is a better predictor of mutability at G:C bases in Ig hypermutation than the widely accepted RGYW/WRCY motif and probably reflects a two-step activation-induced cytidine deaminase-triggered process.* J Immunol, 2004. **172**(6): p. 3382-4.

70.   Di Noia, J.M. and M.S. Neuberger, *Molecular mechanisms of antibody somatic hypermutation.* Annu Rev Biochem, 2007. **76**: p. 1-22.

71.   Alt, F. and M. Reth, *Michael Neuberger (1953-2013).* Immunity, 2013. **39**(6): p. 987-8.

72.   Geisberger, R., M. Lamers, and G. Achatz, *The riddle of the dual expression of IgM and IgD.* Immunology, 2006. **118**(4): p. 429-37.

73.   Zarrin, A.A., et al., *An evolutionarily conserved target motif for immunoglobulin class-switch recombination.* Nat Immunol, 2004. **5**(12): p. 1275-81.

74.   Jung, S., K. Rajewsky, and A. Radbruch, *Shutdown of Class Switch Recombination by Deletion of a Switch Region Control Element.* Science, 1993. **259**(5097): p. 984-987.

75.   Stavnezer, J. and C.E. Schrader, *IgH chain class switch recombination: mechanism and regulation.* J Immunol, 2014. **193**(11): p. 5370-8.

76.   Snapper, C.M., F.D. Finkelman, and W.E. Paul, *Regulation of Igg1 and Ige Production by Interleukin-4.* Immunological Reviews, 1988. **102**: p. 51-75.

77.   Malisan, F., et al., *Interleukin-10 induces immunoglobulin G isotype switch recombination in human CD40-activated naive B lymphocytes.* J Exp Med, 1996. **183**(3): p. 937-47.

78.   Ratcliffe, M.J., *Antibodies, immunoglobulin genes and the bursa of Fabricius in chicken B cell development.* Dev Comp Immunol, 2006. **30**(1-2): p. 101-18.

79.   Butler, J.E., *Immunoglobulin diversity, B-cell and antibody repertoire development in large farm animals.* Rev Sci Tech, 1998. **17**(1): p. 43-70.

80.   Arakawa, H. and J.M. Buerstedde, *Immunoglobulin gene conversion: insights from bursal B cells and the DT40 cell line.* Dev Dyn, 2004. **229**(3): p. 458-64.

81.   Bastianello, G. and H. Arakawa, *A double-strand break can trigger immunoglobulin gene conversion.* Nucleic Acids Res, 2017. **45**(1): p. 231-243.

82. McCormack, W.T. and C.B. Thompson, *Chicken IgL variable region gene conversions display pseudogene donor preference and 5' to 3' polarity.* Genes Dev, 1990. **4**(4): p. 548-58.

83. Muramatsu, M., et al., *Specific expression of activation-induced cytidine deaminase (AID), a novel member of the RNA-editing deaminase family in germinal center B cells.* J Biol Chem, 1999. **274**(26): p. 18470-6.

84. Maul, R.W., et al., *Uracil residues dependent on the deaminase AID in immunoglobulin gene variable and switch regions.* Nat Immunol, 2011. **12**(1): p. 70-6.

85. Wang, Q., et al., *The cell cycle restricts activation-induced cytidine deaminase activity to early G1.* J Exp Med, 2017. **214**(1): p. 49-58.

86. Revy, P., et al., *Activation-induced cytidine deaminase (AID) deficiency causes the autosomal recessive form of the Hyper-IgM syndrome (HIGM2).* Cell, 2000. **102**(5): p. 565-75.

87. Muramatsu, M., et al., *Class switch recombination and hypermutation require activation-induced cytidine deaminase (AID), a potential RNA editing enzyme.* Cell, 2000. **102**(5): p. 553-63.

88. Arakawa, H., J. Hauschild, and J.M. Buerstedde, *Requirement of the activation-induced deaminase (AID) gene for immunoglobulin gene conversion.* Science, 2002. **295**(5558): p. 1301-6.

89. Gu, X., V. Shivarov, and M.P. Strout, *The role of activation-induced cytidine deaminase in lymphomagenesis.* Curr Opin Hematol, 2012. **19**(4): p. 292-8.

90. Robbiani, D.F. and M.C. Nussenzweig, *Chromosome translocation, B cell lymphoma, and activation-induced cytidine deaminase.* Annu Rev Pathol, 2013. **8**: p. 79-103.

91. Staszewski, O., et al., *Activation-induced cytidine deaminase induces reproducible DNA breaks at many non-Ig Loci in activated B cells.* Mol Cell, 2011. **41**(2): p. 232-42.

92. Haluska, F.G., Y. Tsujimoto, and C.M. Croce, *The t(8;14) chromosome translocation of the Burkitt lymphoma cell line Daudi occurred during immunoglobulin gene rearrangement and involved the heavy chain diversity region.* Proc Natl Acad Sci U S A, 1987. **84**(19): p. 6835-9.

93. Schmitz, K.M. and S.K. Petersen-Mahrt, *AIDing the immune system-DIAbolic in cancer.* Semin Immunol, 2012. **24**(4): p. 241-5.

94. Rush, J.S. and P.D. Hodgkin, *B cells activated via CD40 and IL-4 undergo a division burst but require continued stimulation to maintain division, survival and differentiation.* Eur J Immunol, 2001. **31**(4): p. 1150-9.

95. Duan, Z., et al., *AID expression increased by TNF-alpha is associated with class switch recombination of Igalpha gene in cancers.* Cell Mol Immunol, 2016. **13**(4): p. 484-91.

96. Tran, T.H., et al., *B cell-specific and stimulation-responsive enhancers derepress Aicda by overcoming the effects of silencers.* Nature Immunology, 2010. **11**(2): p. 148-U67.

97. Kim, H.A., G.Y. Seo, and P.H. Kim, *Macrophage-derived BAFF induces AID expression through the p38MAPK/CREB and JNK/AP-1 pathways.* J Leukoc Biol, 2011. **89**(3): p. 393-8.

98. Park, S.R., et al., *APRIL stimulates NF-kappaB-mediated HoxC4 induction for AID expression in mouse B cells.* Cytokine, 2013. **61**(2): p. 608-13.

99. Pone, E.J., et al., *BCR-signalling synergizes with TLR-signalling for induction of AID and immunoglobulin class-switching through the non-canonical NF-kappaB pathway.* Nat Commun, 2012. **3**: p. 767.

100. Pauklin, S., et al., *Estrogen directly activates AID transcription and function.* J Exp Med, 2009. **206**(1): p. 99-111.

101. Dedeoglu, F., et al., *Induction of activation-induced cytidine deaminase gene expression by IL-4 and CD40 ligation is dependent on STAT6 and NFkappaB.* Int Immunol, 2004. **16**(3): p. 395-404.

102. Schoetz, U., et al., *E2A expression stimulates Ig hypermutation.* J Immunol, 2006. **177**(1): p. 395-400.

103. Gonda, H., et al., *The balance between Pax5 and Id2 activities is the key to AID gene expression.* J Exp Med, 2003. **198**(9): p. 1427-37.

104. Basso, K., et al., *BCL6 positively regulates AID and germinal center gene expression via repression of miR-155.* J Exp Med, 2012. **209**(13): p. 2455-65.

105. Vasanwala, F.H., et al., *Repression of AP-1 function: a mechanism for the regulation of Blimp-1 expression and B lymphocyte differentiation by the B cell lymphoma-6 protooncogene.* J Immunol, 2002. **169**(4): p. 1922-9.

106. Rada, C., J.M. Jarvis, and C. Milstein, *AID-GFP chimeric protein increases hypermutation of Ig genes with no evidence of nuclear localization.* Proc Natl Acad Sci U S A, 2002. **99**(10): p. 7003-8.

107. Orthwein, A., et al., *Regulation of activation-induced deaminase stability and antibody gene diversification by Hsp90.* J Exp Med, 2010. **207**(12): p. 2751-65.

108. Orthwein, A., et al., *Optimal functional levels of activation-induced deaminase specifically require the Hsp40 DnaJa1.* EMBO J, 2012. **31**(3): p. 679-91.

109. Methot, S.P., et al., *Consecutive interactions with HSP90 and eEF1A underlie a functional maturation and storage pathway of AID in the cytoplasm.* J Exp Med, 2015. **212**(4): p. 581-96.

110. Aoufouchi, S., et al., *Proteasomal degradation restricts the nuclear lifespan of AID.* J Exp Med, 2008. **205**(6): p. 1357-68.

111. Patenaude, A.M. and J.M. Di Noia, *The mechanisms regulating the subcellular localization of AID.* Nucleus, 2010. **1**(4): p. 325-31.

112. Ito, S., et al., *Activation-induced cytidine deaminase shuttles between nucleus and cytoplasm like apolipoprotein B mRNA editing catalytic polypeptide 1.* Proc Natl Acad Sci U S A, 2004. **101**(7): p. 1975-80.

113. McBride, K.M., et al., *Somatic hypermutation is limited by CRM1-dependent nuclear export of activation-induced deaminase.* J Exp Med, 2004. **199**(9): p. 1235-44.

114. Dickerson, S.K., et al., *AID mediates hypermutation by deaminating single stranded DNA.* J Exp Med, 2003. **197**(10): p. 1291-6.

115. Chaudhuri, J., C. Khuong, and F.W. Alt, *Replication protein A interacts with AID to promote deamination of somatic hypermutation targets.* Nature, 2004. **430**(7003): p. 992-8.

116. Zou, Y., et al., *Functions of human replication protein A (RPA): from DNA replication to DNA damage and stress responses.* J Cell Physiol, 2006. **208**(2): p. 267-73.

117. Chaudhuri, J., et al., *Transcription-targeted DNA deamination by the AID antibody diversification enzyme.* Nature, 2003. **422**(6933): p. 726-30.

118. Nambu, Y., et al., *Transcription-coupled events associating with immunoglobulin switch region chromatin.* Science, 2003. **302**(5653): p. 2137-40.

119. Willmann, K.L., et al., *A role for the RNA pol II-associated PAF complex in AID-induced immune diversification.* J Exp Med, 2012. **209**(11): p. 2099-111.

120. Pavri, R., et al., *Activation-induced cytidine deaminase targets DNA at sites of RNA polymerase II stalling by interaction with Spt5.* Cell, 2010. **143**(1): p. 122-33.

121. Wang, X., et al., *A source of the single-stranded DNA substrate for activation-induced deaminase during somatic hypermutation.* Nat Commun, 2014. **5**: p. 4137.

122. Rajagopal, D., et al., *Immunoglobulin switch mu sequence causes RNA polymerase II accumulation and reduces dA hypermutation.* J Exp Med, 2009. **206**(6): p. 1237-44.

123. Basu, U., et al., *The RNA exosome targets the AID cytidine deaminase to both strands of transcribed duplex DNA substrates.* Cell, 2011. **144**(3): p. 353-63.

124. Qian, J., et al., *B cell super-enhancers and regulatory clusters recruit AID tumorigenic activity.* Cell, 2014. **159**(7): p. 1524-37.

125. Meng, F.L., et al., *Convergent transcription at intragenic super-enhancers targets AID-initiated genomic instability.* Cell, 2014. **159**(7): p. 1538-48.

126. Basu, U., et al., *The AID antibody diversification enzyme is regulated by protein kinase A phosphorylation.* Nature, 2005. **438**(7067): p. 508-11.

127. Vuong, B.Q., et al., *Specific recruitment of protein kinase A to the immunoglobulin locus regulates class-switch recombination.* Nat Immunol, 2009. **10**(4): p. 420-6.

128. Vuong, B.Q., et al., *A DNA break- and phosphorylation-dependent positive feedback loop promotes immunoglobulin class-switch recombination.* Nat Immunol, 2013. **14**(11): p. 1183-1189.

129. Methot, S.P., et al., *A licensing step links AID to transcription elongation for mutagenesis in B cells.* Nat Commun, 2018. **9**(1): p. 1248.

130. Le, Q. and N. Maizels, *Cell Cycle Regulates Nuclear Stability of AID and Determines the Cellular Response to AID.* PLoS Genet, 2015. **11**(9): p. e1005411.

131. Ordinario, E.C., et al., *Temporal regulation of Ig gene diversification revealed by single-cell imaging.* J Immunol, 2009. **183**(7): p. 4545-53.

132. Le, Q. and N. Maizels, *Activation-induced deaminase (AID) localizes to the nucleus in brief pulses.* PLoS Genet, 2019. **15**(2): p. e1007968.

133. Alvarez-Prado, A.F., et al., *A broad atlas of somatic hypermutation allows prediction of activation-induced deaminase targets.* J Exp Med, 2018. **215**(3): p. 761-771.

134. Liu, M., et al., *Two levels of protection for the B cell genome during somatic hypermutation.* Nature, 2008. **451**(7180): p. 841-5.

135. Xue, K., C. Rada, and M.S. Neuberger, *The in vivo pattern of AID targeting to immunoglobulin switch regions deduced from mutation spectra in msh2-/- ung-/- mice.* J Exp Med, 2006. **203**(9): p. 2085-94.

136. Shen, H.M., et al., *Somatic hypermutation and class switch recombination in Msh6(-/-)Ung(-/-) double-knockout mice.* J Immunol, 2006. **177**(8): p. 5386-92.

137. Rada, C., J.M. Di Noia, and M.S. Neuberger, *Mismatch recognition and uracil excision provide complementary paths to both Ig switching and the A/T-focused phase of somatic mutation.* Mol Cell, 2004. **16**(2): p. 163-71.

138. Di Noia, J.M., et al., *Dependence of antibody gene diversification on uracil excision.* J Exp Med, 2007. **204**(13): p. 3209-19.

139. Di Noia, J. and M.S. Neuberger, *Altering the pathway of immunoglobulin hypermutation by inhibiting uracil-DNA glycosylase.* Nature, 2002. **419**(6902): p. 43-8.

140. Imai, K., et al., *Human uracil-DNA glycosylase deficiency associated with profoundly impaired immunoglobulin class-switch recombination.* Nat Immunol, 2003. **4**(10): p. 1023-8.

141. Rada, C., et al., *Immunoglobulin isotype switching is inhibited and somatic hypermutation perturbed in UNG-deficient mice.* Curr Biol, 2002. **12**(20): p. 1748-55.

142. Simpson, L.J. and J.E. Sale, *Rev1 is essential for DNA damage tolerance and non-templated immunoglobulin gene mutation in a vertebrate cell line.* EMBO J, 2003. **22**(7): p. 1654-64.

143. Jansen, J.G., et al., *Strand-biased defect in C/G transversions in hypermutating immunoglobulin genes in Rev1-deficient mice.* J Exp Med, 2006. **203**(2): p. 319-23.

144. Pena-Diaz, J., et al., *Noncanonical Mismatch Repair as a Source of Genomic Instability in Human Cells.* Mol Cell, 2017. **67**(1): p. 162.

145. Delbos, F., et al., *DNA polymerase eta is the sole contributor of A/T modifications during immunoglobulin gene hypermutation in the mouse.* J Exp Med, 2007. **204**(1): p. 17-23.

146. Delbos, F., et al., *Contribution of DNA polymerase eta to immunoglobulin gene hypermutation in the mouse.* J Exp Med, 2005. **201**(8): p. 1191-6.

147. Langerak, P., et al., *A/T mutagenesis in hypermutated immunoglobulin genes strongly depends on PCNAK164 modification.* J Exp Med, 2007. **204**(8): p. 1989-98.

148. Roa, S., et al., *Ubiquitylated PCNA plays a role in somatic hypermutation and class-switch recombination and is required for meiotic progression.* Proc Natl Acad Sci U S A, 2008. **105**(42): p. 16248-53.

149. Zhao, Y., et al., *Mechanism of somatic hypermutation at the WA motif by human DNA polymerase eta.* Proc Natl Acad Sci U S A, 2013. **110**(20): p. 8146-51.

150. Girelli Zubani, G., et al., *Pms2 and uracil-DNA glycosylases act jointly in the mismatch repair pathway to generate Ig gene mutations at A-T base pairs.* J Exp Med, 2017. **214**(4): p. 1169-1180.

151. Frieder, D., et al., *The concerted action of Msh2 and UNG stimulates somatic hypermutation at A . T base pairs.* Mol Cell Biol, 2009. **29**(18): p. 5148-57.

152. Krijger, P.H., et al., *Dependence of nucleotide substitutions on Ung2, Msh2, and PCNA-Ub during somatic hypermutation.* J Exp Med, 2009. **206**(12): p. 2603-11.

153. Thientosapol, E.S., et al., *Proximity to AGCT sequences dictates MMR-independent versus MMR-dependent mechanisms for AID-induced mutation via UNG2.* Nucleic Acids Res, 2017. **45**(6): p. 3146-3157.

154. Schanz, S., et al., *Interference of mismatch and base excision repair during the processing of adjacent U/G mispairs may play a key role in somatic hypermutation.* Proc Natl Acad Sci U S A, 2009. **106**(14): p. 5593-8.

155. Krokan, H.E., F. Drablos, and G. Slupphaug, *Uracil in DNA--occurrence, consequences and repair.* Oncogene, 2002. **21**(58): p. 8935-48.

156. Stavnezer, J., J.E. Guikema, and C.E. Schrader, *Mechanism and regulation of class switch recombination.* Annu Rev Immunol, 2008. **26**: p. 261-92.

157. Stavnezer, J., et al., *Differential expression of APE1 and APE2 in germinal centers promotes error-prone repair and A:T mutations during somatic hypermutation.* Proc Natl Acad Sci U S A, 2014. **111**(25): p. 9217-22.

158. Masani, S., L. Han, and K. Yu, *Apurinic/apyrimidinic endonuclease 1 is the essential nuclease during immunoglobulin class switch recombination.* Mol Cell Biol, 2013. **33**(7): p. 1468-73.

159. Schrader, C.E., et al., *Inducible DNA breaks in Ig S regions are dependent on AID and UNG.* J Exp Med, 2005. **202**(4): p. 561-8.

160. Stavnezer, J. and C.E. Schrader, *Mismatch repair converts AID-instigated nicks to double-strand breaks for antibody class-switch recombination.* Trends Genet, 2006. **22**(1): p. 23-8.

161. Barreto, V., et al., *C-terminal deletion of AID uncouples class switch recombination from somatic hypermutation and gene conversion.* Mol Cell, 2003. **12**(2): p. 501-8.

162. Ta, V.T., et al., *AID mutant analyses indicate requirement for class-switch-specific cofactors.* Nat Immunol, 2003. **4**(9): p. 843-8.

163. Ranjit, S., et al., *AID recruits UNG and Msh2 to Ig switch regions dependent upon the AID C terminus [corrected].* J Immunol, 2011. **187**(5): p. 2464-75.

164. Ucher, A.J., et al., *Mismatch repair proteins and AID activity are required for the dominant negative function of C-terminally deleted AID in class switching.* J Immunol, 2014. **193**(3): p. 1440-50.

165. Hirth, G., et al., *Regulation of the Germinal Center Reaction and Somatic Hypermutation Dynamics by Homologous Recombination.* J Immunol, 2019. **203**(6): p. 1493-1501.

166. Hasham, M.G., et al., *Widespread genomic breaks generated by activation-induced cytidine deaminase are prevented by homologous recombination.* Nat Immunol, 2010. **11**(9): p. 820-6.

167. Hasham, M.G., et al., *Activation-induced cytidine deaminase-initiated off-target DNA breaks are detected and resolved during S phase.* J Immunol, 2012. **189**(5): p. 2374-82.

168. Yamane, A., et al., *RPA accumulation during class switch recombination represents 5'-3' DNA-end resection during the S-G2/M phase of the cell cycle.* Cell Rep, 2013. **3**(1): p. 138-47.

169. Ranuncolo, S.M., et al., *Bcl-6 mediates the germinal center B cell phenotype and lymphomagenesis through transcriptional repression of the DNA-damage sensor ATR.* Nat Immunol, 2007. **8**(7): p. 705-14.

170. Ranuncolo, S.M., J.M. Polo, and A. Melnick, *BCL6 represses CHEK1 and suppresses DNA damage pathways in normal and malignant B-cells.* Blood Cells Mol Dis, 2008. **41**(1): p. 95-9.

171. Phan, R.T. and R. Dalla-Favera, *The BCL6 proto-oncogene suppresses p53 expression in germinal-centre B cells.* Nature, 2004. **432**(7017): p. 635-9.

172. Phan, R.T., et al., *BCL6 interacts with the transcription factor Miz-1 to suppress the cyclin-dependent kinase inhibitor p21 and cell cycle arrest in germinal center B cells.* Nat Immunol, 2005. **6**(10): p. 1054-60.

173. Phan, R.T., et al., *Genotoxic stress regulates expression of the proto-oncogene Bcl6 in germinal center B cells.* Nat Immunol, 2007. **8**(10): p. 1132-9.

174. Lindahl, T. and D.E. Barnes, *Repair of endogenous DNA damage.* Cold Spring Harb Symp Quant Biol, 2000. **65**: p. 127-33.

175. Lawley, P.D., *Effects of some chemical mutagens and carcinogens on nucleic acids.* Prog Nucleic Acid Res Mol Biol, 1966. **5**: p. 89-131.

176. Skipper, P.L., et al., *Monocyclic aromatic amines as potential human carcinogens: old is new again.* Carcinogenesis, 2010. **31**(1): p. 50-8.

177. Yu, H., *Environmental carcinogenic polycyclic aromatic hydrocarbons: photochemistry and phototoxicity.* J Environ Sci Health C Environ Carcinog Ecotoxicol Rev, 2002. **20**(2): p. 149-83.

178. Hecht, S.S., *DNA adduct formation from tobacco-specific N-nitrosamines.* Mutat Res, 1999. **424**(1-2): p. 127-42.

179. Yager, J.D. and N.E. Davidson, *Estrogen carcinogenesis in breast cancer.* N Engl J Med, 2006. **354**(3): p. 270-82.

180. Davies, R.J., *Royal Irish Academy Medal Lecture. Ultraviolet radiation damage in DNA.* Biochem Soc Trans, 1995. **23**(2): p. 407-18.

181. Hutchinson, F., *Chemical changes induced in DNA by ionizing radiation.* Prog Nucleic Acid Res Mol Biol, 1985. **32**: p. 115-54.

182. Lindahl, T., *Instability and decay of the primary structure of DNA.* Nature, 1993. **362**(6422): p. 709-15.

183. Cadet, J., T. Douki, and J.L. Ravanat, *Oxidatively generated base damage to cellular DNA.* Free Radic Biol Med, 2010. **49**(1): p. 9-21.

184. De Bont, R. and N. van Larebeke, *Endogenous DNA damage in humans: a review of quantitative data.* Mutagenesis, 2004. **19**(3): p. 169-85.

185. Bebenek, A. and I. Ziuzia-Graczyk, *Fidelity of DNA replication-a matter of proofreading.* Curr Genet, 2018. **64**(5): p. 985-996.

186. Pommier, Y., et al., *Repair of topoisomerase I-mediated DNA damage.* Prog Nucleic Acid Res Mol Biol, 2006. **81**: p. 179-229.

187. Branzei, D. and M. Foiani, *The DNA damage response during DNA replication.* Curr Opin Cell Biol, 2005. **17**(6): p. 568-75.

188. Llorente, B., C.E. Smith, and L.S. Symington, *Break-induced replication: what is it and what is it for?* Cell Cycle, 2008. **7**(7): p. 859-64.

189. Branzei, D. and M. Foiani, *Regulation of DNA repair throughout the cell cycle.* Nat Rev Mol Cell Biol, 2008. **9**(4): p. 297-308.

190. Vermeulen, K., D.R. Van Bockstaele, and Z.N. Berneman, *The cell cycle: a review of regulation, deregulation and therapeutic targets in cancer.* Cell Prolif, 2003. **36**(3): p. 131-49.

191. Bartek, J. and J. Lukas, *DNA damage checkpoints: from initiation to recovery or adaptation.* Curr Opin Cell Biol, 2007. **19**(2): p. 238-45.

192. Norbury, C.J. and B. Zhivotovsky, *DNA damage-induced apoptosis.* Oncogene, 2004. **23**(16): p. 2797-808.

193. Jacobs, A.L. and P. Schar, *DNA glycosylases: in DNA repair and beyond.* Chromosoma, 2012. **121**(1): p. 1-20.

194. Schormann, N., R. Ricciardi, and D. Chattopadhyay, *Uracil-DNA glycosylases-structural and functional perspectives on an essential family of DNA repair enzymes.* Protein Sci, 2014. **23**(12): p. 1667-85.

195. Bailly, V. and W.G. Verly, *AP endonucleases and AP lyases.* Nucleic Acids Res, 1989. **17**(9): p. 3617-8.

196. Svilar, D., et al., *Base excision repair and lesion-dependent subpathways for repair of oxidative DNA damage.* Antioxid Redox Signal, 2011. **14**(12): p. 2491-507.

197. Mjelle, R., et al., *Cell cycle regulation of human DNA repair and chromatin remodeling genes.* DNA Repair (Amst), 2015. **30**: p. 53-67.

198. Braithwaite, E.K., et al., *DNA polymerase lambda mediates a back-up base excision repair activity in extracts of mouse embryonic fibroblasts.* J Biol Chem, 2005. **280**(18): p. 18469-75.

199. Krokan, H.E. and M. Bjoras, *Base excision repair.* Cold Spring Harb Perspect Biol, 2013. **5**(4): p. a012583.

200. Almeida, K.H. and R.W. Sobol, *A unified view of base excision repair: lesion-dependent protein complexes regulated by post-translational modification.* DNA Repair (Amst), 2007. **6**(6): p. 695-711.

201. Hanssen-Bauer, A., et al., *XRCC1 coordinates disparate responses and multiprotein repair complexes depending on the nature and context of the DNA damage.* Environ Mol Mutagen, 2011. **52**(8): p. 623-35.

202. Reynolds, P., et al., *Disruption of PARP1 function inhibits base excision repair of a sub-set of DNA lesions.* Nucleic Acids Res, 2015. **43**(8): p. 4028-38.

203. Spivak, G., *Nucleotide excision repair in humans.* DNA Repair (Amst), 2015. **36**: p. 13-18.

204. Sugasawa, K., *Molecular mechanisms of DNA damage recognition for mammalian nucleotide excision repair.* DNA Repair (Amst), 2016. **44**: p. 110-117.

205. Mehta, A. and J.E. Haber, *Sources of DNA double-strand breaks and models of recombinational DNA repair.* Cold Spring Harb Perspect Biol, 2014. **6**(9): p. a016428.

206. Sonoda, E., et al., *Differential usage of non-homologous end-joining and homologous recombination in double strand break repair.* DNA Repair (Amst), 2006. **5**(9-10): p. 1021-9.

207. Ira, G., et al., *DNA end resection, homologous recombination and DNA damage checkpoint activation require CDK1.* Nature, 2004. **431**(7011): p. 1011-7.

208. Aylon, Y., B. Liefshitz, and M. Kupiec, *The CDK regulates repair of double-strand breaks by homologous recombination during the cell cycle.* EMBO J, 2004. **23**(24): p. 4868-75.

209. Orthwein, A., et al., *A mechanism for the suppression of homologous recombination in G1 cells.* Nature, 2015. **528**(7582): p. 422-6.

210. Lieber, M.R., et al., *Mechanism and regulation of human non-homologous DNA end-joining.* Nat Rev Mol Cell Biol, 2003. **4**(9): p. 712-20.

211. Bonetti, D., et al., *Processing of DNA Ends in the Maintenance of Genome Stability.* Front Genet, 2018. **9**: p. 390.

212. Ceccaldi, R., B. Rondinelli, and A.D. D'Andrea, *Repair Pathway Choices and Consequences at the Double-Strand Break.* Trends Cell Biol, 2016. **26**(1): p. 52-64.

213. Liu, T. and J. Huang, *DNA End Resection: Facts and Mechanisms.* Genomics Proteomics Bioinformatics, 2016. **14**(3): p. 126-130.

214. Davis, A.J., B.P. Chen, and D.J. Chen, *DNA-PK: a dynamic enzyme in a versatile DSB repair pathway.* DNA Repair (Amst), 2014. **17**: p. 21-9.

215. Pannunzio, N.R., G. Watanabe, and M.R. Lieber, *Nonhomologous DNA end-joining for repair of DNA double-strand breaks.* J Biol Chem, 2018. **293**(27): p. 10512-10523.

216. Grawunder, U., et al., *Requirement for an interaction of XRCC4 with DNA ligase IV for wild-type V(D)J recombination and DNA double-strand break repair in vivo.* J Biol Chem, 1998. **273**(38): p. 24708-14.

217. Rodgers, K. and M. McVey, *Error-Prone Repair of DNA Double-Strand Breaks.* J Cell Physiol, 2016. **231**(1): p. 15-24.

218. Lieber, M.R., et al., *Nonhomologous DNA end joining (NHEJ) and chromosomal translocations in humans.* Subcell Biochem, 2010. **50**: p. 279-96.

219. Jiricny, J., *The multifaceted mismatch-repair system.* Nat Rev Mol Cell Biol, 2006. **7**(5): p. 335-46.

220. Li, G.M., *Mechanisms and functions of DNA mismatch repair.* Cell Res, 2008. **18**(1): p. 85-98.

221. Acharya, S., et al., *hMSH2 forms specific mispair-binding complexes with hMSH3 and hMSH6.* Proc Natl Acad Sci U S A, 1996. **93**(24): p. 13629-34.

222. Genschel, J. and P. Modrich, *Mechanism of 5'-directed excision in human mismatch repair.* Mol Cell, 2003. **12**(5): p. 1077-86.

223. Kadyrov, F.A., et al., *Endonucleolytic function of MutLalpha in human mismatch repair.* Cell, 2006. **126**(2): p. 297-308.

224. Ramilo, C., et al., *Partial reconstitution of human DNA mismatch repair in vitro: characterization of the role of human replication protein A.* Mol Cell Biol, 2002. **22**(7): p. 2037-46.

225. Longley, M.J., A.J. Pierce, and P. Modrich, *DNA polymerase delta is required for human mismatch repair in vitro.* J Biol Chem, 1997. **272**(16): p. 10917-21.

226. Umar, A., et al., *Requirement for PCNA in DNA mismatch repair at a step preceding DNA resynthesis.* Cell, 1996. **87**(1): p. 65-73.

227. Zhang, Y., et al., *Reconstitution of 5'-directed human mismatch repair in a purified system.* Cell, 2005. **122**(5): p. 693-705.

228. Hagen, L., et al., *Cell cycle-specific UNG2 phosphorylations regulate protein turnover, activity and association with RPA.* EMBO J, 2008. **27**(1): p. 51-61.

229. Liang, F., et al., *Homology-directed repair is a major double-strand break repair pathway in mammalian cells.* Proc Natl Acad Sci U S A, 1998. **95**(9): p. 5172-7.

230. Li, X. and W.D. Heyer, *Homologous recombination in DNA repair and DNA damage tolerance.* Cell Res, 2008. **18**(1): p. 99-113.

231. Vriend, L.E. and P.M. Krawczyk, *Nick-initiated homologous recombination: Protecting the genome, one strand at a time.* DNA Repair (Amst), 2017. **50**: p. 1-13.

232. Hinz, J.M., *Role of homologous recombination in DNA interstrand crosslink repair.* Environ Mol Mutagen, 2010. **51**(6): p. 582-603.

233. Long, D.T., et al., *Mechanism of RAD51-dependent DNA interstrand cross-link repair.* Science, 2011. **333**(6038): p. 84-7.

234. Sun, Y., et al., *Structural basis of homologous recombination.* Cell Mol Life Sci, 2020. **77**(1): p. 3-18.

235. Limbo, O., et al., *Ctp1 is a cell-cycle-regulated protein that functions with Mre11 complex to control double-strand break repair by homologous recombination.* Mol Cell, 2007. **28**(1): p. 134-46.

236. Sartori, A.A., et al., *Human CtIP promotes DNA end resection.* Nature, 2007. **450**(7169): p. 509-14.

237. Nimonkar, A.V., et al., *BLM-DNA2-RPA-MRN and EXO1-BLM-RPA-MRN constitute two DNA end resection machineries for human DNA break repair.* Genes Dev, 2011. **25**(4): p. 350-62.

238. Bahassi, E.M., et al., *The checkpoint kinases Chk1 and Chk2 regulate the functional associations between hBRCA2 and Rad51 in response to DNA damage.* Oncogene, 2008. **27**(28): p. 3977-85.

239. Wright, W.D., S.S. Shah, and W.D. Heyer, *Homologous recombination and the repair of DNA double-strand breaks.* J Biol Chem, 2018. **293**(27): p. 10524-10535.

240. Kim, J.S., et al., *Independent and sequential recruitment of NHEJ and HR factors to DNA damage sites in mammalian cells.* J Cell Biol, 2005. **170**(3): p. 341-7.

241. Shibata, A., *Regulation of repair pathway choice at two-ended DNA double-strand breaks.* Mutation Research-Fundamental and Molecular Mechanisms of Mutagenesis, 2017. **803**: p. 51-55.

242. Clouaire, T. and G. Legube, *DNA double strand break repair pathway choice: a chromatin based decision?* Nucleus, 2015. **6**(2): p. 107-13.

243. Saberi, A., et al., *RAD18 and poly(ADP-ribose) polymerase independently suppress the access of nonhomologous end joining to double-strand breaks and facilitate homologous recombination-mediated repair.* Mol Cell Biol, 2007. **27**(7): p. 2562-71.

244. Hochegger, H., et al., *Parp-1 protects homologous recombination from interference by Ku and Ligase IV in vertebrate cells.* EMBO J, 2006. **25**(6): p. 1305-14.

245. Boulton, S.J., *DNA repair: Decision at the break point.* Nature, 2010. **465**(7296): p. 301-2.

246. Marians, K.J., *Lesion Bypass and the Reactivation of Stalled Replication Forks.* Annu Rev Biochem, 2018. **87**: p. 217-238.

247. Powers, K.T. and M.T. Washington, *Eukaryotic translesion synthesis: Choosing the right tool for the job.* DNA Repair (Amst), 2018. **71**: p. 127-134.

248. Hedglin, M., et al., *Replication protein A dynamically regulates monoubiquitination of proliferating cell nuclear antigen.* J Biol Chem, 2019. **294**(13): p. 5157-5168.

249. Andersen, P.L., F. Xu, and W. Xiao, *Eukaryotic DNA damage tolerance and translesion synthesis through covalent modifications of PCNA.* Cell Res, 2008. **18**(1): p. 162-73.

250. Freudenthal, B.D., et al., *Structure of monoubiquitinated PCNA and implications for translesion synthesis and DNA polymerase exchange.* Nat Struct Mol Biol, 2010. **17**(4): p. 479-84.

251. Plosky, B.S. and R. Woodgate, *Switching from high-fidelity replicases to low-fidelity lesion-bypass polymerases.* Curr Opin Genet Dev, 2004. **14**(2): p. 113-9.

252. Bienko, M., et al., *Ubiquitin-binding domains in Y-family polymerases regulate translesion synthesis.* Science, 2005. **310**(5755): p. 1821-4.

253. Zhao, L. and M.T. Washington, *Translesion Synthesis: Insights into the Selection and Switching of DNA Polymerases.* Genes (Basel), 2017. **8**(1).

254. Rattray, A.J. and J.N. Strathern, *Error-prone DNA polymerases: when making a mistake is the only way to get ahead.* Annu Rev Genet, 2003. **37**: p. 31-66.

255. Sale, J.E., *Translesion DNA synthesis and mutagenesis in eukaryotes.* Cold Spring Harb Perspect Biol, 2013. **5**(3): p. a012708.

256. Motegi, A., et al., *Polyubiquitination of proliferating cell nuclear antigen by HLTF and SHPRH prevents genomic instability from stalled replication forks.* Proc Natl Acad Sci U S A, 2008. **105**(34): p. 12411-6.

257. Sancar, A., et al., *Molecular mechanisms of mammalian DNA repair and the DNA damage checkpoints.* Annu Rev Biochem, 2004. **73**: p. 39-85.

258. Nojima, K., et al., *Multiple repair pathways mediate tolerance to chemotherapeutic cross-linking agents in vertebrate cells.* Cancer Res, 2005. **65**(24): p. 11704-11.

259. Lazzaro, F., et al., *Checkpoint mechanisms at the intersection between DNA damage and repair.* DNA Repair (Amst), 2009. **8**(9): p. 1055-67.

260. Warmerdam, D.O. and R. Kanaar, *Dealing with DNA damage: relationships between checkpoint and repair pathways.* Mutat Res, 2010. **704**(1-3): p. 2-11.

261. Blackford, A.N. and S.P. Jackson, *ATM, ATR, and DNA-PK: The Trinity at the Heart of the DNA Damage Response.* Mol Cell, 2017. **66**(6): p. 801-817.

262. Wang, H., et al., *The interaction of CtIP and Nbs1 connects CDK and ATM to regulate HR-mediated double-strand break repair.* PLoS Genet, 2013. **9**(2): p. e1003277.

263. Cortez, D., et al., *Requirement of ATM-dependent phosphorylation of brca1 in the DNA damage response to double-strand breaks.* Science, 1999. **286**(5442): p. 1162-6.

264. Salguero, I., et al., *MDC1 PST-repeat region promotes histone H2AX-independent chromatin association and DNA damage tolerance.* Nat Commun, 2019. **10**(1): p. 5191.

265. Li, J. and D.F. Stern, *Regulation of CHK2 by DNA-dependent protein kinase.* J Biol Chem, 2005. **280**(12): p. 12041-50.

266. Matsuoka, S., et al., *Ataxia telangiectasia-mutated phosphorylates Chk2 in vivo and in vitro.* Proc Natl Acad Sci U S A, 2000. **97**(19): p. 10389-94.

267. Zannini, L., D. Delia, and G. Buscemi, *CHK2 kinase in the DNA damage response and beyond.* J Mol Cell Biol, 2014. **6**(6): p. 442-57.

268. Gatei, M., et al., *Role for ATM in DNA damage-induced phosphorylation of BRCA1.* Cancer Res, 2000. **60**(12): p. 3299-304.

269. Wang, X., P.R. Andreassen, and A.D. D'Andrea, *Functional interaction of monoubiquitinated FANCD2 and BRCA2/FANCD1 in chromatin.* Mol Cell Biol, 2004. **24**(13): p. 5850-62.

270. Tan, Y., P. Raychaudhuri, and R.H. Costa, *Chk2 mediates stabilization of the FoxM1 transcription factor to stimulate expression of DNA repair genes.* Mol Cell Biol, 2007. **27**(3): p. 1007-16.

271. Falck, J., et al., *The ATM-Chk2-Cdc25A checkpoint pathway guards against radioresistant DNA synthesis.* Nature, 2001. **410**(6830): p. 842-7.

272. Matsuoka, S., M. Huang, and S.J. Elledge, *Linkage of ATM to cell cycle regulation by the Chk2 protein kinase.* Science, 1998. **282**(5395): p. 1893-7.

273. Shiloh, Y. and Y. Ziv, *The ATM protein kinase: regulating the cellular response to genotoxic stress, and more.* Nat Rev Mol Cell Biol, 2013. **14**(4): p. 197-210.

274. Hirao, A., et al., *DNA damage-induced activation of p53 by the checkpoint kinase Chk2.* Science, 2000. **287**(5459): p. 1824-7.

275. Zou, L. and S.J. Elledge, *Sensing DNA damage through ATRIP recognition of RPA-ssDNA complexes.* Science, 2003. **300**(5625): p. 1542-8.

276. Jazayeri, A., et al., *ATM- and cell cycle-dependent regulation of ATR in response to DNA double-strand breaks.* Nat Cell Biol, 2006. **8**(1): p. 37-45.

277. Kumagai, A., et al., *TopBP1 activates the ATR-ATRIP complex.* Cell, 2006. **124**(5): p. 943-55.

278. Lee, J., A. Kumagai, and W.G. Dunphy, *The Rad9-Hus1-Rad1 checkpoint clamp regulates interaction of TopBP1 with ATR.* J Biol Chem, 2007. **282**(38): p. 28036-44.

279. Zhao, H. and H. Piwnica-Worms, *ATR-mediated checkpoint pathways regulate phosphorylation and activation of human Chk1.* Mol Cell Biol, 2001. **21**(13): p. 4129-39.

280. Bartek, J., C. Lukas, and J. Lukas, *Checking on DNA damage in S phase.* Nat Rev Mol Cell Biol, 2004. **5**(10): p. 792-804.

281. Barber, L.J. and S.J. Boulton, *BRCA1 ubiquitylation of CtIP: Just the tIP of the iceberg?* DNA Repair (Amst), 2006. **5**(12): p. 1499-504.

282. Mladenov, E., et al., *DNA-PKcs and ATM epistatically suppress DNA end resection and hyperactivation of ATR-dependent G2-checkpoint in S-phase irradiated cells.* Sci Rep, 2019. **9**(1): p. 14597.

283. Gonzalez Besteiro, M.A. and V. Gottifredi, *The fork and the kinase: a DNA replication tale from a CHK1 perspective.* Mutat Res Rev Mutat Res, 2015. **763**: p. 168-80.

284. Ge, X.Q. and J.J. Blow, *Chk1 inhibits replication factory activation but allows dormant origin firing in existing factories.* J Cell Biol, 2010. **191**(7): p. 1285-97.

285. Liu, P., et al., *The Chk1-mediated S-phase checkpoint targets initiation factor Cdc45 via a Cdc25A/Cdk2-independent mechanism.* J Biol Chem, 2006. **281**(41): p. 30631-44.

286. Katou, Y., et al., *S-phase checkpoint proteins Tof1 and Mrc1 form a stable replication-pausing complex.* Nature, 2003. **424**(6952): p. 1078-83.

287. Speroni, J., et al., *Kinase-independent function of checkpoint kinase 1 (Chk1) in the replication of damaged DNA.* Proc Natl Acad Sci U S A, 2012. **109**(19): p. 7344-9.

288. Yamada, M., et al., *ATR-Chk1-APC/CCdh1-dependent stabilization of Cdc7-ASK (Dbf4) kinase is required for DNA lesion bypass under replication stress.* Genes Dev, 2013. **27**(22): p. 2459-72.

289. Yang, X.H., et al., *Chk1 and Claspin potentiate PCNA ubiquitination.* Genes Dev, 2008. **22**(9): p. 1147-52.

290. Frankenberger, S., et al., *Checkpoint kinase 1 negatively regulates somatic hypermutation.* Nucleic Acids Res, 2014. **42**(6): p. 3666-74.

291. Sharbeen, G., et al., *Ectopic restriction of DNA repair reveals that UNG2 excises AID-induced uracils predominantly or exclusively during G1 phase.* J Exp Med, 2012. **209**(5): p. 965-74.

292. Yabuki, M., et al., *E2A acts in cis in G1 phase of cell cycle to promote Ig gene diversification.* J Immunol, 2009. **182**(1): p. 408-15.

293. Schrader, C.E., et al., *Activation-induced cytidine deaminase-dependent DNA breaks in class switch recombination occur during G1 phase of the cell cycle and depend upon mismatch repair.* J Immunol, 2007. **179**(9): p. 6064-71.

294. Wiedemann, E.M., M. Peycheva, and R. Pavri, *DNA Replication Origins in Immunoglobulin Switch Regions Regulate Class Switch Recombination in an R-Loop-Dependent Manner.* Cell Rep, 2016. **17**(11): p. 2927-2942.

295. Thientosapol, E.S., et al., *SAMHD1 enhances immunoglobulin hypermutation by promoting transversion mutation.* Proc Natl Acad Sci U S A, 2018. **115**(19): p. 4921-4926.

296. Schuler, F., et al., *Checkpoint kinase 1 is essential for normal B cell development and lymphomagenesis.* Nat Commun, 2017. **8**(1): p. 1697.

297. Schoeler, K., et al., *CHK1 dosage in germinal center B cells controls humoral immunity.* Cell Death Differ, 2019. **26**(12): p. 2551-2567.

298. Lam, M.H., et al., *Chk1 is haploinsufficient for multiple functions critical to tumor suppression.* Cancer Cell, 2004. **6**(1): p. 45-59.

299. Hobeika, E., et al., *Testing gene function early in the B cell lineage in mb1-cre mice.* Proc Natl Acad Sci U S A, 2006. **103**(37): p. 13789-94.

300. Sakaguchi, N., et al., *B lymphocyte lineage-restricted expression of mb-1, a gene with CD3-like structural properties.* EMBO J, 1988. **7**(11): p. 3457-64.

301. Jacob, J., R. Kassir, and G. Kelsoe, *In situ studies of the primary immune response to (4-hydroxy-3-nitrophenyl)acetyl. I. The architecture and dynamics of responding cell populations.* J Exp Med, 1991. **173**(5): p. 1165-75.

302. Liu, Y.J., et al., *Sites of specific B cell activation in primary and secondary responses to T cell-dependent and T cell-independent antigens.* Eur J Immunol, 1991. **21**(12): p. 2951-62.

303. Cumano, A. and K. Rajewsky, *Clonal recruitment and somatic mutation in the generation of immunological memory to the hapten NP.* EMBO J, 1986. **5**(10): p. 2459-68.

304. Jolly, C.J., N. Klix, and M.S. Neuberger, *Rapid methods for the analysis of immunoglobulin gene hypermutation: application to transgenic and gene targeted mice.* Nucleic Acids Res, 1997. **25**(10): p. 1913-9.

305. Pilzecker, B. and H. Jacobs, *Mutating for Good: DNA Damage Responses During Somatic Hypermutation.* Front Immunol, 2019. **10**: p. 438.

306. Allen, D., et al., *Antibody engineering for the analysis of affinity maturation of an anti-hapten response.* EMBO J, 1988. **7**(7): p. 1995-2001.

307. Dunnick, W., et al., *DNA sequences at immunoglobulin switch region recombination sites.* Nucleic Acids Res, 1993. **21**(3): p. 365-72.

308. Reboldi, A. and J.G. Cyster, *Peyer's patches: organizing B-cell responses at the intestinal frontier.* Immunol Rev, 2016. **271**(1): p. 230-45.

309. Gramlich, H.S., T. Reisbig, and D.G. Schatz, *AID-targeting and hypermutation of non-immunoglobulin genes does not correlate with proximity to immunoglobulin genes in germinal center B cells.* PLoS One, 2012. **7**(6): p. e39601.

310. Sakaue-Sawano, A., et al., *Visualizing spatiotemporal dynamics of multicellular cell-cycle progression.* Cell, 2008. **132**(3): p. 487-98.

311. Buerstedde, J.M., et al., *Light chain gene conversion continues at high rate in an ALV-induced cell line.* EMBO J, 1990. **9**(3): p. 921-7.

312. Sale, J.E. and M.S. Neuberger, *TdT-accessible breaks are scattered over the immunoglobulin V domain in a constitutively hypermutating B cell line.* Immunity, 1998. **9**(6): p. 859-69.

313. Feng, Y., et al., *AID in Antibody Diversification: There and Back Again.* Trends Immunol, 2020. **41**(7): p. 586-600.

314. Saribasak, H., et al., *Uracil DNA glycosylase disruption blocks Ig gene conversion and induces transition mutations.* J Immunol, 2006. **176**(1): p. 365-71.

315. Arakawa, H. and J.M. Buerstedde, *Activation-induced cytidine deaminase-mediated hypermutation in the DT40 cell line.* Philos Trans R Soc Lond B Biol Sci, 2009. **364**(1517): p. 639-44.

316. Arakawa, H., H. Saribasak, and J.M. Buerstedde, *Activation-induced cytidine deaminase initiates immunoglobulin gene conversion and hypermutation by a common intermediate.* PLoS Biol, 2004. **2**(7): p. E179.

317. Reynaud, C.A., et al., *A hyperconversion mechanism generates the chicken light chain preimmune repertoire.* Cell, 1987. **48**(3): p. 379-88.

318. Zhang, W., et al., *Clonal instability of V region hypermutation in the Ramos Burkitt's lymphoma cell line.* Int Immunol, 2001. **13**(9): p. 1175-84.

319. Pasqualucci, L., et al., *Expression of the AID protein in normal and neoplastic B cells.* Blood, 2004. **104**(10): p. 3318-25.

320. Allman, D., et al., *BCL-6 expression during B-cell activation.* Blood, 1996. **87**(12): p. 5257-68.

321. Jinek, M., et al., *A programmable dual-RNA-guided DNA endonuclease in adaptive bacterial immunity.* Science, 2012. **337**(6096): p. 816-21.

322. Ran, F.A., et al., *Genome engineering using the CRISPR-Cas9 system.* Nat Protoc, 2013. **8**(11): p. 2281-2308.

323. Izon, D.J., et al., *Notch1 regulates maturation of CD4+ and CD8+ thymocytes by modulating TCR signal strength.* Immunity, 2001. **14**(3): p. 253-64.

324. Takai, H., et al., *Aberrant cell cycle checkpoint function and early embryonic death in Chk1(-/-) mice.* Genes Dev, 2000. **14**(12): p. 1439-47.

325. Liu, Q., et al., *Chk1 is an essential kinase that is regulated by Atr and required for the G(2)/M DNA damage checkpoint.* Genes Dev, 2000. **14**(12): p. 1448-59.

326. Zaugg, K., et al., *Cross-talk between Chk1 and Chk2 in double-mutant thymocytes.* Proc Natl Acad Sci U S A, 2007. **104**(10): p. 3805-10.

327. Greenow, K.R., A.R. Clarke, and R.H. Jones, *Chk1 deficiency in the mouse small intestine results in p53-independent crypt death and subsequent intestinal compensation.* Oncogene, 2009. **28**(11): p. 1443-53.

328. Schuler, F., et al., *Checkpoint kinase 1 is essential for fetal and adult hematopoiesis.* EMBO Rep, 2019. **20**(8): p. e47026.

329. Spanopoulou, E., et al., *Functional immunoglobulin transgenes guide ordered B-cell differentiation in Rag-1-deficient mice.* Genes Dev, 1994. **8**(9): p. 1030-42.

330. Young, F., et al., *Influence of immunoglobulin heavy- and light-chain expression on B-cell differentiation.* Genes Dev, 1994. **8**(9): p. 1043-57.

331. Davari, K., et al., *Checkpoint kinase 2 is required for efficient immunoglobulin diversification.* Cell Cycle, 2014. **13**(23): p. 3659-69.

332. Sorensen, C.S., et al., *The cell-cycle checkpoint kinase Chk1 is required for mammalian homologous recombination repair.* Nat Cell Biol, 2005. **7**(2): p. 195-201.

333. Zachos, G., M.D. Rainey, and D.A. Gillespie, *Chk1-deficient tumour cells are viable but exhibit multiple checkpoint and survival defects.* EMBO J, 2003. **22**(3): p. 713-23.

334. Dalla-Favera, R., et al., *Human c-myc onc gene is located on the region of chromosome 8 that is translocated in Burkitt lymphoma cells.* Proc Natl Acad Sci U S A, 1982. **79**(24): p. 7824-7.

335. Baba, T.W., B.P. Giroir, and E.H. Humphries, *Cell lines derived from avian lymphomas exhibit two distinct phenotypes.* Virology, 1985. **144**(1): p. 139-51.

336. Ulrich, E., et al., *Immortalization of conditionally transformed chicken cells: loss of normal p53 expression is an early step that is independent of cell transformation.* Genes Dev, 1992. **6**(5): p. 876-87.

337. Gaidano, G., et al., *p53 mutations in human lymphoid malignancies: association with Burkitt lymphoma and chronic lymphocytic leukemia.* Proc Natl Acad Sci U S A, 1991. **88**(12): p. 5413-7.

338. Kleinstein, S.H., Y. Louzoun, and M.J. Shlomchik, *Estimating hypermutation rates from clonal tree data.* J Immunol, 2003. **171**(9): p. 4639-49.

339. Kocks, C. and K. Rajewsky, *Stepwise intraclonal maturation of antibody affinity through somatic hypermutation.* Proc Natl Acad Sci U S A, 1988. **85**(21): p. 8206-10.

340. Kepler, T.B. and A.S. Perelson, *Cyclic re-entry of germinal center B cells and the efficiency of affinity maturation.* Immunol Today, 1993. **14**(8): p. 412-5.

341. Oprea, M. and A.S. Perelson, *Somatic mutation leads to efficient affinity maturation when centrocytes recycle back to centroblasts.* J Immunol, 1997. **158**(11): p. 5155-62.

342. He, M., et al., *Cyclin-dependent kinases regulate Ig class switching by controlling access of AID to the switch region.* J Immunol, 2015. **194**(9): p. 4231-9.

343. Meyer-Hermann, M., *Injection of Antibodies against Immunodominant Epitopes Tunes Germinal Centers to Generate Broadly Neutralizing Antibodies.* Cell Rep, 2019. **29**(5): p. 1066-1073 e5.

344. Anderson, S.M., et al., *Taking advantage: high-affinity B cells in the germinal center have lower death rates, but similar rates of division, compared to low-affinity cells.* J Immunol, 2009. **183**(11): p. 7314-25.

345. Zineldeen, D.H., N.M. Shafik, and S.F. Li, *Alternative Chk1-independent S/M checkpoint in somatic cells that prevents premature mitotic entry.* Med Oncol, 2017. **34**(4): p. 70.

346. Leimbacher, P.A., et al., *MDC1 Interacts with TOPBP1 to Maintain Chromosomal Stability during Mitosis.* Mol Cell, 2019. **74**(3): p. 571-583 e8.

347. Deckbar, D., P.A. Jeggo, and M. Lobrich, *Understanding the limitations of radiation-induced cell cycle checkpoints.* Crit Rev Biochem Mol Biol, 2011. **46**(4): p. 271-83.

348. Cortez, D., *Replication-Coupled DNA Repair.* Mol Cell, 2019. **74**(5): p. 866-876.

349. Sirbu, B.M., et al., *Analysis of protein dynamics at active, stalled, and collapsed replication forks.* Genes Dev, 2011. **25**(12): p. 1320-7.

350. Petermann, E., et al., *Hydroxyurea-stalled replication forks become progressively inactivated and require two different RAD51-mediated pathways for restart and repair.* Mol Cell, 2010. **37**(4): p. 492-502.

351. Castedo, M., et al., *Cell death by mitotic catastrophe: a molecular definition.* Oncogene, 2004. **23**(16): p. 2825-37.

352. Qiu, Z., N.L. Oleinick, and J. Zhang, *ATR/CHK1 inhibitors and cancer therapy.* Radiother Oncol, 2018. **126**(3): p. 450-464.

353. Yoshioka, K., Y. Yoshioka, and P. Hsieh, *ATR kinase activation mediated by MutSalpha and MutLalpha in response to cytotoxic O6-methylguanine adducts.* Mol Cell, 2006. **22**(4): p. 501-10.

354. Adamson, A.W., et al., *Methylator-induced, mismatch repair-dependent G2 arrest is activated through Chk1 and Chk2.* Mol Biol Cell, 2005. **16**(3): p. 1513-26.

355. Gupta, D., et al., *ATR-Chk1 activation mitigates replication stress caused by mismatch repair-dependent processing of DNA damage.* Proc Natl Acad Sci U S A, 2018. **115**(7): p. 1523-1528.

356. Ratnam, S., et al., *The pattern of somatic hypermutation of Ig genes is altered when p53 is inactivated.* Mol Immunol, 2010. **47**(16): p. 2611-8.

357. Martomo, S.A., W.W. Yang, and P.J. Gearhart, *A role for Msh6 but not Msh3 in somatic hypermutation and class switch recombination.* J Exp Med, 2004. **200**(1): p. 61-8.

358. Kuppers, R. and R. Dalla-Favera, *Mechanisms of chromosomal translocations in B cell lymphomas.* Oncogene, 2001. **20**(40): p. 5580-94.

359. Alt, F.W., et al., *Mechanisms of programmed DNA lesions and genomic instability in the immune system.* Cell, 2013. **152**(3): p. 417-29.

360. Basso, K., et al., *Integrated biochemical and computational approach identifies BCL6 direct target genes controlling multiple pathways in normal germinal center B cells.* Blood, 2010. **115**(5): p. 975-84.

361. Shen, H.M., et al., *Mutation of BCL-6 gene in normal B cells by the process of somatic hypermutation of Ig genes.* Science, 1998. **280**(5370): p. 1750-2.

362. Basso, K. and R. Dalla-Favera, *Roles of BCL6 in normal and transformed germinal center B cells.* Immunol Rev, 2012. **247**(1): p. 172-83.

363. Leeman-Neill, R.J. and G. Bhagat, *BCL6 as a therapeutic target for lymphoma.* Expert Opin Ther Targets, 2018. **22**(2): p. 143-152.

364. Niu, H., B.H. Ye, and R. Dalla-Favera, *Antigen receptor signaling induces MAP kinase-mediated phosphorylation and degradation of the BCL-6 transcription factor.* Genes Dev, 1998. **12**(13): p. 1953-61.

365. Polo, J.M., et al., *Reversible disruption of BCL6 repression complexes by CD40 signaling in normal and malignant B cells.* Blood, 2008. **112**(3): p. 644-51.

366. Liu, Y.J., et al., *Within germinal centers, isotype switching of immunoglobulin genes occurs after the onset of somatic mutation.* Immunity, 1996. **4**(3): p. 241-50.

367. Klein, U., et al., *Transcriptional analysis of the B cell germinal center reaction.* Proc Natl Acad Sci U S A, 2003. **100**(5): p. 2639-44.

368. Dominguez-Sola, D., et al., *The FOXO1 Transcription Factor Instructs the Germinal Center Dark Zone Program.* Immunity, 2015. **43**(6): p. 1064-74.

369. Faili, A., et al., *AID-dependent somatic hypermutation occurs as a DNA single-strand event in the BL2 cell line.* Nat Immunol, 2002. **3**(9): p. 815-21.

370. Mayer, C.T., et al., *The microanatomic segregation of selection by apoptosis in the germinal center.* Science, 2017. **358**(6360).

371. Schweighoffer, E. and V.L. Tybulewicz, *Signalling for B cell survival.* Curr Opin Cell Biol, 2018. **51**: p. 8-14.

372. Sander, S., et al., *Synergy between PI3K signaling and MYC in Burkitt lymphomagenesis.* Cancer Cell, 2012. **22**(2): p. 167-79.

373. Delker, R.K., et al., *Solubility-based genetic screen identifies RING finger protein 126 as an E3 ligase for activation-induced cytidine deaminase.* Proc Natl Acad Sci U S A, 2013. **110**(3): p. 1029-34.

374. Ordinario, E.C., et al., *RAD51 paralogs promote homology-directed repair at diversifying immunoglobulin V regions.* BMC Mol Biol, 2009. **10**: p. 98.

375. Conlon, T.M. and K.B. Meyer, *The chicken Ig light chain 3'-enhancer is essential for gene expression and regulates gene conversion via the transcription factor E2A.* Eur J Immunol, 2006. **36**(1): p. 139-48.

376. Kawamoto, T., et al., *Dual roles for DNA polymerase eta in homologous DNA recombination and translesion DNA synthesis.* Mol Cell, 2005. **20**(5): p. 793-9.

377. McIlwraith, M.J., et al., *Human DNA polymerase eta promotes DNA synthesis from strand invasion intermediates of homologous recombination.* Mol Cell, 2005. **20**(5): p. 783-92.

378. Zhou, J., et al., *Replication and subnuclear location dynamics of the immunoglobulin heavy-chain locus in B-lineage cells.* Mol Cell Biol, 2002. **22**(13): p. 4876-89.

379. Ballana, E. and J.A. Este, *SAMHD1: at the crossroads of cell proliferation, immune responses, and virus restriction.* Trends Microbiol, 2015. **23**(11): p. 680-692.

380. Boldinova, E.O., et al., *DNA Damage Tolerance by Eukaryotic DNA Polymerase and Primase PrimPol.* Int J Mol Sci, 2017. **18**(7).

381. Pilzecker, B., et al., *PrimPol prevents APOBEC/AID family mediated DNA mutagenesis.* Nucleic Acids Res, 2016. **44**(10): p. 4734-44.

382. Tepper, S., et al., *PARP activation promotes nuclear AID accumulation in lymphoma cells.* Oncotarget, 2016. **7**(11): p. 13197-208.

383. Niwa, H., K. Yamamura, and J. Miyazaki, *Efficient selection for high-expression transfectants with a novel eukaryotic vector.* Gene, 1991. **108**(2): p. 193-9.

384. Morita, S., T. Kojima, and T. Kitamura, *Plat-E: an efficient and stable system for transient packaging of retroviruses.* Gene Ther, 2000. **7**(12): p. 1063-6.

385. Schneider, C.A., W.S. Rasband, and K.W. Eliceiri, *NIH Image to ImageJ: 25 years of image analysis.* Nat Methods, 2012. **9**(7): p. 671-5.

386. Maccarthy, T., et al., *SHMTool: a webserver for comparative analysis of somatic hypermutation datasets.* DNA Repair (Amst), 2009. **8**(1): p. 137-41.

387. Lefranc, M.P., *IMGT, the international ImMunoGeneTics database.* Nucleic Acids Res, 2003. **31**(1): p. 307-10.

7 Acknowledgments

First and foremost, I want to thank Prof. Berit Jungnickel for patient supervision and guidance throughout these years. The scientific pieces of advice and the fruitful discussions have shaped my critical thinking, while trust and encouragement have helped me overcome moments of frustration.

Special thanks also go to Dr. Christian Kosan for keeping a close eye on my signs of progress since the beginning, for the insightful comments and the constructive suggestions.

I am grateful to Dr. Jeroen Guikema for the intellectual excitement we had the chance to share in the occasion of the 19th International Conference on Germinal Centers; my passion for science has grown even stronger from that moment on.

Heartfelt thanks go to the wonderful people of the lab crew I had the fortune to work with and get to know. I can't thank Gianna Hirth enough for all the valuable inputs and feedbacks in countless hours of discussion and for joining me in every single step of this journey, not only by being there "with" me as a colleague and then also as a flatmate but by choosing, in all those moments, to be there "for" me as a friend. My deepest gratitude also goes to Marta O'Connell for her friendship, for being always available, since the very first step I took on Jena's ground, and for the contagious positivity she irradiates people with. I want to thank Katrin Böttcher for troubleshooting any technical problem, for the cheerful atmosphere, and for the great coffee-break distractions, sometimes very badly needed. I thank Sandra Tepper for always having an answer to my questions and Sally Böde for her indispensable help in the immunization experiments. I thank Antonia Müller and Liane Nadja Giebeler for the contribution to the research they provided with their Bachelor thesis and with their work as student lab assistants, together with Jana Efremova and Charline Sommer. I thank Ana, Ewelina, Geli, Gleice, Katrin T., Kev, Sarah, Steph, and Vanessa for the friendly working atmosphere and the moments of celebration we shared; special thanks go to Melissa for the nice conversations and the boost of energy in the form of chocolate. I am grateful to Petra and Gunther for their great help in the animal facility and to the staff of the FACS facility of the Leibniz Institute on Aging for the sorting experiments.

I want to thank Gianna, Steffen, and Wolfgang for being like a family in these years I spent far from home. I am grateful to Amod, Bela, Maricel, Martina, and Sofia for the beautiful moments we shared, which have helped me face the challenges of every-day life in the last years. I am grateful to Marika, Elisa, and Silvia for being there for each other even at kilometers apart, as

8 Publication of the present work

- **Impact of Chk1 dosage on somatic hypermutation *in vivo***
  Amanda Bello and Berit Jungnickel
  Immunology & Cell Biology 2021; 1–15

- **Cell cycle-mediated regulation of secondary immunoglobulin diversification**
  Amanda Bello, Antonia Müller, Liane Nadja Giebeler and Berit Jungnickel
  Yet unpublished work

9 Declaration of Authorship

I hereby declare that I am aware of the relevant examination regulation on the conferral of the doctoral degree at the Faculty of Biological Science of the Friedrich Schiller University Jena. In accordance, I declare that the submitted dissertation was composed entirely by me and that I have not used any sources other than those cited in the text and identified as references. People who have provided technical support and/or have assisted me in the evaluation and the interpretation of the data have been properly acknowledged. I have not received the assistance of a doctoral consultant, neither have I provided directly or indirectly monetary compensation to third parties for the work related to the content of the submitted thesis. This thesis has not been previously submitted for examination to the Friedrich Schiller University Jena, nor elsewhere.

_____   _____

Place, date   Signature (Amanda Bello)